Design Principles for Robust Grasping in Unstructured Environments

A thesis presented

by

Aaron Michael Dollar

to

The Division of Engineering and Applied Sciences

in partial fulfillment of the requirements for the degree of

Doctor of Philosophy

in the subject of

Engineering Sciences

Harvard University

Cambridge, Massachusetts

October 25, 2006

Robert D. Howe
Thesis Advisor

Aaron Michael Dollar
Author

Design Principles for Robust Grasping in Unstructured Environments

Abstract

Grasping in unstructured environments is one of the most challenging issues currently facing robotics. The inherent uncertainty about the properties of the target object and its surroundings makes the use of traditional robot hands, which typically involve complex mechanisms, sensing suites, and control, difficult and impractical. In this dissertation I investigate how the challenges associated with grasping under uncertainty can be addressed by careful mechanical design of robot hands. In particular, I examine the role of three characteristics of hand design as they affect performance: passive mechanical compliance, adaptability (or underactuation), and durability. I present design optimization studies in which the kinematic structure, compliance configuration, and joint coupling are varied in order to determine the effect on the allowable error in positioning that results in a successful grasp, while keeping contact forces low. I then describe the manufacture of a prototype hand created using a particularly durable process called polymer-based Shape Deposition Manufacturing (SDM). This process allows fragile sensing and actuation components to be embedded in tough polymers, as well as the creation of heterogeneous parts, eliminating the need for fasteners and seams that are

often the cause of failure. Finally, I present experimental work in which the effectiveness of the prototype hand was tested in real, unstructured tasks. The results show that the grasping system, even with three positioning degrees of freedom and extremely simple hand control, can grasp a wide range of target objects in the presence of large positioning errors.

Contents

Title Page i
Abstract iii
Table of Contents v
Acknowledgements viii
Dedication xi

1 Introduction 1
1.1 Compliance 3
1.1.1 Active Compliance 3
1.1.2 Passive Mechanical Compliance 4
1.1.3 Inspiration from Biology 5
1.2 Underactuation 6
1.3 Survey of Compliant and Coupled Robot Hands 7
1.4 Robustness 11
1.5 Thesis Overview 12

2 Compliance and Configuration Optimization 15
2.1 Methods 16
2.1.1 Grasping Scenario 16
2.1.2 Grasp Analysis 18
2.1.3 Simulation 22
2.1.4 Experimental Apparatus and Procedure 24
2.2 Results 26
2.2.1 Simulation Results 26
2.2.2 Experimental Results 32
2.3 Discussion 34
2.3.1 Within Parameterizations 35
2.3.2 Between Parameterizations 37
2.3.3 Comparison to 'Intuitive' Configurations 38
2.3.4 Experimental Validation 39
2.3.5 Generalizations 40

3 Joint Coupling and Actuation 42
3.1 Methods 43
3.1.1 Basic Grasping Scenario 44

3.1.2 Specific Grasping Scenarios 51
3.1.3 Parametric Analysis 55
3.2 Results 57
3.2.1 One Actuator 57
3.2.2 Two Actuators 66
3.3 Discussion 67

4 Finger Design, Fabrication, and Evaluation 71
4.1 Shape Deposition Manufacturing 71
4.2 Finger Design and Fabrication 73
4.2.1 Fabrication Procedure 73
4.2.2 Finger Design 75
4.3 Mechanism Behavior 78

5 Sensor Design and Fabrication 85
5.1 Joint Angle Sensor 86
5.2 Strain Gage Force Sensor 87
5.3 Tactile Sensor 89
5.4 Piezofilm Contact Sensor 91
5.5 Future Work 92

6 Hand Implementations 94
6.1 Two-fingered Hand 94
6.1.1 Experimental Evaluation 95
6.2 Four-fingered Hand 99
6.2.1 Hand Design 100
6.2.2 Hand Performance 102

7 Autonomous Grasping Experiments 104
7.1 Grasp Range and Contact Force Experiment 104
7.1.1 Experimental Setup 104
7.1.2 Experimental Procedure 106
7.1.3 Results 109
7.2 Visual-Guided Grasping Experiment 113
7.2.1 Experimental Setup 114
7.2.2 Experimental Procedure 116
7.2.3 Results 117
7.3 Discussion 120

8 Conclusions and Future Directions **122**
8.1 Implications 123
8.1.1 New Approach 123
8.1.2 New Frameworks 124
8.2 Applications 124
8.2.1 Within Robotics 125
8.2.2 Outside of Robotics 126
8.3 Limitations 127
8.3.1 Current Hardware Implementation 127
8.3.2 Overall Approach 128
8.4 Future Work 129
8.4.1 Extension to Manipulation 129
8.4.2 Quality Measures for Grasping in Unstructured Environments 129
8.4.3 Sensing for Unstructured Grasping Tasks 130

Bibliography **131**

Acknowledgements

Wow. It's been quite a journey. Now I get the opportunity to thank all of the people who have helped me get here.

Thanks to my thesis committee, Professors Pierre Dupont and Rob Wood, for all of the time they invested in meeting with me with to discuss my ideas and guide my progress. Professor Fred Abernathy, for faithfully serving up until the end, when he was gladly relieved of duty. Thanks for all of your grandfatherly encouragement and guidance. Thanks also to Professors Jack Dennerlein, Garrett Stanley, Joost Vlassak, and John Hutchinson, all of whom provided valuable guidance in areas from concept to nitty-gritty details, and spending time hashing out solutions with me on most of the boards in Pierce Hall and 60 Oxford.

Unending thanks to my thesis advisor, Professor Robert D. Howe. You have been an amazing mentor and friend. I can't express how grateful I am to have had the good fortune of being taken on as a student in your lab and having the privilege of your attention for at least an hour a week for the last six years. I am leaving here with overwhelming confidence, excitement, and energy due to your thoughtful guidance, and

feel prepared to move on to the next level. I will strive to model myself after you in my own career. Thank you.

I also want to thank my school teachers throughout the years. All have been wonderful and have contributed to my education and getting this far. Some, however, stand out in particular: Susan Roetzel, my first grade teacher at Yellow Springs Elementary School in Frederick, MD; Mrs. Bush and Mrs. Hargraves at Page School in Ayer, MA; Judy Schaefer and Don Seltzer at Darmstadt Middle School in Darmstadt, Germany; and Dolly Sullivan, John Clarke, Daniel Rogacki, Elisabeth Gaffney, and Susan Patterson at Tewksbury Memorial High School in Tewksbury, MA.

Thanks to the professors of Mechanical Engineering at UMass Amherst who inspired me to carve out a career in their field as well as go to graduate school. In particular, John Ritter, Donald Fisher, James Rinderle, G. Albert Russell, Karl Jakus, Shantikumar Nair, Sundar Krishnamurty, Yossi Chait, and Corrodo Poli.

My friends throughout graduate school, who have helped me get through numerous hard times and have lots of fun throughout: Peter Massumi, Brian Murphy, Dan Gallagher, Cliff Brangwyne, Brian Roland, Matt Kanan, Bola George, Patrick Everley, Tunde Agumbiade, and Chris Zillman.

All of my labmates in the Biorobotics lab. In particular, Chris Wagner, Ryan Beasley, Paul Novotny, Amy Kerdok, Doug Perrin, Solomon Gilbert Diamond, Petr Jordan, Shelten Yuen, Yoky Matsuoka, Shin Park, and Marius Linguraru, all of whom helped me learn and work through sticking points in my research and school life. Also to the undergraduate students who worked with me over the summers: Chris Johnson and Francisco (Paco) Isenberg.

My sister, Andrea (Dollar) Dixon, for being a great friend and confidante throughout our childhood and into our adult years. My grandparents, Jack Gibbs and Joan (Weiland) Gibbs and Leonard Dollar and Ruth (Henry) Dollar, for always encouraging me in my thirst for knowledge, particularly when I was young, impressionable, and asking too many questions. My aunt, Cathy Sheppeck, mostly because I can't think of anyone else who would be more excited to know that her name will forever reside in a book on a shelf in one of Harvard's libraries.

My girlfriend and best friend, Stacy Jethroe, who has been amazingly supportive of me and tolerant of my long hours in the lab and short hours with her, especially over these last six months. I'll make up for it, I promise.

Thanks most of all to the greatest teachers in my life – my parents. Mom, all of your work with me before I started school was what put me on this path to begin with. Because of you I started school way ahead of my classmates, and you helped me stay there through most of my education. Dad, you were the driving force behind my development in my teen years and onward. You taught me the value of hard work and you allowed me the freedom to mature independently. And you both have always been so proud.

For my parents, Susan (Gibbs) Dollar and Gary Dollar

Chapter 1

Introduction

One of the greatest challenges of robotics is grasping and manipulating objects in unstructured environments, where object properties are not known *a priori* and sensing is prone to error. The resulting uncertainty in the relationship between the object and gripper makes it difficult to control contact forces and establish a successful grasp. One way to describe such an environment is to discuss what it *isn't*. An example of a "structured" grasping task is a manufacturing assembly-line: the location, orientation, and properties of the object are known with only a small amount of error. A machine can then fairly easily be designed and programmed specifically for that object and task, with little need for sensory feedback during the execution of the task. An "unstructured" grasping task, therefore, can be thought of as one that is performed without a precise knowledge of the relevant properties of the object and environment: object size, shape, mass, surface properties, position and orientation, and properties of the surroundings.

Human environments – the spaces we operate in day to day – are great examples of unstructured environments. Consider if you will the true complexity involved in a

relatively mundane task that we perform every day – picking up a filled drinking glass. After years of "training" in this type of task, we have a fairly good internal model of the properties of the glass – by looking at it we can see how much liquid is in it, and therefore have a good estimate of what it will weigh. We see that it is in a glass container, and therefore know approximately what the frictional properties will be between the cup and our fingers. We see where it is located and its approximate size and shape, so we can move our hand to it and have a good idea where to place our fingers in order to stably grasp it. After placing our fingers, we will use information from the sensors in our fingerpads and muscles in order to sense contact with the object, the forces that we are applying, and when slip occurs in order to ensure a successful grasp (picking up the glass and manipulating it without spilling). If one or more of our sensing modalities is impaired, we modify our approach strategy depending on the quality of the sensory information and our prior experience with the task [1]. For instance, we will take a much different approach if we are attempting to pick up the glass in the dark.

In robotics, the traditional approach to the problem of grasping in unstructured environments has been to design hands with similar capabilities of a human hand – many degrees of freedom and actuators and a rich suite of sensors. However, there are a number of problems with this approach:

- Complexity - integrating the sensory information to create a model of the task which can then be used to control the many degrees of freedom of the hand can be prohibitively difficult.

- Lack of adaptability – because of the need to actively control every degree of freedom of these hands, even small errors in sensing or positioning can lead to failure of the grasp.
- Expense – due to the number of sensors and actuators, and complexity of construction, the hardware alone can easily exceed $100,000.
- Fragility – not surprisingly, with so many subcomponents, there is an increased likelihood of some part failing. On-board sensors, which are typically located close to the source of the information to be sensed (i.e. on or near the fingertips), are easily damaged. And finally, crashes that can easily occur during use or the debugging phase can put the hardware offline for months at a time.

In order to address these pitfalls, I approach the design of robot hands for unstructured environments in three directions: mechanical compliance to keep contact forces low and allow passive deflection under unwanted contact, adaptive actuation to simplify the sensing and control, and robust construction to prevent damage when unplanned contact occurs.

1.1. Compliance

One approach to dealing with the uncertainty inherent in unstructured grasping task is through compliance, so that positioning errors do not result in large forces and the grasper conforms to the object.

1.1.1. Active Compliance

Robot compliance or stiffness has often been considered in the context of active control, where sensors and actuators are used to achieve a desired force-deflection relationship. Many studies have been devoted to impedance analysis and control techniques for robot arms and hands (e.g. [2]-[7]).

However, this approach requires the active use of position/velocity and force/torque sensor signals in the robot joints or end-effector. This presents a number of undesirable effects for grasping in unstructured environments. First, the sensors required to help create the active compliant behavior are both fragile and expensive. In an unstructured environment, where unintended contact commonly occurs and results in large contact forces, expensive, fragile sensors that are often mounted on the external surfaces of robot are easily damaged. Additionally, active stiffness control schemes fail in impacts, where the speed of the force transients is too fast to use sensing and control to avoid damage.

1.1.2. Passive Mechanical Compliance

In contrast, passive compliance, implemented through springs in robot joints, offers a number of additional benefits that cannot be provided with active control of stiffness. Passive joint compliance that allows for large joint deflections can ensure low contact forces, thus minimizing disturbance or damage to objects during the first phases of acquisition and in impacts, where active stiffness control often fails. The elimination of the sensing required to create active compliance can also lower implementation costs. Ideally, carefully designed passive compliance can also eliminate the need for a good deal of traditional sensor-based control.

A number of researchers in robotics (e.g. [8] -[13]) have used the concept of employing mechanical compliance to accommodate for robot positioning errors. They developed remote center of compliance (RCC) devices for use in assembly tasks that were typically wrists incorporating elastomer pads or deformable rods that allowed for small angular deflections of the robot end-effector. The devices aided tasks such as peg-in-hole insertion where *small* alignment errors can prevent the completion of the assembly task, or edge-tracking, where contact with the surface must be kept despite irregularities.

In addition to grasping, passive mechanical compliance can aid in robot locomotion. Recent results with legged robots demonstrate that judiciously tuned leg stiffness and kinematic configurations can permit stable high-speed locomotion over rough terrain using only open-loop commands (e.g. [14] and [15]). Unlike legs, which undergo fast, repetitive motion with relatively small cycle-to-cycle variation in load and interaction with the environment, a compliant grasper will have highly variable interactions that must, to a considerable extent, utilize sensing. Further comparison of these modalities may lend insight into common passive "control" mechanisms.

A number of authors have dealt with the analysis of compliance in robotics (e.g.[3]), and even applied it to grasping ([4]-[6] and [16]). But these deal with the computation and analysis of the compliance of a given robot or grasper and do not address the issue of the utilization of compliance. I seek to understand how compliance can be purposefully used in the design of robot graspers to increase performance, particularly in unstructured environments and/or for grasping objects of unknown physical properties.

1.1.3. Inspiration from Biology

Nature uses compliance in joints to increase performance. There are many examples of this in arthropods, which are particularly interesting to the application of robotics in that their mechanical design is similar to robot design: stiff links (due to the exoskeleton) with flexure-based, actuated joints. Unlike those of mainstream robots, most arthropod joints are compliant, including the joints in arthropod pincers and claws [17]. Arthropods often have a 'living hinge' joint that allows passive motion between the two links. This hinge is primarily made of a rubber-like substance called resilin, and serves to seal the joint, provide passive compliance to the environment (such as uneven ground), and sometimes provides useful elastic potential energy [18].

1.2. Underactuation

After years of experimenting with complex, fully-articulated anthropomorphic hands, researchers have begun to embrace the idea that much of the functionality of a hand can be retained by careful selection of joint coupling schemes, reducing the number of actuators and the overall complexity of the grasping mechanism. Many of these grippers are "underactuated", having fewer actuators than degrees of freedom. These hands have also been referred to as "adaptive" or "self-adaptable". In an underactuated hand, motion of the distal links can continue after contact on the coupled proximal links occurs, allowing the finger to passively adapt to the object shape. Other simplified hands have fixed-motion coupling between joints, reducing the overall degrees-of-freedom of the mechanism. These two classes of simplified grippers can be easier to control, lighter, and less expensive than their fully-actuated counterparts.

The joint coupling necessary for underactuation is often accomplished through compliance in the manipulator structure. Compliance is perhaps the simplest way to allow for coupling between joints without enforcing the fixed-motion coupling relationship inherent with many gear or linkage couplings. Finger compliance allows the gripper to passively conform to a wide range of objects while minimizing contact forces.

The very nature of unstructured environments hinders full utilization of a complex, fully-actuated hand. In order to appropriately use the added degrees of actuation, an accurate model of the task environment is necessary. This model can be built from real-time sensing, but requires a great deal of sensors, processing, and control that may be difficult for the task at hand. A gripper with a reduced number of actuators is not only simpler to use, it is more appropriate based on the quality of information available in unstructured environments.

1.3. Survey of Compliant and Coupled Robot Hands

Table 1.1 provides an overview of some of the most well-known underactuated and fixed-motion coupled robotic hands. An "underactuated" hand has fewer actuators than degrees-of-freedom, and therefore demonstrates adaptive behavior. In these hands, motion of the distal links can continue after contact on the coupled proximal links occurs, allowing the finger to passively adapt to the object shape. A 'fixed-motion coupled' hand has more joints than degrees-of-freedom, each actuator controls a single degree-of-freedom, and the mechanism has no "adaptability" (final column). In these hands, motion of one joint always results in a proportional motion of the joint(s) coupled to it. In the

Table 1.1: Underactuated and Fixed-Motion Coupled Robot Hands

Hand	*# fingers*	*Pitch joints per finger*	*Pitch actuators per finger*	*Coupling scheme* (*indicates compliant coupling ^indicates adaptive mechanism)	*Coupling ratio*	*Source of compliance and/or adaptability*
100G [19]	2	2	1/2	prox*:dist	unknown	tendon routing, spring-loaded joints
Barrett [20]	3	2	1	prox^:dist	(3:4)	"TorqueSwitch" differential
Belgrade/USC [21,22]	4+1	3+0	1/2+1	(prox;med;dist)+(prox;dist)	(~9;8;7)	rocker arm coupling of fingers
DLR I and II [23,24]	4	3	2	med;dist	(1;1)	none
Domo [25]	3	3	1	prox;med:*:dist	(1;1:passive)	unactuated compliant distal joint
Graspar [26]	3	3	1	prox^:med:^:dist	(~5:4.2:2.9)	tendon differential mechanism
Hirose [27]	2	10	1/2	prox(all):distal	(55:::28:::10::1)	tendon routing
Laval 10-DOF [28]	3	3	1/3	prox^:med:^:dist	unknown	adaptive mechanism
NAIST [29]	3+1	3+3	2+2	(med;dist)+(med;dist)	(1;1.15)	none
Obrero [30]	3	2	1	prox*:dist	(4:3)	series elastic actuation
Robonaut [31]	2+2+1	3+3+2	2+1+2	(med;dist)+(prox;med;dist)+0	(1;1)+(1;1;1)+0	none
Rutgers [32]	4+1	3+3	2+2	med:dist	unknown	tendon routing
Salford [33]	4+1	3+3	2+3	(med;dist)+0	unknown	none
SDM [34]	4	2	1/4	(prox*:dist)	(1:1)	tendon routing, joints made of springs
Shadow[35]	4+1	3+2	2+2	(med:dist)+0	unknown	unknown
Southampton [36]	3	3	1	prox^:med:^:dist	unknown	differential unit
SPRING [37]	2+1	3+2	1/3+1/3	(prox*:med:*:dist)+(prox*:dist)	(2.9:1.6:1)	series elastic actuation
TBM [38]	4+1	3+2	1+1	(prox;med;dist)+(prox;dist)	(~2;1;1)+(~2;1)	none
UB III [39]	2+2+1	3+3+3	3+2+2	0+(med:*:dist)+(med:*:dist)	(~6:7)	tendon routing, joints made of springs

same way, if contact occurs on one joint fixing its position, all coupled joints are thereby fixed.

The "# fingers" column gives the number of fingers of each different type used in the hand, separated by "+". Cases where two types are given indicate that some number of identical fingers and one thumb are used in the design. Cases where three types are given mean that two different finger designs are used in addition to a thumb. For example, the Robonaut hand [31] incorporates two "grasping" fingers, two "dexterous" fingers, and a thumb.

The second column indicates the number of "pitch" joints per finger, leaving out "yaw" and "roll" joints, if any exist. Entries correspond to the data in the "# fingers" column. For the Robonaut hand, the grasping and dexterous fingers have three pitch joints each while the thumb has two.

The next column corresponds to the number of actuators per finger that control the pitch joints. Note that the degree of underactuation ranges from a single actuator for twenty joints (Hirose's "Soft Gripper" [27]) to twelve actuators for fifteen joints (UB III hand [39]).

The coupling scheme is indicated in the next column. "Prox" indicates the proximal joint (nearest to the base), "med" is the medial joint (for three phalanx fingers), and "dist" is the distal joint (farthest from the base). The notation ":*:" between two joints indicates that the coupling between the two joints is compliant, such as those hands with joints made of springs. A ":^:" between two joints indicates that the coupling between the two joints is based on a mechanism that allows for decoupling. The BarrettHand [20], for example, achieves this effect by means of a "TorqueSwitch"

differential gear mechanism that actively decouples the two joints once contact has been made on the inner link and a preset torque limit has been reached. A ";" between joints indicates that the coupling is fixed-motion, and therefore has no adaptability.

The next column indicates the coupling ratio (prox:med:dist) between the joints. For a finger with some method of adaptability, this ratio is the relative angular motion between joints when the finger is freely actuated (i.e. no external contact). For Hirose's "Soft Gripper" [27], every third value is given. The final column indicates the method by which the hand is passively compliant and/or adaptive, if at all.

Note that every one of these hands has some coupling scheme, yet few of the designers give any systematic justification for the choice. Notable exceptions are the 100G hand [19] and the Laval 10-DOF hand [28].

A number of insights can be gleaned from this survey. Six of the anthropomorphic hands (which, in general, have three or four fingers and an opposing thumb) employ fixed-motion (non-adaptive) coupling, and most often between the medial and distal joints of the fingers (presumably mimicking the human hand). However, the coupling between the medial and distal joints in human fingers (PIP and DIP joints) is adaptive and not fixed-motion. Interestingly, of the hands surveyed, fixed-motion coupling is only employed in anthropomorphic hands, even though this type of coupling does not exist in the human hand. The other 13 hands (3 anthropomorphic) employ adaptability in the finger structure, indicating a widespread interest in the value of this property in grasping and/or manipulation.

Anthropomorphic hands are generally intended to be dexterous, yet as reflected in this survey, many have little or no adaptabililty. However, it is not clear that fixed control

of each joint is necessary or even desirable to perform dexterous tasks. When actuation configuration and/or lack of sensing preclude the use of force or stiffness control, an adaptive mechanism with passive stiffness can help ensure contact while an object is actively perturbed by another finger.

1.4. Robustness

A gripper for unstructured environments needs to be robust in two ways: it needs to be able to reliably grasp objects in the presence of large sensory uncertainty or errors, and it needs to be able to withstand large impact and other forces due to the unintended contact likely to occur due to this uncertainty. Underactuation can lead to adaptive behavior that allows for large positioning errors and compliance can enhance both the adaptability and robustness of robot grippers by allowing passive deflection of robot joints. However, traditional approaches to the fabrication of robot hands make them unsuitable for withstanding large forces due to unintended contact.

Designing durable robots, although rarely addressed in robotics research, is essential in industrial, space, and military applications. Examples include iRobot's "PackBot" [40], University of Minnesota's "Scout" family of launchable robots [41], and MIT manipulator arms for the NASA/JPL Pathfinder and Surveyor Mars missions [42]. However, robustness has become a limiting factor in experimental development of multifingered robot hands: the expense and fragility of these hands precludes casual experimentation, restricting the type of experimental tasks that can be reasonably attempted and slowing implementation due to the need for careful validation of programs.

The unintended contact that is likely to occur in unstructured environments can also happen in laboratory experiments, particularly in the debugging phase. Researchers are often reluctant to risk crashes with expensive multi-degree-of-freedom robot hands, so implementations must be carefully validated and experimental scope must be limited. In research, the durability associated with a robust robot hand would expand the type of experimental tasks that can be reasonably attempted and speed implementation due to the reduced need for careful validation of programs.

1.5. Thesis Overview

The overall strategy taken in this dissertation is to address these issues as a design problem. The first two of the remaining chapters of this dissertation describe optimization studies used to investigate the effects of variations in mechanical design parameters on the performance of a robot hand operating in unstructured environments. In the first (Chapter 2), I examine the role of various grasper compliance schemes and kinematic configurations (preshape). A simplified grasper consisting of a pair of two-link planar fingers with compliant revolute joints was simulated as it passively deflected during contact with a target object. The kinematic configuration and joint stiffness values of the grasper were varied in order to find the design parameters that maximize successful grasp range and minimize contact forces for a wide range of target object size. The second chapter (Chapter 3) examines the effects of variations in joint coupling schemes in adaptive, underactuated robotic grippers. The joint coupling configuration of the same simplified gripper was varied in order to again maximize successful grasp range and minimize contact forces for a wide range of target object size and position. The number

of actuators was also varied in order to test the performance of the gripper for varying degrees of underactuation. In order to model the sensing uncertainty inherent in unstructured grasping tasks, a normal distribution of object position was assumed and the results weighted accordingly.

In the second section of this thesis, the design, construction, and evaluation of the components of a robust robot hand are described. Chapter 4 introduces an emerging layered-manufacturing technique called polymer-based Shape Deposition Manufacturing (SDM) ([43] and [44]) which was used to create the prototype hands. I then describe the construction and evaluation of robot fingers with the functionality of conventional metal prototypes but with robustness properties that allow for uncertainty in object location and large impact forces. Chapter 5 presents the design and evaluation of a number of novel sensors created using the SDM technique which will add to the functionality of our robot hands. These include Hall-effect sensors for joint angle sensing, embedded strain gauges for force measurements, optical reflectance sensors for tactile sensing, and piezoelectric polymers for contact detection. Chapter 6 then describes the design and evaluation of two novel hands built using SDM. The first is a two-fingered hand developed primarily as a proof-of-concept model to test the results of the preshape and stiffness optimization study in Chapter 2 as well as to begin to investigate the use of SDM in the construction of robot hands. The second hand, a four-fingered model driven by a single actuator, was developed to provide a capstone to all of the previous design and fabrication investigations. This hand, using extremely simple positioning and control schemes, can grasp objects spanning a wide range of size, shape, and mass under a great deal of uncertainty while demonstrating superior robustness.

In the final section of the document (Chapter 7), two experiments using the four-fingered hand presented in Chapter 6 are presented. In the first, I evaluate the amount of allowable positioning error in the grasping task that results in a successful grasp. In the second experiment, I autonomously grasp a wide range of spherical objects positioned randomly across the workspace, guided using only a single image from an overhead camera, with feed-forward control of the manipulator and hand. Chapter 8 provides a summary of the entire work and discusses implications and limitations of the results as well as directions for future work.

Chapter 2

Compliance and Configuration Optimization

In this chapter, I explore the role of compliance and kinematic configuration in grasping in unstructured environments, where errors in sensing mean that object size and location uncertainty can span a wide range. In contrast to manipulators for unstructured environments that rely on active control for compliance [12], [42], I am interested in passive joint compliance that results in large joint deflections and low contact forces, thus minimizing disturbance or damage to objects during the first phases of acquisition. In particular, I examine the performance of a two-fingered gripper as joint compliance and configuration are varied. This simple configuration allows detailed analysis of parametric trade-offs, which is difficult for complex anthropomorphic hands (e.g. [45] and [46]). Performance is compared on the basis of the maximum range of object size and location that can be successfully grasped and the magnitude of contact forces. The results are analyzed to determine the ways that compliance and kinematic configuration contribute to grasping performance without the need for extensive sensing.

2.1 Methods

The general problem of manipulation in unstructured environments is, by its very nature, so broad that assumptions are required to limit the scope of the problem to a tractable size. I thus select for this initial study a simple gripper with two fingers, each with two revolute degrees of freedom (Figure 2.1). This gripper is perhaps the simplest configuration that is able to grasp a wide range of objects [27]. I assume that the links are rigid lines between joints and that each joint of the gripper includes a passive linear spring in series with an actuator. Our goal is then to determine how variations in the joint stiffnesses and initial rest angles affect the ability to grasp objects. For this purpose, I must define the scenario in which the grasper will operate and determine its grasping ability by simulating the grasping process for a range of object sizes and locations.

2.1.1 Grasping Scenario

The basic grasping process follows a simple scenario. I assume that sensing (e.g. vision) provides rudimentary information about the target object location, and that the

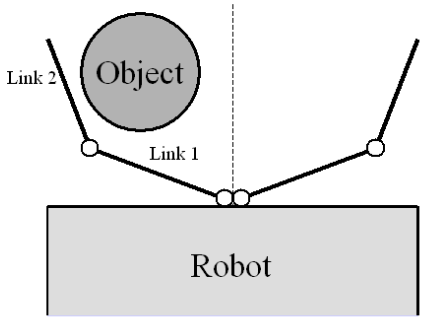

Figure 2.1. A grasper mounted on a robot vehicle approaching an object to be grasped. The grasper consists of two fingers, each a 2 degree of freedom planar manipulator with revolute joints.

robot arm or vehicle moves straight towards this location. As the robot advances, the grasper comes into contact with an object with unknown properties and location. This results in contact forces, which deflect the grasper due to its passive compliance. If the grasp is successful, the forward motion and joint deflection continues until one finger makes two-point contact with the object as described below. At this point the joint actuators can be activated and both fingers brought into contact with the object. This study investigates the behavior of the compliant grasper before actuation and so the details of the actuation scheme need not be specified.

To evaluate the potential of each grasper configuration to successfully grasp objects, I must define a "successful grasp." In an unstructured environment, the mechanical properties of the target object (particularly mass, frictional properties, and detailed shape) are uncertain, making it difficult to predict the precise finger configuration and grasp force necessary to secure the object. To maximize grasp robustness, I require an enveloping grasp [47], [48], in which the object is physically constrained by the grasper regardless of friction and contact between the fingers and object is maintained for infinitesimal displacements in all directions in the plane. For this simple grasper, this equates to three- or four-point contact enclosing greater than 180 degrees along the object's surface. Therefore, at least one grasper finger must have two-point contact with the object. The possibility of achieving two-point contact on one grasper finger such that an enveloping grasp can be achieved is therefore the criterion by which a successful grasp configuration is judged in this analysis (Figure 2.2).

In order to simplify the analysis and simulation, I ignore inertial effects and assume quasi-static conditions. To simplify the geometrical calculations, the links were

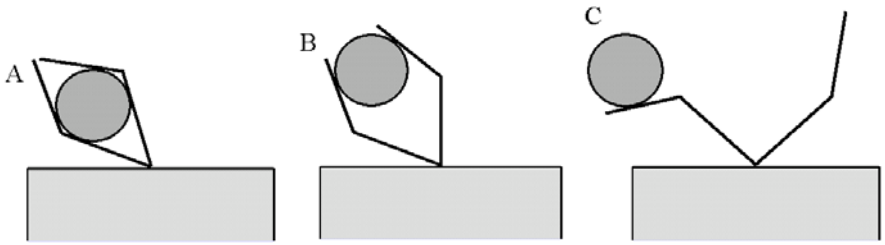

Figure 2.2. Examples of (A) successful enveloping grasp, (B) non-enveloping grasp, and (C) unsuccessful grasp.

assumed to be simple lines through the joint axes. The object to be grasped was assumed to be circular (a frequent assumption in the grasping literature [49], [50] and a reasonable approximation for many objects), and sufficiently massive such that the contact forces with the gripper do not displace or rotate it.

2.1.2 Grasp Analysis

Within this grasping scenario, I can examine the role of compliance and link configuration through simulation of the grasping process. I begin by analyzing the deflection of the grasper due to contact with the object as the robot advances. Three cases of object contact on a finger are possible. The first case is object contact with the tip of the grasper. In the presence of friction, the tip will stick until static friction is overcome as the robot moves forward, begins to roll and slide, and possibly transitions to contact along the length of link 2 (the second case described below). A successful grasp will not often be achieved in this case. The second case is initial contact along the length of link 2 (pictured in Figure 2.3). In this case the robot must continue moving forward, causing the object to roll and slide along the length of link 2, until a successful grasp can be achieved,

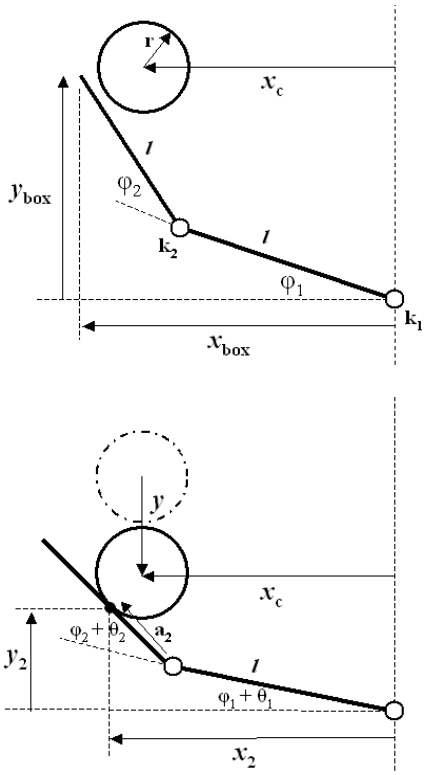

Figure 2.3. The manipulator before contact with the object (top) and after contact and deflection (bottom)

if at all. The third and simplest is contact on link 1. In this case, joint 2 can often be immediately actuated to achieve two-point contact and successfully grasp the object.

Except for cases of tip contact, contact with the object gives a unique solution for an object of a given radius at a given position. To arrive at this solution, the inverse kinematics of the mechanism must be solved, along with a torque balance for each joint and equations describing the geometry of the grasper and object. Table 2.1 gives the parameters used to describe the grasper/object configuration and their definitions.

TABLE 2.1
NOMENCLATURE

parameter	*definition*
φ_1, φ_2	spring rest link angles
θ_1, θ_2	angular deflections from φ_1 and φ_2
k_1, k_2	joint stiffness values
k_T	total stiffness (k_1,k_2/ k_1+k_2)
x_{box}, y_{box}	bounding box of the undeflected mechanism in the x and y directions
x_0,y_0 x_1,y_1 x_2,y_2	coordinates of the initial contact point and the contact points on each of the two links
x_c	distance from the center of the circle to the centerline of the grasper
r	object radius
y	distance the manipulator has traveled since first contact with the object
l	grasper link length
a_2	distance from joint 2 to contact point on link 2
α	angle between radius normal to the finger and the approach direction.
f_R	resultant contact force = $\sqrt{f_T^2 + f_N^2}$
f_T	contact force tangential to the link surface
f_N	contact force normal to the link surface
μ_s, μ_k	coefficients of static and kinetic friction

2.1.2.1 Contact at the tip of link 2

Two sets of equations are needed to describe this case. The first set describes tip contact with static friction; assuming Coulomb friction, $f_T \leq \mu_s f_N$. Since the tip "sticks" to the object at the point of initial contact as described above, the closed-form solution to the joint angles is

$$\theta_2 = \gamma - \varphi_2 \tag{2.1}$$

$$\theta_1 = \cos^{-1}\left(\frac{x_2}{2l\cos[\gamma/2]}\right) - \frac{\gamma}{2} - \varphi_1$$

$$\text{where} \qquad \gamma = \cos^{-1}\left(\frac{x_2^2 + y_2^2}{2l^2} - 1\right).$$

If the applied forces overcome static friction so $f_T > \mu_s f_N$, dynamic or sliding frictional tip contact occurs. I can then calculate the coordinates of the changing point of contact

$$x_2 = r\sin\alpha + x_c \tag{2.2}$$

$$y_2 = y_0 - y + \sqrt{r^2 - (x_0 - x_c)^2} - r\cos\alpha$$

The changing contact point can also be calculated using the forward kinematics of the grasper

$$x_2 = l\cos(\varphi_1 + \theta_1) + l\cos(\varphi_1 + \varphi_2 + \theta_1 + \theta_2) \tag{2.3}$$

$$y_2 = l\sin(\varphi_1 + \theta_1) + l\sin(\varphi_1 + \varphi_2 + \theta_1 + \theta_2)$$

For this contact scenario kinetic friction applies, so

$$f_T = \mu_k f_N. \tag{2.4}$$

And finally, the torque balance of the two joints yields

$$\begin{aligned} \frac{-k_2\theta_2}{f_N l} &= \cos[\varphi_1 + \varphi_2 + \theta_1 + \theta_2 + \sin^{-1}(\frac{x_2 - x_c}{r})] \\ &\quad -\mu_k \cos[\frac{\pi}{2} - \varphi_1 - \varphi_2 - \theta_1 - \theta_2 - \sin^{-1}(\frac{x_2 - x_c}{r})] \end{aligned} \tag{2.5}$$

$$\begin{aligned} \frac{-k_1\theta_1}{f_N\sqrt{x_2^2 + y_2^2}} &= \cos[\frac{\pi}{2} - \tan^{-1}(\frac{x_2}{y_2}) - \sin^{-1}(\frac{x_2 - x_c}{r})] \\ &\quad -\mu_k \cos[\tan^{-1}(\frac{x_2}{y_2}) + \sin^{-1}(\frac{x_2 - x_c}{r})] \end{aligned} \quad .$$

The coordinates of the initial point of contact, x_0 and y_0, are calculated using Eq. (2.3) with θ_1 and θ_2 =0. The entire set of equations (2.1) - (2.5) can be solved simultaneously to find θ_1 and θ_2 as a function of y, the object position in the approach

direction. In certain configurations, sliding tip contact can transition to contact along the length of link 2 as described below.

Two analogous sets of equations are similarly derived to describe contact along the length of link 2 and contact on link 1 (closest to the base). Each case is based on the kinematics and torque balance relationships, with kinetic friction.

2.1.3 Simulation

In the absence of a closed-form solution to the foregoing sets of coupled nonlinear equations, a numerical method was used to solve for the deflection behavior of the mechanism in the different contact states. The grasping scenario was simulated for a wide range of grasper parameter values, measuring the successful grasp range and recording contact forces across object locations within that range.

The algorithm, implemented in Matlab (The Mathworks, Natick, MA), found the passive deflection of the mechanism for incremented values of y (the robot travel) until two-point contact was established with the object, if it occurred at all. A constraint was imposed on the travel of the fingers such that they do not deflect past the line horizontal from the base joint (i.e. $\varphi_1+\theta_1 = 0$). Deflection past this line can be thought of as the fingers or object hitting the face of the robot structure.

If two-point contact occurs for a certain configuration, the program checks the locations of the contact points to verify that the grasp would enclose the object, allowing an enveloping grasp to be attained. Due to symmetry, if the other finger is actuated at the two-point contact configuration, the object will be in four-point contact with the grasper. An enveloping grasp occurs when these four points of contact enclose greater than 180

degrees of the object surface. It is also assumed that the fingers will not interfere with each other, as is the case if they are slightly offset in the out-of-plane direction.

The simulation was used to investigate the performance across the space of design parameters. For the grasp range evaluation, the joint stiffnesses were used as a ratio, since the individual magnitudes only affect the magnitude of the applied force and not the deflection behavior of the mechanism. For the contact force evaluation, the forces were normalized by the length term and the total stiffness, defined as

$$k_T = \frac{k_1 k_2}{k_1 + k_2} \tag{2.6}$$

The static and kinetic friction coefficients were set equal to further reduce the dimension of the parameter space.

Due to the geometric constraints, only three of the five geometric parameters (φ_1, φ_2, l, x_{box}, y_{box}) can be chosen independently, as well as the ratio of k_1/k_2 and the coefficient of friction, μ. The object parameters x_c and r are varied since the scenario is to grasp an unfamiliar object at an unknown location.

Two categories of model parameterization were simulated. In the first, distances were normalized by l, the link length. This normalization can be thought of as comparison of graspers of equal link length, allowing the grasper to take any shape. In this simulation, φ_1 and φ_2 were chosen to be the geometric parameters varied. These angles were varied from 0 to 90 degrees at 5-degree increments.

In the second parameterization, the lengths were normalized by x_{box} (the width of the half-grasper before contact), which is an indication of the size of the grasper, regardless of configuration. In this simulation, φ_1 and y_{box}/x_{box} were chosen to be the

geometric parameters varied. The rest angle for joint 1, φ_1, was varied from 0 to 90 degrees at 5 degree increments and y_{box}/x_{box} was tested between 0.5 and 3 at 0.125 increments. For both cases, the ratio k_1/k_2 was tested at values {0.1, 1, 10}. The coefficient of friction was tested at μ=2, based on previous studies that suggest high friction increases grasp stability ([51] and [52]).

The performance of each mechanism configuration was evaluated for normalized object radius, r/l or r/x_{box}={0.1, 0.5, 0.9} and object location, x_c/l or x_c/x_{box}, incremented by 0.01 from the center toward the outside of the grasping range. The maximum normalized distance of the object from the centerline for which a successful grasp was attained was recorded for each configuration. This value represents the successful grasp range. The largest contact force applied to the object during the grasping process was also recorded for each tested value of object location, x_c. This information was used to calculate the average maximum contact force over the grasp range for each grasper configuration tested.

2.1.4 Experimental Apparatus and Procedure

In order to experimentally validate the results of the simulation, I built a prototype grasper with the same kinematics as the simulated mechanism (Figure 2.4). Each link consisted of an aluminum bar 2.54 cm wide and 1.27 cm thick, with 12.7 cm between joint axes. Optical encoders with 1200 counts/revolution allow measurement of joint angle and testing for object enclosure. Interchangeable metal torsional springs are mounted in each joint to provide passive compliance; stiffness values used in these experiments are 0.18 - 4.5 mN-m/deg.

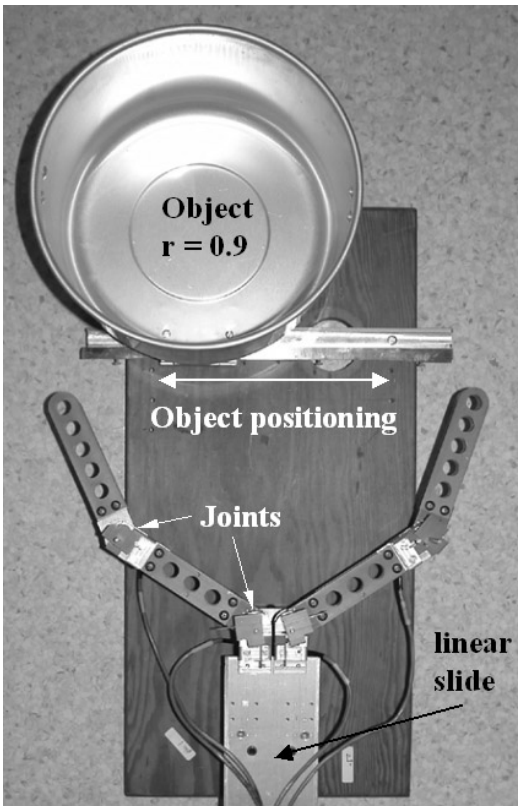

Figure 2.4. The experimental grasper mounted on a linear slide approaching an object to be grasped. The grasper consists of two fingers, each a 2 degree of freedom planar manipulator with compliant revolute joints.

The grasper is mounted on a low-friction linear slide so that it can be pushed against the target object, which can be securely positioned in the lateral direction. The objects were metal cylinders chosen to reflect the sizes studied in the simulation, and were mounted on a multi-axis force/torque sensor (Nano 43, ATI Industrial Automation, Apex, NC; resolution 1/64 N) to record the contact forces in the plane.

The grasping scenario studied in the simulation was repeated to determine the successful grasp space and contact forces of this grasper for the chosen target objects. The grasper was pushed forward by hand on the linear slide until an enveloping grasp

was attained, based on the information from the measured joint angles and the object position. Force was determined as the average of five samples after the successful grasp configuration was attained, and was averaged over five trials.

2.2 Results

2.2.1 Simulation Results

2.2.1.1 Link length normalization

Figure 2.5 shows the results of the simulation with the length terms normalized by the link length l, which preserves link lengths but allows grasper width to vary across configurations. The nine plots represent combinations of three object radii and three stiffness ratios. For each plot, the axes are the rest angle for link 1 (φ_1) and link 2 (φ_2). The contours correspond to the values of $(x_c)_{max}$ (i..e. the successful grasp range) for each rest angle configuration, normalized by the link length.

Comparison of the plots across each row shows that increasing the stiffness ratio (k_1/k_2) does not affect the maximum value of the successful grasp range, $(x_c)_{max}$. Varying stiffness ratio does, however, affect the size of the optimum region for larger radius objects, as shown in the bottom two rows. In particular, a broader range of values for φ_1 produce the maximum grasp range if the distal joint is stiffer than the base joint (i.e. $k_1<k_2$).

Comparing within the columns of Figure 2.5, the optimum configuration space changes slightly with object radius, becoming smaller and moving toward increasing φ_2 for increasing object radius. Variation around these values is not large, however. For example, for r/l=0.9, the contour directly below the maximum value ($(x_c)_{max}/l$=0.40) is

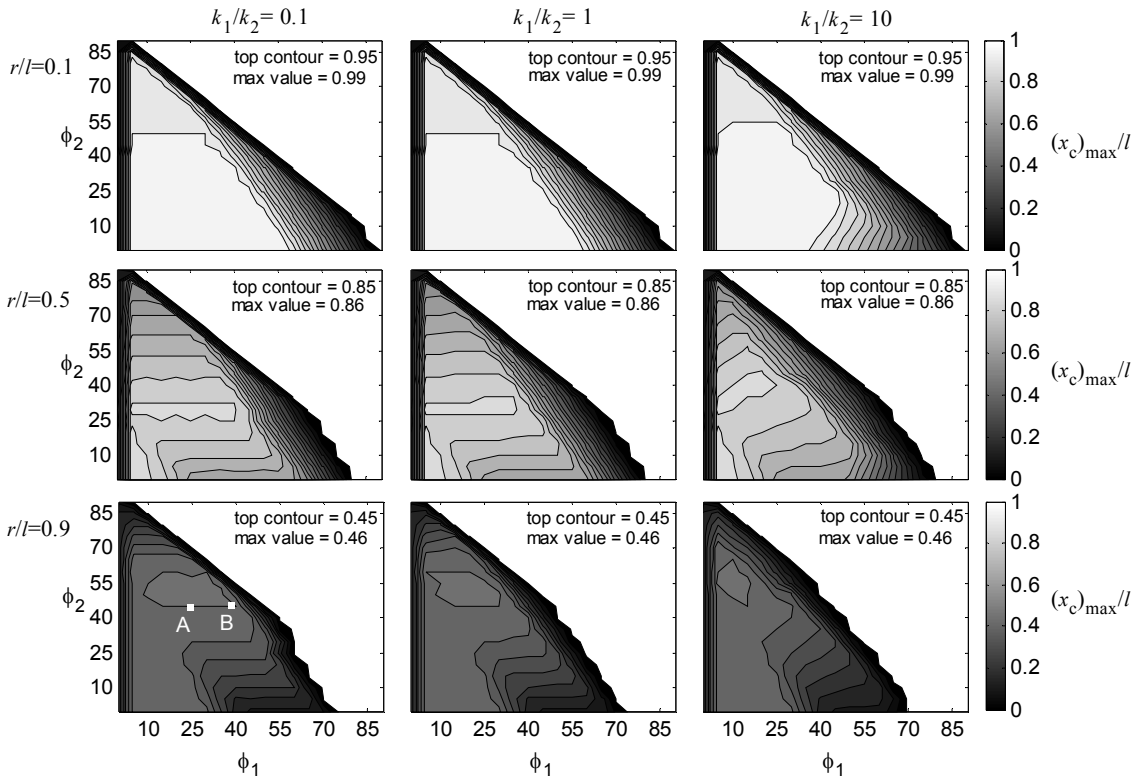

Figure 2.5. Successful grasp range ($(x_c)_{max}$) for link length normalization. Contours are in increments of 0.05. The joint rest angles φ_1 and φ_2 are in degrees. Lighter colors (higher contours) represent larger successful grasp ranges and thus better parameter configurations.

only 11% lower but contains a much larger region. Note that the different combinations of φ_1 and φ_2 have different grasper widths; x_{box} decreases as φ_1 or φ_2 increases.

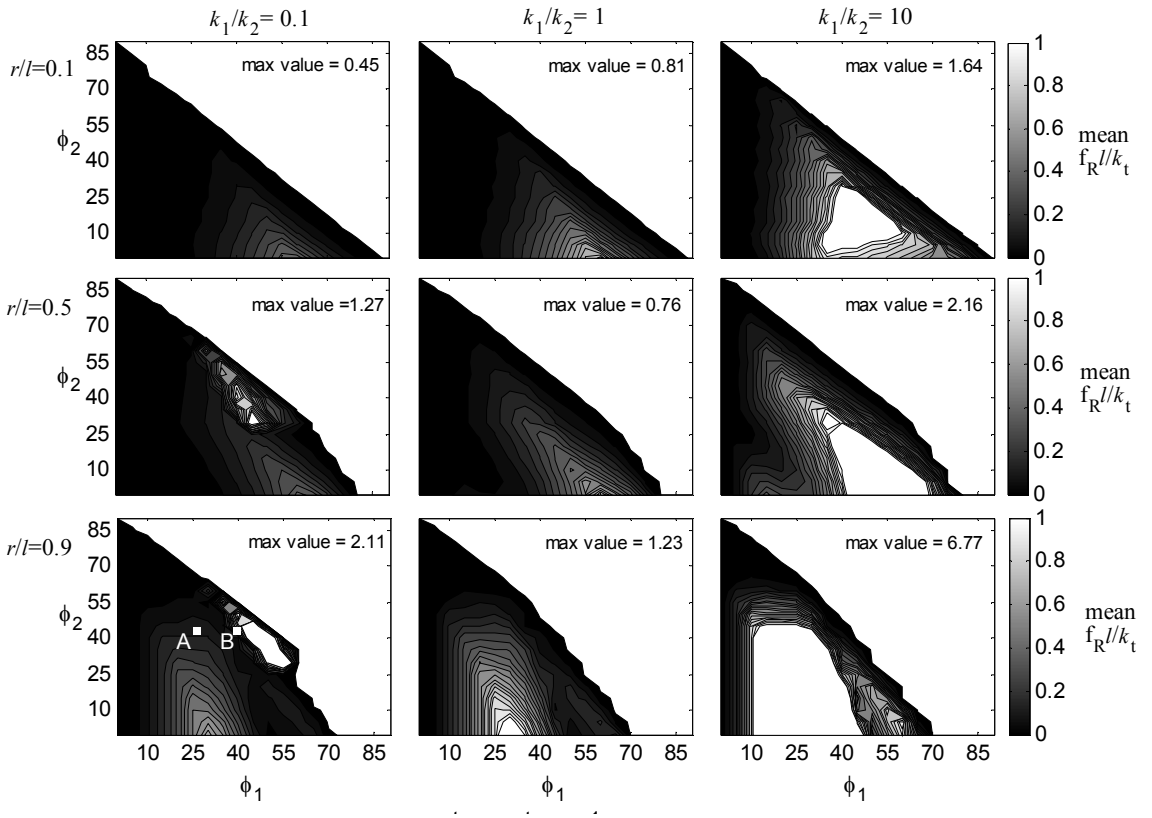

Figure 2.6. Average normalized force ($f_R l/k_T$) for link length normalization. Contours are in increments of 0.05 with peak at 1.00. The joint rest angles φ_1 and φ_2 are in degrees. Darker colors (lower contours) represent lower forces and thus better parameter configurations.

Figure 2.6 shows the results of the force investigation with the length terms normalized by the link length, *l*. The contours correspond to the values of the average normalized force (mean $f_R l/k_T$) for each rest angle configuration. The average resultant force, mean f_R, is the maximum contact force for each object position averaged over the entire successful grasp range.

The largest contact force values in the column of plots for which k_1/k_2=0.1 correspond to the grasper making tip contact with the object during initial contact. In these configurations, large joint deflections occur before the tip begins to roll and slide

along the surface of the object. In the plots corresponding to r/l=0.9, k_1/k_2=1 and k_1/k_2=10, the peak values occur at configurations where the object makes first contact on link 1. In these configurations, the robot must continue moving forward after initial contact in order to reach a configuration enabling an enveloping grasp, resulting in large deflections of joint 1. For the rest of the plots, the maxima simply occur at configurations where initial contact is on link 2 and there are large deflections of joint 1 before two-point contact.

A comparison of Figures 2.5 and 2.6 show that the configurations with the largest successful grasp range also exhibit low average contact force. Also note that in Figure 2.6, the plots appear to be most similar within a column (same stiffness ratio) than within a row (same object size ratio). This result is in contrast to that of the grasp range investigation (Figure 2.4), which shows similar results within object radius. Thus, stiffness is an important determinant of contact force, whereas object size largely affects successful grasp range.

2.2.1.2 Grasper width normalization

Figure 2.7 shows the results of the grasp range investigation with the length terms normalized by the grasper width, x_{box}, which preserves the width of the grasper across configurations. The axes are the rest angle for link 1 (φ_1) and the bounding box height (y_{box}/x_{box}). The contours correspond to the values of the successful grasp range, $(x_c)_{max}/x_{box}$ for each rest angle configuration. The scalloped edges are due to the finite sampling of the parameter space. The attenuation at the bottom of the plots for r/x_{box}=0.9 is due to inadequate link length to achieve an enveloping grasp for large objects in those configurations.

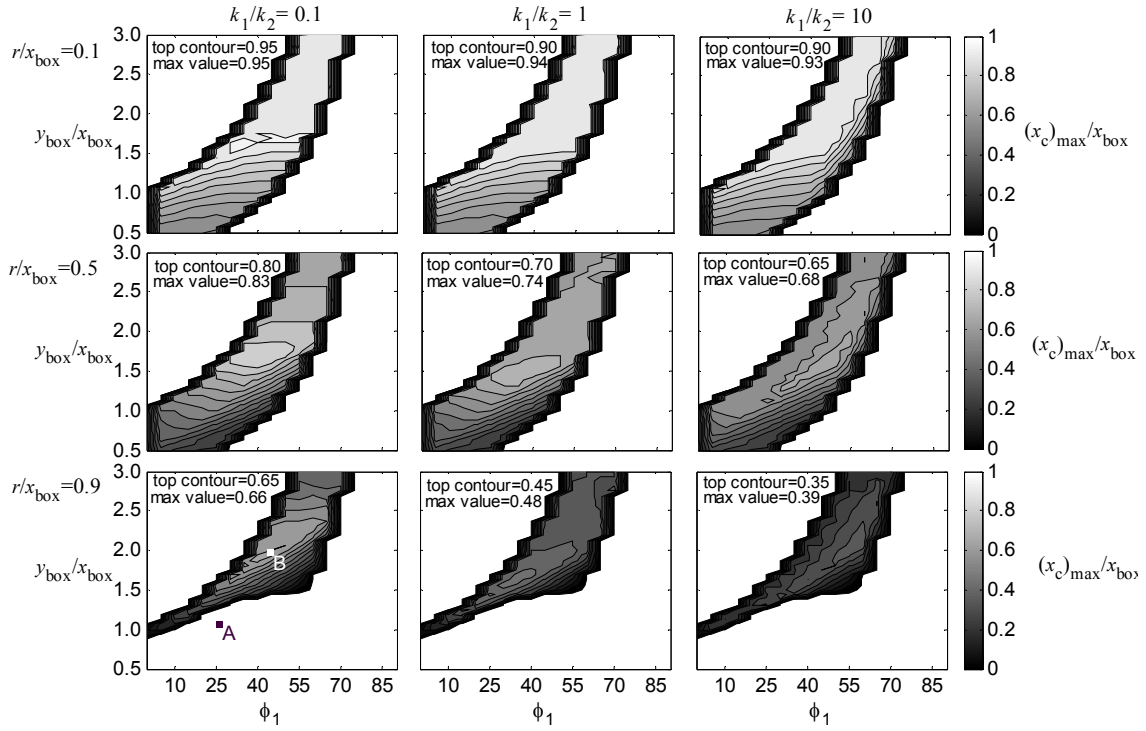

Figure 2.7. Successful grasp range ($(x_c)_{max}$) for grasper width normalization. Contours are in increments of 0.05. The joint rest angles φ_1 and φ_2 are in degrees.

It is clear from the figure that increasing the stiffness ratio (k_1/k_2) decreases the successful grasp range, most significantly for larger objects. This suggests that the intermediate joint should be stiffer than the base joint.

Note that the different combinations of y_{box}/x_{box} and φ_1 have different link lengths. In particular, as φ_1 increases, l decreases for a given y_{box}/x_{box}, and as y_{box}/x_{box} increases, l increases for a given φ_1. The changing link length is a significant factor in the performance of a given grasper configuration using this geometric scheme.

Figure 2.8 shows the results of the force investigation with the length terms normalized by the grasper width, x_{box}. The contours correspond to the values of the

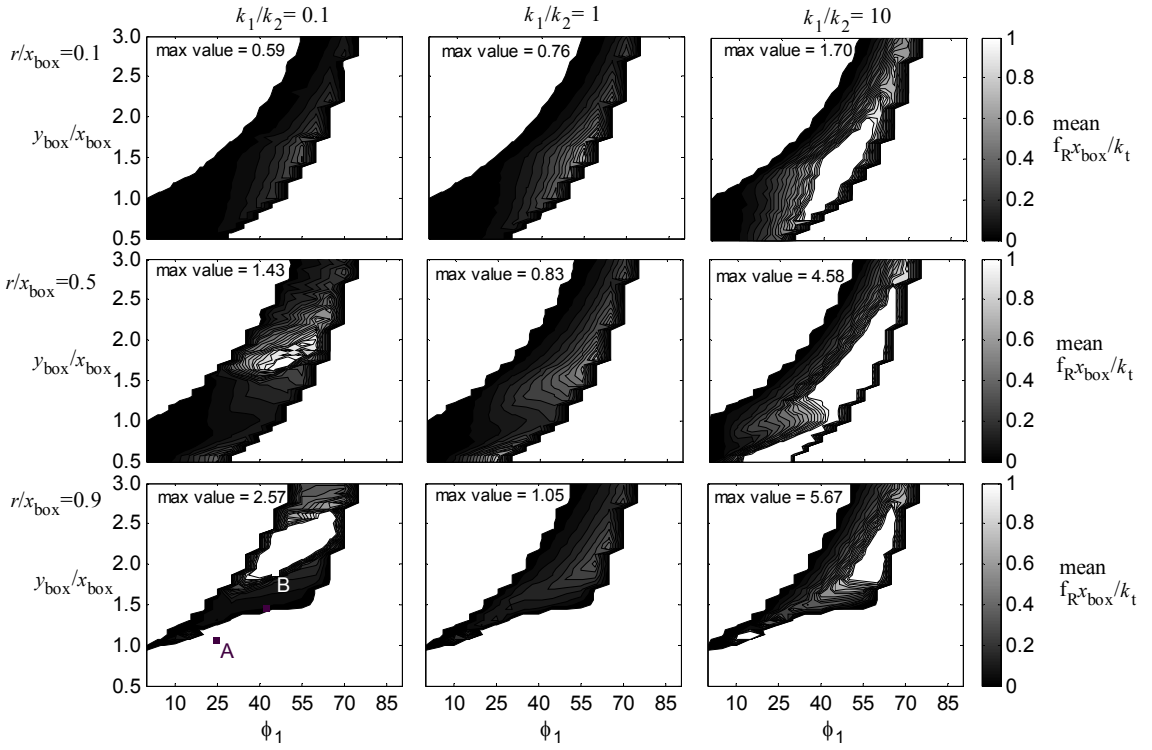

Figure 2.8. Average normalized force ($f_R x_{box}/k_T$) for grasper width normalization. Contours are in increments of 0.05. The joint rest angles φ_1 and φ_2 are in degrees.

average normalized force ($f_R x_{box}/k_T$) for each rest angle configuration. The largest contact force values in the column of plots for which k_1/k_2=0.1 correspond to the grasper making tip contact with the object during initial contact. In these configurations, large joint deflections occur before the tip begins to roll and slide along the surface of the object. In the plots corresponding to k_1/k_2=10, the peak values largely occur at configurations where the object makes first contact on link 2 and large joint deflections occur before two-point contact is made.

Although not presented in detail here, a simulation was carried out to investigate how coefficient of friction affects the successful grasp range. Friction within the range

$0.1 \geq \mu \geq 2.0$ does not affect the maximum successful grasp range, but does slightly change the kinematic configuration of the optimum. This lends weight to preferring a large coefficient of friction to increase stability during the grasping phase ([51] and [52]).

2.2.2 Experimental Results

Figure 2.9 shows the successful grasp range of the experimental grasper and the analogous simulation results. The grasper configuration was tested at joint angle increments of 15 deg. varied from 0 to 90 degrees. The simulation plots were resampled at this resolution for comparison. The grasp range was tested for r/l=0.5 and r/l=0.9, with stiffness ratios k_1/k_2=0.1 and k_1/k_2=10. Overall shape and peak values of the experimental grasp range show good agreement with the simulation. For the corresponding to around φ_1=60 deg and φ_2=15 deg, the fall off seen on the simulation results is due to the tip sticking until the deflection limit of the grasper is hit. However, in the experimental results, this fall off is not seen, but can be attributed to a much lower coefficient of friction, allowing the tip to slip before the limit is reached.

The experimental results for contact force are shown in Figure 2.10. The contours correspond to the values of the average normalized force (mean $f_R l/k_T$) for each rest angle configuration, tested at the same increments as the grasp range investigation. A plot of the simulation results for the comparable case are also shown for comparison. Note that the contour intervals for the two plots are different for better resolution. The overall shape of the experimental and simulation plots are closely similar, although the magnitudes differ by over an order of magnitude. This is due in large part to the normalization scheme used to nondimensionalize the force measure, as discussed below.

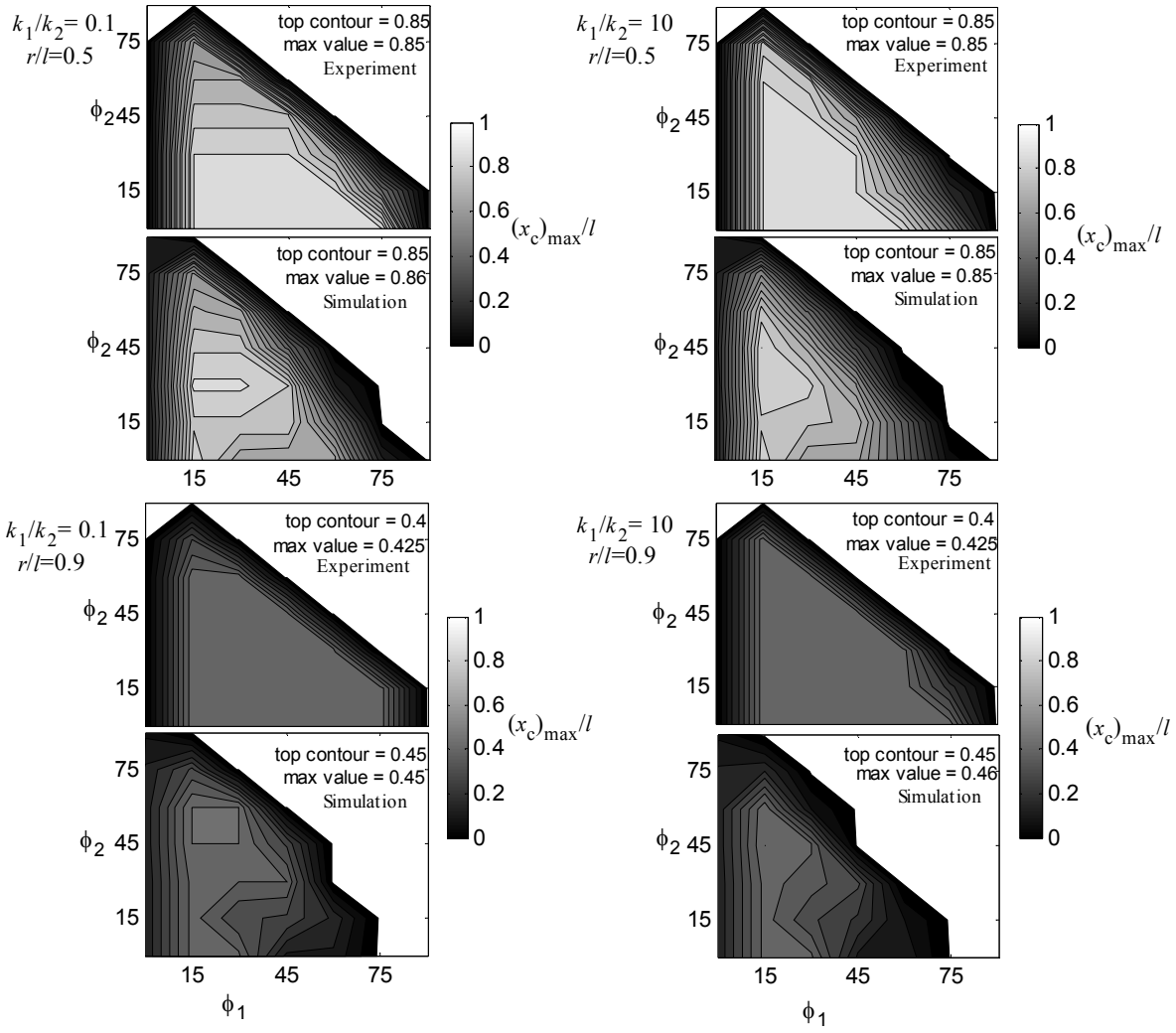

Figure 2.9. Comparison of successful grasp range from experiment and simulation. Contours are in increments of 0.05. The joint rest angles φ_1 and φ_2 are in degrees.

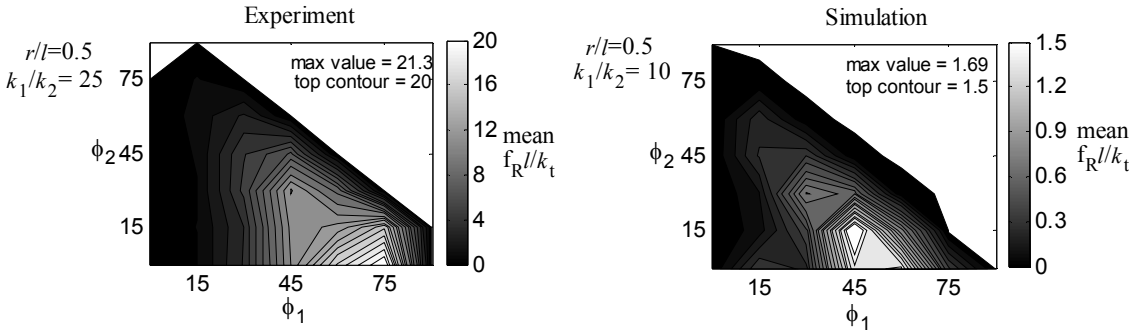

Figure 2.10. Comparison of force results from experiment (left) and simulation (right). Note that the colorbars for the two plots have different scales to better show the resolution of the two results. The joint rest angles φ_1 and φ_2 are in degrees.

2.3 Discussion

This is, to my knowledge, the first study to quantify the ability of passive stiffness to enhance grasper performance, particularly in terms of successful grasp range and applied force. The optimum configurations allow the links to conform to large objects, permitting an enveloping grasp that is not possible for other link configurations and joint stiffness ratios when the object is far from the centerline.

The results presented above consider the behavior of the grasper for a wide range of object size with respect to grasper size. However, these results are most pertinent for the large object radius cases, as performance is largely unaffected by the configuration or stiffness parameters for the smallest objects (top row of Figures 2.5-2.8). In addition, if the object size range is known, a design goal may be to find the smallest grasper that can acquire these objects, or equivalently, it is often desired to maximize the size of object that can be acquired for a gripper of a given size. In this case, the results for the large object (bottom row of Figures 2.5-2.8) are the most important. However, the larger the grasper with respect to the target object, the larger the allowable positioning error, which may be more important in some contexts.

The magnitude of the individual joint stiffness values are directly related to the force applied to the object (i.e. lower absolute stiffness will result in lower applied forces). In order to avoid damaging or disturbing the target object, these values should be kept low. However, to avoid undesired resonant behavior, grasper dynamics must be taken into account when choosing these parameters.

2.3.1 Within Parameterizations

For the link length normalization results, the grasp range is particularly sensitive to variations in the distal joint rest angle, φ_2, while variations in φ_1 are not as significant for small values of the stiffness ratio k_1/k_2. The stiffness ratio of the joints, k_1/k_2, does not affect the maximum successful grasp range that can be achieved. However, it does affect the size of the "sweet spot," and therefore should be minimized. On the other hand, for the grasper width normalization results, the stiffness ratio of the joints significantly affects the maximum successful grasp range that can be achieved. This optimum configuration corresponds to a link length normalized configuration that is sensitive to changes in stiffness ratio.

The optimum configurations from the contact force investigation largely concur with those from the grasp range investigation, particularly within the link length parameterization study. The configurations showing largest successful grasp range also demonstrated low contact forces. The results of the width parameterization study show slightly different results. These configurations demonstrated large joint deformation due to the tip sticking. However, this type of contact occurs only for a small range of object positions when the object is furthest from the centerline.

For the link length normalization, a near-optimum link configuration across the parameter range studied is around φ_1=25 deg and φ_2=45 deg for a stiffness ratio of k_1/k_2=0.1 (Figure 2.11). This choice is within the optimum range for r/l=0.9 and is slightly off maximum for r/l=0.5. As noted above, φ_1 can vary across about 30 degrees with little effect on the successful grasp range for this best stiffness ratio case. This configuration is represented by the letter 'A' on the bottom left plot of Figures 2.5-2.8.

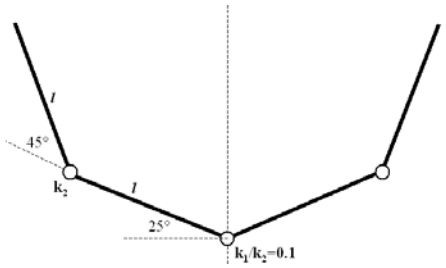

Figure 2.11. Optimum grasper configuration based on normalization by link length.

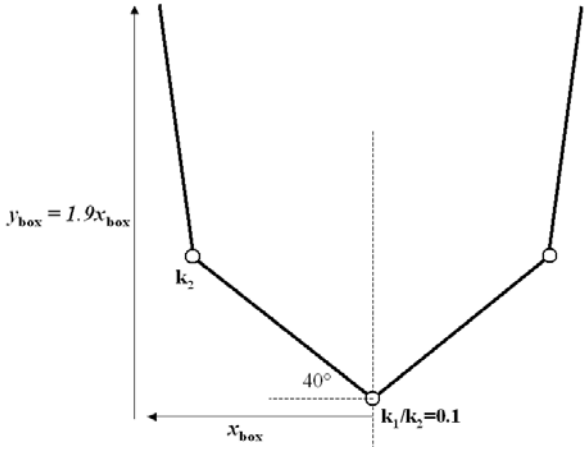

Figure 2.12. Optimum grasper configuration based on normalization by grasper width. The width of this figure has been scaled to approximate that of Figure 2.11.

For the width parameterization, a near-optimum link configuration is around φ_1=40 deg and y_{box}/x_{box}=1.875 (Figure 2.12). However, variation around these values is not large. This configuration is represented by the letter 'B' on the bottom left plot of Figures 2.5-2.8.

I also note that the failure mode for the best configurations in both cases is incomplete enclosure. This lends weight to preferring these values since *force* closure might be achieved in practice, thus successfully grasping the object although outside the bounds of the assumed scenario.

TABLE 2.2
COMPARISON OF OPTIMUM CONFIGURATIONS, BOTH NORMALIZED BY GRASPER WIDTH, x_{box}. (A) AND (B) ARE THE RESULT OF THE LINK LENGTH AND WIDTH PARAMETERIZATIONS, RESPECTIVELY.

	φ_1,φ_2 (deg)	x_{box}/x_{box}, y_{box}/x_{box}	$(x_c)_{max}/x_{box}$			mean $f_R x_{box}/k_t$		
			r/l=0.1	0.5	0.9	r/l=0.1	0.5	0.9
A	25,45	1.00,1.00	0.68	0.50	0.00	0.03	0.06	N/A
B	40,45	1.00,1.88	0.94	0.79	0.66	0.02	0.54	1.36

TABLE 2.3
COMPARISON OF OPTIMUM CONFIGURATIONS, BOTH NORMALIZED BY GRASPER LINK LENGTH, l. (A) AND (B) ARE THE RESULT OF THE LINK LENGTH AND WIDTH PARAMETERIZATIONS, RESPECTIVELY.

	φ_1,φ_2 (deg)	$x_{box}/l, y_{box}/l$	$(x_c)_{max}/l$			mean $f_R l/k_t$		
			r/l=0.1	0.5	0.9	r/l=0.1	0.5	0.9
A	25,45	1.35,1.35	0.96	0.81	0.44	0.03	0.06	0.15
B	40,45	0.90,1.60	0.79	0.66	0.45	0.01	0.89	0.78

2.3.2 Between Parameterizations

Tables 2.2 and 2.3 show a comparison of the two optimum configurations. Table 2.2 shows the successful grasp range and average force when both configurations have equal width. Note the differences in link length and that configuration A (the link-normalized optimum) is unable to grasp the large object (i.e. r/x_{box}=0.9). Table 2.3 shows the two with equal link length. Note the difference in grasper width.

The two tables above quantify the difference in performance between the two grasper shapes for the two normalizations. From Table 2.2, grasper B is clearly a better option than grasper A in terms of successful grasp range, $(x_c)_{max}$, but is slightly larger and exerts larger contact forces. Under this parameterization, configuration A cannot achieve an enveloping grasp on the large object anywhere in the grasp range, as reflected in Figures 2.7 and 2.8.

From Table 2.3, grasper A shows a larger successful grasp range for the large and medium sized objects, and about the same as grasper B for small objects. Contact forces are either the same or lower than B.

The two parameterizations (by l and x_{box}) reflect two different ways of approaching the grasper design analysis. The first, normalization by link length, l, can be thought of as comparison of graspers of equal link length, while allowing the grasper to take any shape. This is useful if the size of the deployed grasper is not critical due to space constraints. In the second, the lengths were normalized by x_{box} (the width of the half-grasper), which constrains the size of the grasper, regardless of configuration. These results are useful in a cluttered or space-restricted environment, where the size of the grasper must be limited.

2.3.3 Comparison to 'Intuitive' Configurations

Figure 2.13 shows some "intuitive" configurations that one might guess to be an appropriate design configuration for a compliant grasper. Table 2.4 shows the performance of these and allows for comparison to the optimum configurations. Note that these results are for equal link-length graspers with stiffness ratio k_1/k_2=0.1.

From Table 2.4, it is clear that many "intuitive" configurations, particularly 'D'-'F', have a substantially smaller successful grasp range, $(x_c)_{max}$, than the optimum configuration, 'A'. However, note that configuration 'C' shows a slightly greater successful grasp range for the smaller objects (r/l=0.1,0.5), and a slightly smaller successful grasp range for large objects (r/l=0.9). This highlights the point that there is a range of effective grasper configurations as shown in the fairly wide plateaus in Figures 2.5-2.8.

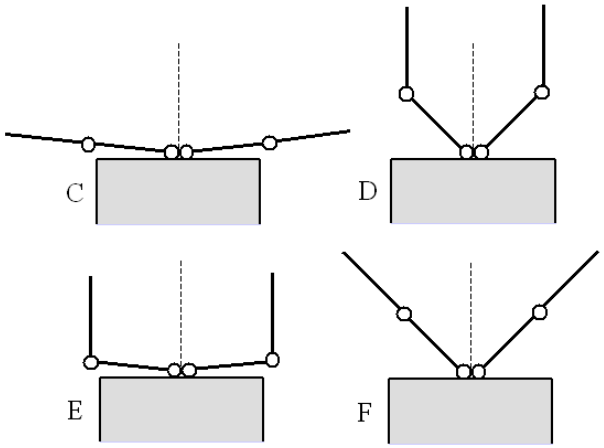

Figure 2.13. "Intuitive" grasper configurations

TABLE 2.4
COMPARISON OF OPTIMUM AND "INTUITIVE" CONFIGURATIONS, NORMALIZED BY LINK LENGTH, l, CORRESPONDING TO FIGS 11-13.

	φ_1,φ_2 (deg)	$x_{box}/l, y_{box}/l$	$(x_c)_{max}/l$			mean $f_R l/k_t$		
			r/l=0.1	0.5	0.9	r/l=0.1	0.5	0.9
A	25,45	1.35,1.35	0.96	0.81	0.44	0.03	0.06	0.15
B	40,45	0.90,1.60	0.79	0.66	0.45	0.01	0.89	0.78
C	5,0	1.95,0.00	0.98	0.86	0.42	0.00	0.00	0.00
D	45,45	0.70,1.70	0.60	0.43	0.29	0.00	0.33	1.56
E	5,85	0.98,1.01	0.89	0.54	0.17	0.00	0.00	0.00
F	45,0	1.40,1.40	0.98	0.66	0.14	0.24	0.13	0.15

The specifics of a particular application must be taken into account when choosing the grasper layout. For example, configuration 'C' does not allow the robot much reaction time to contact with an object before the grasper deflects and hits the robot face. Other potential issues include grasper width, ability to achieve *force*-closure grasps, and range of target object size.

2.3.4 Experimental Validation

The results from the experimental work corroborate the results from the simulation study. The successful grasp range was nearly identical across the range of tested configurations and the differences can be attributed to dissimilar friction between

grasper and object. The contact force evaluation shows that the lower forces were exhibited in the configurations predicted from the simulation. Large differences in the magnitudes of these forces between simulation and experiment are largely due to the normalization scheme used to nondimensionalize the contact force values. The total stiffness defined in Eq. (2.6) endeavors to take into account the stiffness of both joints. However, in many object locations, x_c, the object is not in contact with joint 2, and therefore the deflection of the base joint generates the contact force. This joint had a stiffness value of 4.5 mN-m/deg in the experiments and 174.5 mN-m/deg in the corresponding simulation. Taking this into consideration, the differences in normalized contact force between experiment and simulation are reduced to a maximum factor of three. The relative magnitudes of the experimental forces is consistent with the simulation result that magnitude of the contact force increases with the base/intermediate joint stiffness ratio, giving weight to the conclusion that this ratio should be kept low.

2.3.5 Generalizations

This study was based on a specific grasping scenario, in order to limit the scope of the problem of grasping in an unstructured environment. While a complete understanding of the issues will require exploration of alternative scenarios, these results appear to hold for relaxation of some of the assumptions. For example, sensing and actuation have been treated here in a simplified fashion, with the assumption that once two-point contact is achieved, sensors will detect this condition, the robot will be stopped, and the other gripper finger actuated to form a force closure grasp. In simulation, however, further forward travel of the robot for some distance after two-point contact was achieved did not result in the loss of an enveloping grasp in most cases, thus relaxing the sensing and

actuation requirements. Likewise, preliminary consideration of other object shapes suggests that the optimum configurations also apply to a range of convex objects. A possible direction for future work is expanding the scope of this optimization study to cover a much larger parameter space, including a greater set of object parameters (shape, orientation, mass, etc.) and grasper parameters (number of links, link lengths, etc.), as well as expanding to three dimensions.

One important issue for further investigation is the type of sensing needed. In addition to joint angles sensing, is crude vision enough? Is contact sensing also needed? What is an appropriate actuation scheme incorporating the sensory information? The results presented here consider only the passive deflection of the mechanism (i.e. the "capture" phase) to maximize grasping space and minimize forces. Additional work may reveal ways that passive compliance can contribute to the sensing and actuation processes as well.

Another important assumption was the requirement of an enveloping grasp. This goal is appropriate since the grasping environment is uncertain, but in practice force-closure is sufficient for a stable grasp, and often might be achieved if an enveloping grasp fails. Further work in this area might consider the implications of planning for force-closure instead of an enveloping grasp. The choice of a large value for the coefficient of friction can be debated as well, although informal studies suggest it does not have a large effect on grasp space.

Chapter 3

Joint Coupling and Actuation

There has been little work on understanding design tradeoffs in configuring underactuated hands, with most designs chosen intuitively or anthropomorphically. In this chapter, we examine the role of the joint coupling scheme in grasping in unstructured environments, where poor sensing may mean that object size and location uncertainty may be large. We begin by describing the details of the gripper and grasping scenarios that we are studying. In particular, we examine the performance of a two-fingered compliant underactuated gripper as joint torque ratio and joint compliance are varied. We also examine the role of the number of actuators, contact response time, and target positioning of the hand. Finally, we provide the results of a simulation of the grasping process for a wide range of target object size and position, identifying optimal joint coupling schemes for various levels of sensory information available for the grasping task.

3.1. Methods

In the previous chapter, we examined the optimization of the preshape and joint stiffness of simple two-fingered grippers with passive springs in the joints. This study showed that a particular set of joint stiffnesses and rest angles could accommodate the widest range of range of uncertainty in object size and location. Contact forces were also minimized at approximately the same gripper configuration. In addition to simulation studies, these results were confirmed with experimental tests using a reconfigurable gripper.

Our goal in this chapter is to gain general insight into the advantages and disadvantages of joint coupling and specific actuation configurations. We thus focus on the same simple gripper with two fingers, each with two revolute degrees of freedom (Figure 3.1). This gripper, proposed by Hirose [27], is perhaps the simplest configuration that is able to grasp a wide range of objects. This mechanism is the same as that used in the 100G hand [19], and is similar to the planar, power-grasp configurations of the BarrettHand [20], Domo hand [25], Laval 10-DOF hand [28], Obrero hand [30], SDM hand [34], and SPRING hand [37], among others.

We use a planar analysis and assume that the links are rigid lines between joints and that each joint of the gripper includes a passive torsional spring providing a rotationally compliant joint. Our goal is to determine how variations in the joint coupling scheme and number of actuators affect the ability to grasp objects in the presence of uncertainty. For this purpose, we must define the scenario in which the grasper will operate.

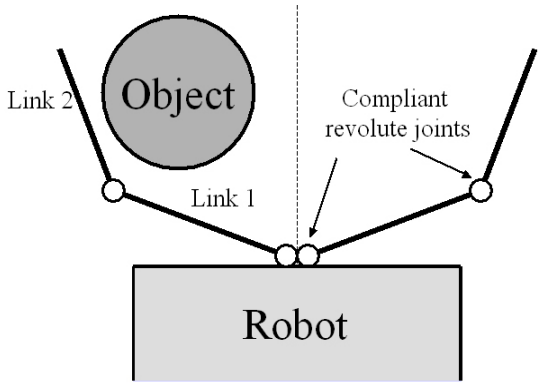

Figure 3.1. A grasper mounted on a robot approaching an object to be grasped. The grasper consists of two fingers, each a two degree of freedom planar manipulator with compliant revolute joints.

3.1.1. Basic Grasping Scenario

The basic grasping process follows a simple scenario. We assume that sensing (e.g. vision) provides rudimentary information about the target object location, and that the robot arm or vehicle moves straight towards this location. As the robot advances, the grasper comes into contact with an object with unknown properties and location. At this point the robot stops its forward progress and the joints of the gripper are actuated to bring both fingers into contact with the object, securing the grasp.

In order to simplify the analysis, we ignore inertial effects and assume quasi-static conditions. To simplify the geometrical calculations, the links were assumed to be simple lines through the joint axes. The object to be grasped was assumed to be circular (a frequent assumption in the grasping literature, and a reasonable approximation for many objects), and sufficiently massive such that the gripper contact forces do not displace or rotate it.

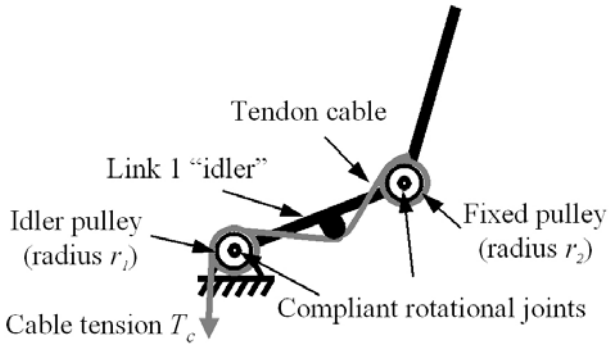

Figure 3.2. Tendon and pulley arrangement for analysis purposes. The tendon is fixed to the distal link.

For the purposes of allowing in-depth analysis of the mechanism, details of the actuation scheme must be specified. While we employed the cable actuation scheme shown in Figure 3.2, this analysis applies to any method of actuation that enforces a constant distal/proximal torque ratio and has compliant joints and fingerpads, as in many underactuated hands (Chapter 1, Table 1.1).

In our scheme, a tendon cable runs over a free-spinning idler pulley at joint 1 (to allow adaptability), over another idler on link 1, and ends at a pulley on joint 2 that is fixed to link 2. Torque is applied about joint 1 via the idler located along the length of link 1, whose position and radius can be set in order to specify the distal/proximal torque ratio, τ_r.

Detailed steps of the grasping scenario are as follows: the grasper has some joint angle preshape of φ_1, φ_2, φ_3, φ_4 (Figure 3.3, top). The robot moves forward, stopping when contact is made with a circular object of radius r at position x_c from the centerline of the grasper.

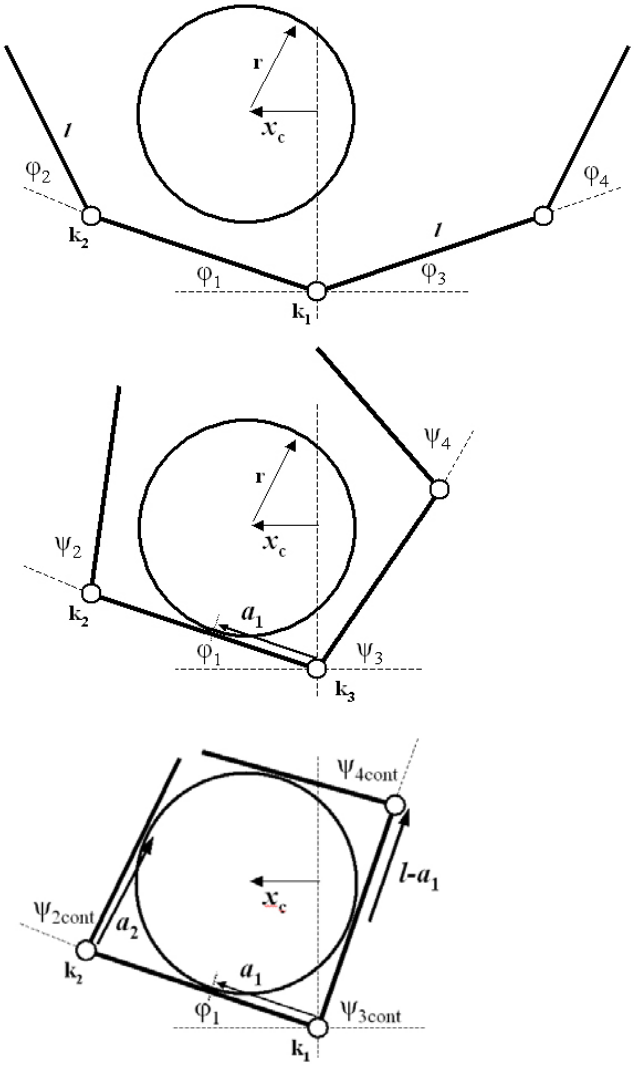

Figure 3.3. Example grasping scenario with relevant terms

3.1.1.1. Contact on the Proximal Link

Due to reasons explained in the results section, the initial contact for a successful grasp is always made on the proximal link. When contact has been made, the joints of the

TABLE 3.1
NOMENCLATURE

parameter	*definition*
φ_1, φ_2	spring rest link angles
ψ_1, ψ_2	deflected angles
$\Delta\psi_i$	small joint deflection due to fingerpad compliance
k_1, k_2	joint stiffness values
k_r	stiffness ratio (k_2/k_1)
k_s	finger skin stiffness
τ_1, τ_2	joint torque values
τ_r	torque ratio (τ_2/τ_1)
r	object radius
x_c	object position from the centerline
l	grasper link length
a_i	distance from joint i to contact point on link i
F_T	contact force tangential to the link surface
F_N	contact force normal to the link surface
F_{Ru}	unbalanced object force
μ	coefficient of friction
σ	standard deviation of object position
T_c	cable tension
s	cable length change
ΔN_j	normal fingerpad spring deflection
ΔT_j	tangential fingerpad spring deflection

grasper are actuated to begin to enclose the object (Figure 3.3 center). At initial contact, the angle of the contact joint remains fixed

$$\psi_1 = \varphi_1$$

where ψ_i is the deflected angle of joint i (Table 3.1 summarizes the nomenclature). Grasper symmetry allows us to assume initial contact is always on the left side (link 1).

When actuated by a joint torque τ_i, the other joints move in proportion to their stiffness, k_i

$$\psi_i = \frac{\tau_i}{k_i} - \varphi_i \ , \ i=2,3,4$$

until the respective link contacts the object (Figure 3.3 bottom). The joint angles at contact (ψ_{icon}) can be found

$$r\sin\psi_{3cont} - a_3\cos\psi_{3cont} - x_c = 0$$

where a_3 is the lever arm length on link 3

$$a_3 = a_1 = \frac{x_c + r\sin\psi_1}{\cos\psi_1} .$$

When contact on the two inner links is made, the outer joints continue to close against the object until they have made contact

$$\psi_{2cont} = \psi_{4cont} = \pi - 2\tan^{-1}\left(\frac{r}{l-a_1}\right)$$

This relationship comes from the symmetry of the two fingers when in complete contact with the object (Figure 3.3 bottom) and that

$$a_2 = l - a_1 .$$

The gripper is assumed to be covered with an elastic, high-friction skin to increase grasp stability [51,52]. This skin is modeled as a linear spring (with stiffness k_s) positioned along the normal to the link surface with some contact friction, μ. (Figure 3.4) As torque τ_j is increased after contact has been made, small deflections $\Delta\psi_j$ of the joint cause the spring to deflect and exert normal force F_{Nj} and tangential force F_{Tj} on the object, where

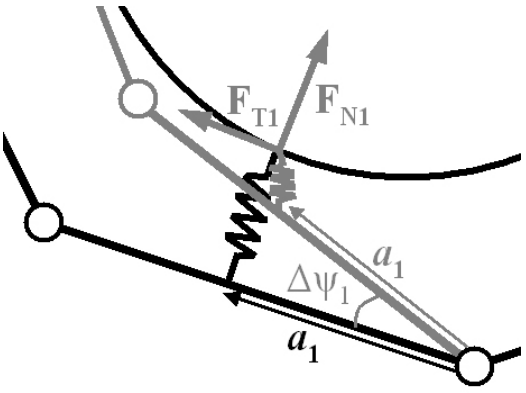

Figure 3.4. Spring model of the elastic finger skin after undergoing a virtual displacement, with relevant terms.

$$\mathrm{F}_{N_j} = (\tau_j - k_j(\psi_j - \varphi_j))/a_j$$

$$\Delta\psi_j = \sin^{-1}\left(\frac{\mathrm{F}_{N_j}}{a_j k_s}\right),\ j = 1,3.$$

These small joint deflections are assumed to be insignificant displacements of the joints and do not affect grasper kinematics. They are, however, necessary to enable calculation of contact forces. The resulting tangential component of the object force is

$$\mathrm{F}_{T_j} = a_j k_s(1 - \cos\Delta\psi_j),\ j = 1,3$$

$$\text{for } \mathrm{F}_{T_j} \le \mu_s \mathrm{F}_{N_j},$$

assuming, for simplicity, that normal skin stiffness and shear skin stiffness are equal (with stiffness k_s). For cases when the coefficient of static friction has been overcome at the contact point, $\mathrm{F}_{T_j} = \mu_s \mathrm{F}_{N_j}$.

Total force on the object is defined as the sum of forces at the individual contact points. For the stages of the grasping process before the outer links have made contact, this force is nonzero and must be balanced by a ground reaction force (most often due to friction) for the object to remain in equilibrium. Nonzero object force will henceforth be referred to as unbalanced object force $F_{Ru}l/k_1$, and will be used as a quality measure that should be minimized.

3.1.1.2. Contact on both proximal and distal links

In order to calculate the normal and tangential components of the contact forces during contact on both links of a finger, the work done by the actuator was balanced with the work done on the springs at the contact points. While we specify cable actuation to enable calculation of work, other methods of actuation can be considered in a similar way. For cable actuation with no slippage at the contact points,

$$\int_0^{s_1} T_c ds = \frac{1}{2} k_s (\Delta N_1^2 + \Delta T_1^2 + \Delta N_2^2 + \Delta T_2^2),$$

where T_c is the cable tension and s is the cable length change. These are integrated over the range from beginning of actuation (s=0) to the end of the grasp sequence (s=s_1, varies from case to case). Motion of the joints after contact is insignificant and does not factor into the work calculation. ΔN_j and ΔT_j are spring deflections normal and tangential to the surface of links j=1,2 and are related to the parameters $\Delta\psi_1$ and $\Delta\psi_2$ described in the previous section. Additionally,

$$s = r_1 \Delta\psi_1 + r_2 \Delta\psi_2$$

$$\text{and} \quad T_c = \tau_2 / r_2$$

where r_1 and r_2 are the pulley radii at joints 1 and 2, respectively.

For the contact point on the proximal link,

$$\Delta N_1 = a_1 \sin \Delta\psi_1$$

$$\Delta T_1 = a_1 (1 - \cos \Delta\psi_1)$$

For contact on the distal link,

$$\Delta N_2 = \tau_2 / a_2 k_s$$

$$\Delta T_2 = \Delta x_2 \cos(\psi_1 + \psi_2) + \Delta y_2 \sin(\psi_1 + \psi_2)$$

where Δx_2 and Δy_2 are the change in location of the contact point on the distal link due to the small joint deflections ($\Delta\psi_1$ and $\Delta\psi_2$) and can be found using the forward kinematics of the mechanism.

Finally, a torque balance is performed on joint 1

$$\tau_1 = a_1 \mathrm{F}_{N_1} + \mathrm{F}_{N_2} l \cos(\psi_2 + \Delta\psi_2) + \mathrm{F}_{T_2} l \sin(\psi_2 + \Delta\psi_2),$$

where $\mathrm{F}_{N_1} = k_s \Delta N_1$, $\mathrm{F}_{N_2} = \tau_2 / a_2$, and $\mathrm{F}_{T_2} = k_s \Delta T_2$.

This system of equations can be used to write the work balance and torque balance on joint 1 in terms of $\Delta\psi_1$ and $\Delta\psi_2$ and then solve them numerically. These equations also apply to links 3 and 4. Additionally, a similar and simpler system of equations describes cases in which forces at a contact point overcome friction and local slip occurs.

Cases in which tip contact on one finger occurs are judged as unsuccessful grasps (Figure 3.5). These cases typically occur at high torque ratios and most often result in the tip slipping and folding in towards the base joint after continued actuation, due to the large relative torque about joint 4.

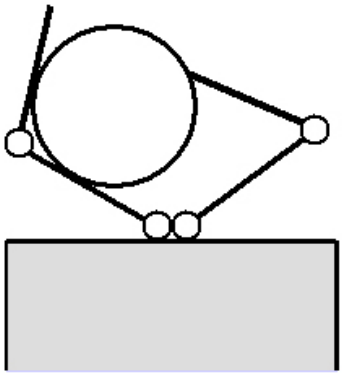

Figure 3.5. Example of an unsuccessful grasp

3.1.2. Specific Grasping Scenarios

In order to test questions related to the actuation design of the grasper, three specific grasping scenarios were studied:

3.1.2.1. One actuator for both fingers

This actuation scenario is analogous to the scheme implemented by Hirose [27] and Kaneko [19]: a single actuator for the four joints (two joints on two fingers). Assuming the transmission configuration in the two fingers is the same,

$$\tau_1 = \tau_3 \text{ and } \tau_2 = \tau_4 .$$

In this scenario, it is assumed that the robot reacts to contact and stops immediately, with initial contact producing negligible contact forces (Figure 3.6A). When the gripper is actuated, forces are exerted at the initial contact point while the second finger is brought into contact (Figure 3.6B). Due to symmetry, the distal links on both fingers contact the object simultaneously (Figure 3.6D). The grasp is successful if

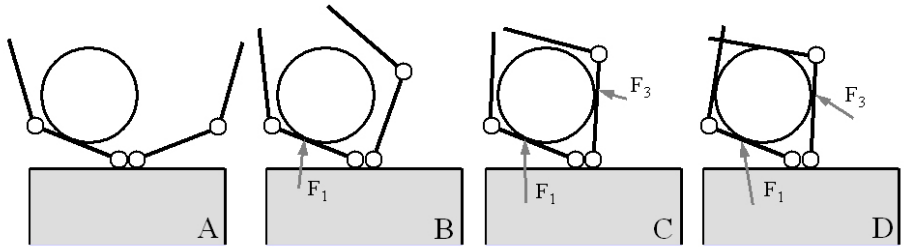

Figure 3.6. Grasp scenario 1

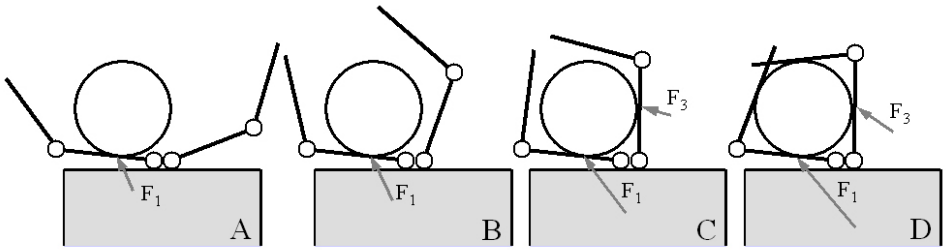

Figure 3.7. Grasp scenario 1a

these contacts envelop the object (enclose more than 180º of the object surface). Note that the direction of the contact forces change as the gripper is actuated, due to a squared relationship between normal and tangential contact forces (until the friction limit has been reached).

3.1.2.2. One actuator, further travel after contact

This scenario is similar to the one above, except that the grasper continues to move forward against the object for some distance after initial contact has been made, passively deflecting the contact finger and thereby exerting force on the object (Figure 3.7A). Due to sliding, the force remains on the friction cone. This scenario is studied to determine the sensitivity of the results from scenario 1 to delays in reacting to contact due to robot inertia and sensing the contact stimulus. As in scenario 1, the distal links on both

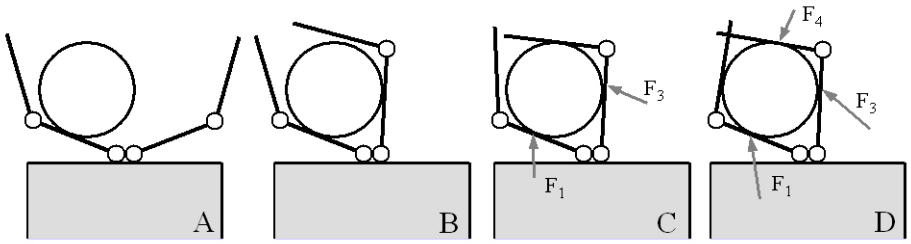

Figure 3.8. Grasp scenario 2

fingers contact the object simultaneously (Figure 3.7D). Again, the grasp is successful if these contacts envelop the object.

3.1.2.3. Two actuators (one per finger)

In this scenario, the contact finger remains unactuated until the second finger is brought into contact with the object. As with scenario 1, the robot stops immediately at initial contact. No force is exerted on the contact link until the second finger has made contact (Figures 3.8A and B). Torque is then applied at an equal rate to the two proximal joints, resulting in equal forces due to symmetry (Figures 3.8C). However, the actuation of the second finger to bring link 3 into contact with the object also causes deflection of link 4, leaving it closer to the object than link 2. When the two fingers are actuated together after contact on links 1 and 3, link 4 makes contact before link 2 (Figures 3.8D).

At the point of link 4 contact, if the three contacts (links 1, 3, and 4) envelop the object, the grasp is considered successful and the unbalanced object force $F_{Ru}l/k_1$ becomes zero since the object can no longer move in the plane. Note that for this gripper, three contacts can only geometrically enclose a circular object with radius less than

r/l=0.5. For all other cases, actuation of the fingers continues until all four links are in contact and the object is enveloped.

A second possible scenario for two actuators can be considered: contact on link 1, actuate the second finger to bring link 3 into contact, actuate both fingers together until link 4 makes contact, then actuate only finger 1 to bring link 2 into contact. This scenario, however, results in identical forces to scenario 1 (one actuator), but applied in a different sequence.

3.1.3. Parametric Analysis

The grasping scenario was simulated for a wide range of grasper parameter values, recording contact forces and the successful grasp range across a range of joint coupling configurations. The algorithm, implemented in Matlab (version 7.0.1, The Mathworks, Natick, MA), found the joint angles and object contact forces as joint torques were increased using the above system of equations. Simulation of the grasping process continued until both fingers enclosed the object.

The joint stiffnesses were applied as a ratio, since the individual magnitudes only affect the magnitude of the applied force and not the deflection behavior of the mechanism. In order to apply the actuation coupling that exists for this mechanism, individual joint torques were also applied as a ratio. Therefore, as the distal joint is brought into contact with the object, the proximal joint applies force to the object due to non-zero torque about that joint. The ratios are defined as

$$\tau_r = \frac{\tau_2}{\tau_1} = \frac{\tau_4}{\tau_3} \text{ and } k_r = \frac{k_2}{k_1} = \frac{k_4}{k_3}.$$

The motion that results when a compliant gripper is actuated is a function of both the torque and the joint stiffness. Therefore, the torque ratio was normalized by the stiffness ratio τ_r/k_r. From this point forward, this independent variable will be referred to simply as 'torque ratio'. Note that without object contact on the specified finger

$$\frac{\tau_r}{k_r} = \frac{\psi_2 - \varphi_2}{\psi_1 - \varphi_1},$$

representing the relative angular motion of the joints during free actuation (no object contact).

The object parameters x_c and r are varied to test the scenario of grasping an unfamiliar object at an unknown location. Distances were normalized by l, the link length. The performance of the gripper for each torque ratio configuration was evaluated for normalized object radius, $r/l=\{0.1:0.1:0.9\}$ and object location, x_c/l, incremented by 0.0025 from the center toward the outside of the grasping range. The maximum normalized distance of the object from the centerline for which a successful enveloping grasp was attained (x_{cmax}) was recorded for each configuration. This value represents the successful grasp range.

The largest force applied to the object during the grasping process before complete object enclosure was also recorded for each tested value of object location, x_c/l. The overall goal is to determine the coupling scheme (torque ratio, τ_r/k_r) that results in the lowest unbalanced object forces $F_{Ru}l/k_1$ and the largest grasp range x_{cmax}.

It is assumed that the fingers will not interfere with each other when the links overlap, as is the case if they are slightly offset in the out-of-plane direction. The static and kinetic friction coefficients were set equal to further reduce the dimension of the

parameter space. The coefficient of friction was tested at μ=2, based on previous studies that suggest high friction increases grasp stability [51,52]. The finger skin stiffness was tested at k_s=1000F/l. The default rest angle configuration was φ_1,φ_2=(25,45º) and was based on the results of a previous study that showed this configuration allowed for the widest range of range of uncertainty in object size and location, while keeping contact forces low [25]. We do, however, examine the behavior of the gripper mechanism for other gripper preshapes as described in section IV.A.2.

3.2. Results

3.2.1. One Actuator

Figure 3.9 shows the results of the simulation for five different object radius values under grasp scenario 1. Maximum unbalanced object force $F_{Ru}l/k_1$ was recorded as object position x_c/l and torque ratio τ_r/k_r were varied. Note that the hatched portions in the upper right of each plot are unsuccessful configurations (no grasp could be achieved), and the jagged edges are an artifact of the torque ratio step size.

These results suggest that, to keep unbalanced object forces low, torque ratio τ_r/k_r should be as large as possible. However, as torque ratios increase, the position range in which an object can be successfully grasped (max(x_c/l)) is decreased. This range is delimited by the outer boundary of the contour plots (max(x_c/l)) in Figure 3.9.

This tradeoff in force versus successful grasp range can be weighed by considering the quality of the sensory information available for the grasping task. For a task in which the location of the target object is well known, the torque ratio can be large, since the gripper can be reliably centered on the object. For this case, the gripper does not

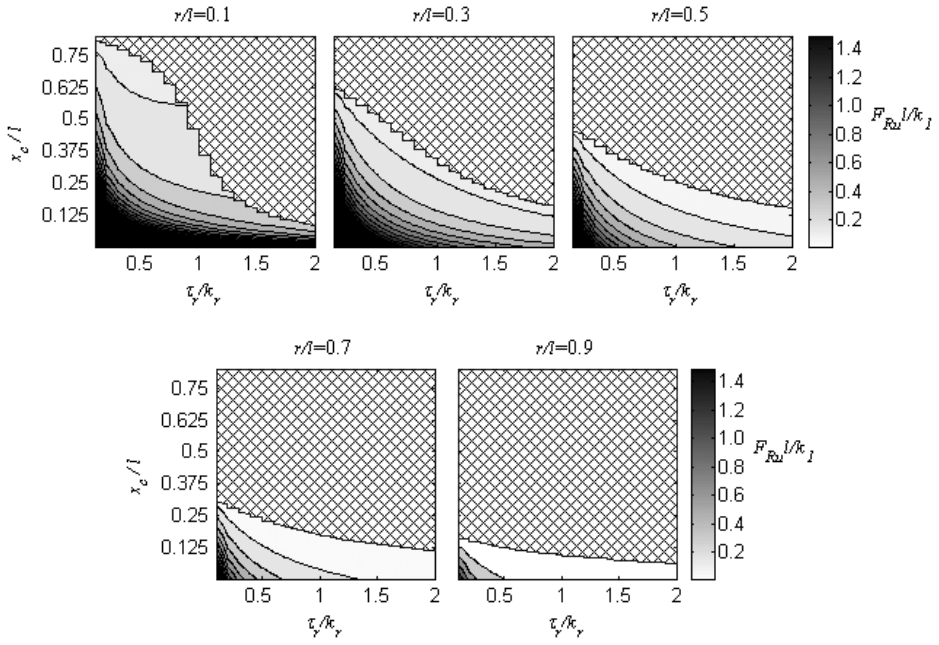

Figure 3.9. Unbalanced object force $F_{Ru}l/k_1$ as object location x_c/l and size r/l are varied for a range of torque ratio values τ_r/k_r.

need to be able to grasp objects at positions, x_c/l, far from the centerline. However, for tasks in which sensory information is poor, the positioning of the gripper is subject to large errors, requiring that the chosen torque ratio should allow for positions far from the centerline.

It should be noted that the successful grasp range results show that a successful grasp can only be achieved for object positions in which initial contact is made with the inner (proximal) link. However, initial contact on the proximal link does not guarantee a successful grasp, as the successful grasp range for any coupling configuration is always less than the maximum position resulting in proximal link contact.

3.2.1.1. Weighted results

The results of Figure 3.9 are further analyzed by weighting the individual data points by a normal distribution of the target object position, x_c/l, for a number of values of standard deviation. Different values of standard deviation of x_c/l correspond to different qualities of sensory information about the object prior to contact (e.g. vision) – large standard deviation corresponding to poor sensing and small standard deviation corresponding to good sensing.

Weighting functions were generated according to the normal Gaussian distribution with mean x_t and standard deviation σ

$$z(x, x_t, \sigma) = \frac{1}{\sigma\sqrt{2\pi}} e^{\frac{-(x-x_t)^2}{2\sigma^2}}$$

with probability density

$$p(x, x_t, \sigma) = \int_{-\infty}^{x} z(x')dx',$$

where $\sigma=\sigma/l$, $x= x_c/l$ and $x_t=x_t/l$ is the "target position" for the hand. As will be discussed later, it is sometimes better to approach the target object at some position offset from the center of the hand, therefore making it necessary to investigate object distributions with nonzero mean. Weighting functions were generated for three values of standard deviation (σ=1.5, 0.5, 0.1) and target positions spanning the entire possible successful grasp range (x_t/l=0,0.05,…0.85).

A weighted average Q_{FRu} of the maximum unbalanced object force over the range of object positions x_c/l for a given torque ratio τ_r/k_r was calculated using the normal distribution function

$$Q_{FRu}(\tau_r / k_r, x_t, \sigma) = \frac{\int_0^{x_{c\max}(\tau_r/k_r)} F_{Ru}(\tau_r / k_r, x_c) z(x_c, x_t, \sigma) dx_c}{\int_0^{x_{c\max}(\tau_r/k_r)} z(x_c, x_t, \sigma) dx_c}.$$

In this quality measure on force, smaller values represent better performance.

To address the tradeoff that high torque ratio leads to low grasp range, the normal probability density function was used to calculate a quality measure of the successful grasp range $Q_{Xc\max}$ for a given torque ratio τ_r/k_r

$$Q_{x_c\max}(\tau_r / k_r, x_c, x_t, \sigma) = p(x_{c\max}(\tau_r / k_r), x_t, \sigma) - p(-x_{c\max}(\tau_r / k_r), x_t, \sigma).$$

This term represents the probability that a given torque ratio configuration will be able to successfully grasp an object with the specified target position and distribution. Under this quality measure on grasp range, larger values represent better performance.

Figure 3.10 shows an example of these weightings for a large object and large standard deviation (r/l=0.9, σ=1.5). Results for the full range of r/l and σ are not shown here because the overall trends after weighting remain the same as in Figure 3.9.

In order to provide a measure of the tradeoffs between minimizing force and maximizing grasp space, the quotient of the two quality measures can be analyzed:

$$Q(\tau_r / k_r, x_c, x_t, \sigma) = \frac{Q_{x_c\max}(\tau_r / k_r, x_c, x_t, \sigma)}{Q_{F_{Ru}}(\tau_r / k_r, x_c, x_t, \sigma)}.$$

By calculating an overall quality measure in this specific way, we are using the force quality measure as a weighting function on the probability of successful grasp. Note that this relative weighting of Q_{FRu} and $Q_{Xc\max}$ is somewhat arbitrary, but gives some sense of the tradeoffs between force and successful grasp range.

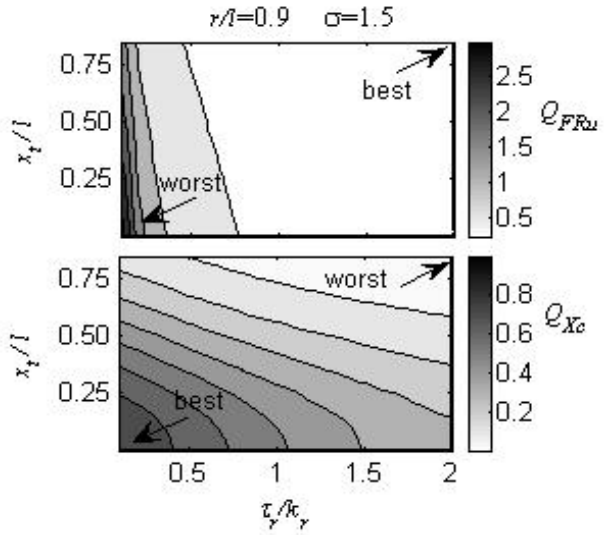

Figure 3.10. Force quality (top) and successful grasp range quality for a large object and poor sensing (r/*l*=0.9, σ =1.5).

Figure 3.11 shows *Q* across a wide range of object size (top three rows - *r*/*l*=0.1,0.5,0.9) and a normalized average (bottom row) over all tested object sizes (*r*/*l*=0.1,0.3,0.5,0.7,0.9) for three different standard deviations (columns - σ=1.5,0.5,0.1). In each plot, the horizontal axes are torque ratio τ_r/k_r, the vertical axes are gripper target position x_t/l, and the contours are the overall quality *Q*, with darker areas having higher quality.

The normalized average (bottom row) is the average over the five objects after each has been normalized by their individual maximum value. The magnitudes of *Q* across object size are not comparable, and a direct average would not give equal weighting to all objects. Alternatively, this quantity could be replaced by an average weighted by the distribution of the expected object size, if known.

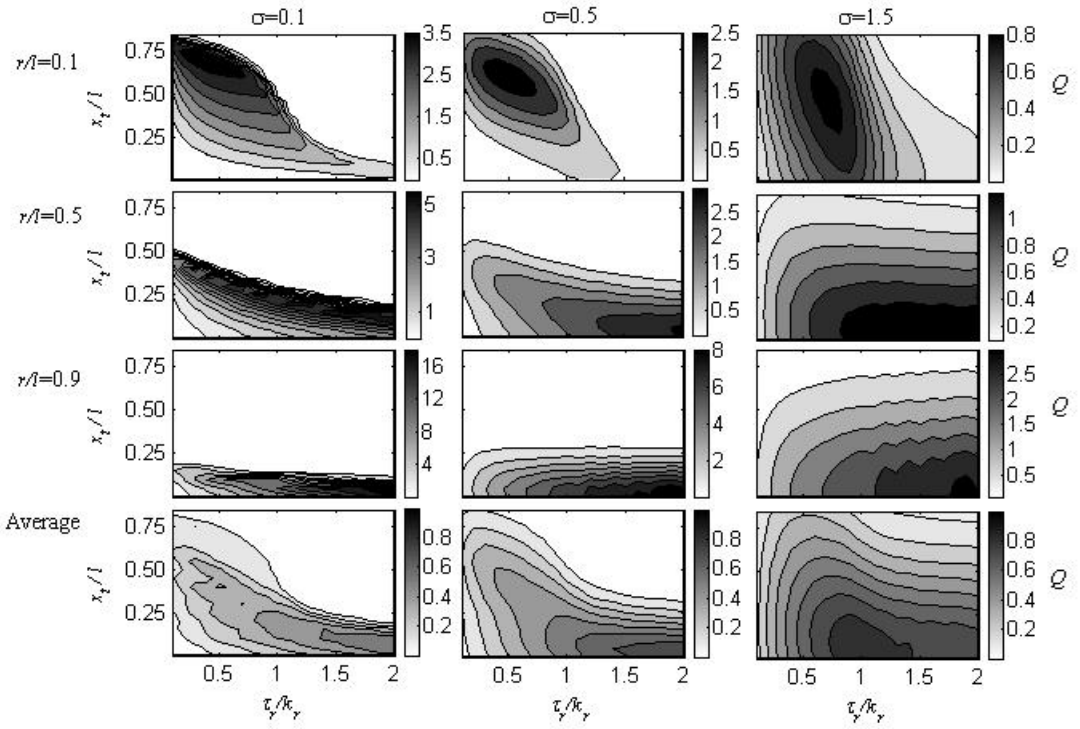

Figure 3.11. Overall quality Q as object size (r/l - rows) and distribution (σ – columns) are varied for a range of torque ratio values (τ_r/k_r – horizontal axes) and target positions (x_t/l – vertical axes). Note that each plot has a different scaling of the contours to show detail.

According to these results, for poor sensing (large standard deviation in object position - σ=1.5), a hand should be designed with a torque ratio of around $\tau_r/k_r = 1$. While this is the optimum when averaged across object size, there is high quality around this value across the entire range of object sizes. These results also show that targeting the object in the center gives the best performance for poor sensing, except for the smaller objects, which are better grasped slightly off-center ($x_t/l \approx 0.4$ for $r/l=0.1$).

As the standard deviation decreases (better sensing), the optimum torque ratio generally shifts towards higher τ_r/k_r and becomes more sensitive to object size. Note that

the results for σ=0.1 are nearly identical to the unweighted data (Figure 3.9), as would be expected.

Based on these results, it is often best to target the object off-center (x_t/l>0), particularly for smaller objects, thereby increasing the distance of the contact location (lever arm) from the base joint and lowering contact forces for a given joint torque. For tasks in which excellent sensing is available, the best positioning strategy is to target the location resulting in the lowest forces that also results in a successful grasp. This location is near the upper boundary of the contours in Figure 3.9. However, the torque ratio resulting in the best performance is less obvious. The averaging done in the last row of Figure 3.10 makes less sense for scenarios with good sensing than for poor sensing, since the target location need not be predetermined and can be decided based on the sensed object size. In this case, the best torque ratio should not be a function of x_t/l.

Figure 3.12 shows the maximum Q across all x_t/l as torque ratio is varied, normalized to the maximum across torque ratio, for three objects (r/l=0.1,0.5,0.9), the average of the normalized curves across all objects, and the minimum Q across the normalize maxima across all objects. Note that the "steps" in the curves are artifacts of the discrete values of object location and applied joint torque. As with Figure 3.9, the results show that a lower torque ratio should be used with small objects ($\tau_r/k_r\approx$0.4) and a large torque ratio for large objects (τ_r/k_r>2.0). The average across object size (dashed line) shows that any value of τ_r/k_r>0.5 performs well.

However, by taking the average, bad performance for one object (e.g. τ_r/k_r=2.0 for r/l=0.1) is sometimes balanced by good performance by another object (e.g. τ_r/k_r=2.0 for r/l=0.9). By looking at the minimum and designing for the "best worst case", acceptable

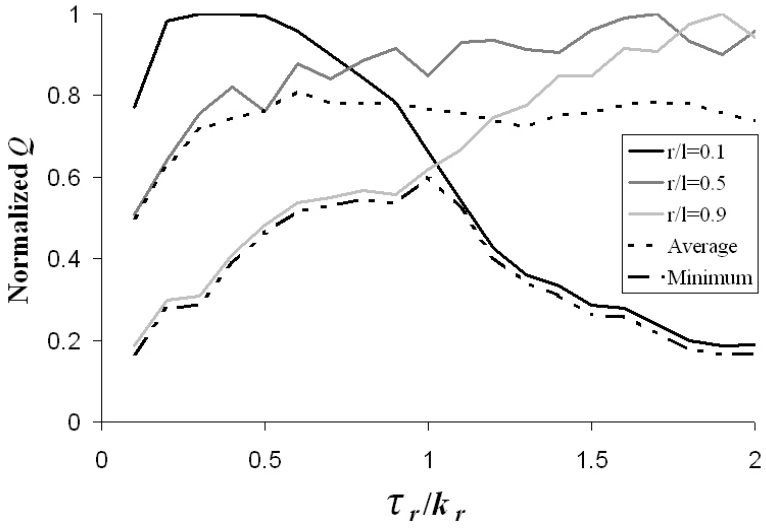

Figure 3.12. Normalized overall quality for σ=0.1 for three object sizes (*r*/*l*=0.1,0.5,0.9) and an average across objects.

performance across all objects is achieved, rather than a mixture of good and poor performance. In this case, a torque ratio of around τ_r/k_r=1.0 ensures that overall quality for all object sizes is above 50% of the maximum for that object. This value is within the maximum range of the average as well.

3.2.1.2. Stop-delay sensitivity

In the previous scenario, the grasper is actuated at the instant of initial contact with the target object. No further travel of the robot vehicle occurs. However, sensing delays and inertia in a real task require time for the robot to react to contact and come to a stop. We model these effects as forward travel after contact with the object (grasp scenario 1a), resulting in passive deflection of the compliant joints of the gripper, and contact force prior to actuation.

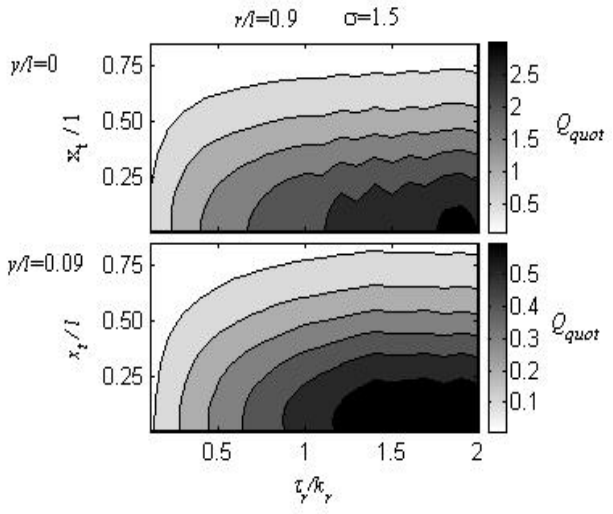

Figure 3.13. Overall quality for a large object and standard deviation (r/*l*=0.9, σ=1.5) when the robot travels forward some distance y/*l* after initial contact.

Figure 3.13 shows the product quality measure for a large object under poor sensing (*r*/*l*=0.9, σ=1.5) for two cases: a large amount of forward travel occurring after contact was made (*y*/*l*=0.09 across the entire successful grasp range), and no forward travel (stop on initial contact – scenario 1). This example result is consistent with the overall observed behavior that forward travel does not greatly affect the optimum torque ratio.

However, since forward travel after contact leads to large contact forces due to the passive joint stiffness, *Q* decreases with forward travel. Note that near the centerline, smaller objects will hit the stiff grasper base joint after just a small amount of forward travel after contact, lending further weight to the idea that grasping the object off-center is oftentimes better.

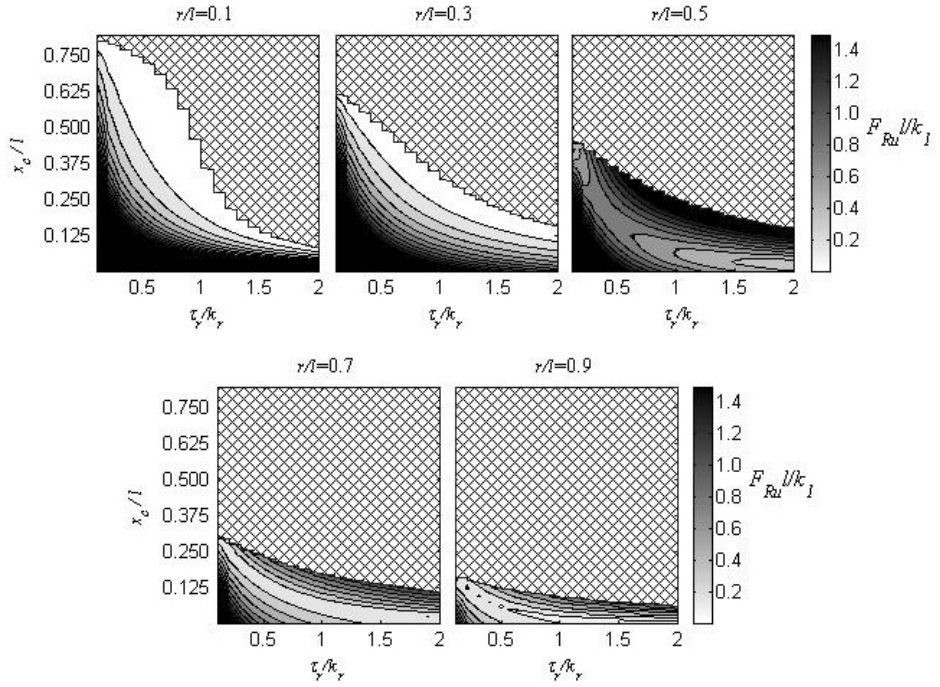

Figure 3.14. Unbalanced object force $F_{Ru}l/k_1$ as object location x_c/l and size r/l are varied for a range of torque ratio values τ_r/k_r for two actuators (scenario 2).

3.2.2. Two Actuators

To investigate whether there is any advantage to using two actuators, grasp scenario 2 was investigated. Figure 3.14 shows the unweighted results of this simulation. The successful grasp ranges for this scenario (boundary of the contour plots) are identical to scenario 1 (Figure 3.9). However, the force results are fairly different. For the smaller objects (r/l=0.1,0.3), most of the forces are smaller than the single-actuator scenario, resulting in better Q (not shown).

For medium and large objects (r/l=0.5,0.7,0.9), the forces are much larger than for a single actuator, resulting in lower Q. For these cases, there is tradeoff in the lower forces exerted on link 1 with the higher forces exerted on link 4. For these objects, four

contact points are needed to envelop the object, requiring that link 4 applies force as the final link (link 2) is being brought into contact. Depending on the torque ratio and contact locations (lever arm), these forces are often much larger than the forces on links 1 and 3, and may result in a large unbalanced object force. The symmetry inherent with scenario 1 necessitates that the object is enveloped when links 2 and 4 make simultaneous contact, and therefore forces applied at these links do not contribute to the unbalanced object force.

These results show that for multi-purpose grippers (intended to grasp a wide range of objects) and grippers specialized for medium and large objects with respect to the gripper size (which makes sense for a "specialized" gripper), one actuator for the four joints of the gripper actually performs better than two actuators, due to the enforced symmetry in the grasping task.

3.3. Discussion

The very nature of unstructured environments hinders full utilization of a complex, fully-actuated hand. In order to appropriately use the added degrees of actuation, an accurate model of the task environment is necessary. This model can be built from real-time sensing, but requires substantial sensing, processing, and control that may be difficult for the task at hand. A gripper with a reduced number of actuators is not only simpler to use, it is more appropriate based on the quality of information available in unstructured environments.

Towards this goal, this chapter evaluated a simple, two-fingered underactuated gripper as it was actuated after contact with a target object. We optimize the performance

of the gripper in an "unstructured environment" by varying the joint coupling configuration and number of actuators of the gripper in order to find configuration with the maximum successful grasp range while minimizing contact forces for a wide range of target object size and position. We also address the issue of positioning the hand with respect to the object and find that for scenarios in which the sensory information is good, targeting the object offset from the center of the hand results in lower forces while keeping the same probability of establishing a successful grasp. For poor sensing, the hand should be targeted to the center of the object, since the drop off in probability of successful grasp outweighs the decrease in force at offset target positions.

A number of key assumptions were made in order to make the study tractable, however. The requirement of an enveloping grasp is appropriate since the grasping environment is uncertain, but in practice force-closure is sufficient for a stable grasp. Evaluating the gripper performance for only circular objects is also simplistic, however, preliminary evaluation of other object shapes suggests that the optimum configurations also apply to a range of convex objects. We also assumed that the object is sufficiently massive such that the gripper contact forces do not displace or rotate it, but this is reasonable from several perspectives: predicting the movement of the object is impossible without knowledge of the object mass and friction properties with the ground (which would not be known in an unstructured environment); the goal of minimizing contact forces also minimizes the likelihood of object motion; and this assumption greatly simplifies the analysis, enabling broader investigation of the design space. The choice of a large value for the coefficient of friction can be debated as well, although informal studies suggest it does not have a large effect on the results. While we employed a

specific actuation scheme in order to allow for analysis of the mechanism, the results of this study apply to any method of actuation that enforces a constant distal/proximal torque ratio.

The weighting scheme used in this study, while providing a general framework for addressing the tradeoffs between successful grasp range and contact force, uses relative weightings that can be specialized for a given application. Our choice in specific weightings makes sense for the conditions that we are most interested in: grasping a broad range of target objects in the presence of large uncertainties in location and object properties. However, these may not be best for other scenarios. For instance, for a task in which target objects are known to be massive, choosing a coupling scheme that weights successful grasp range much larger than low contact forces may be more appropriate.

This work differs from the few systematic design studies identified in the survey in a number of ways. The designers of the 100G hand [19] sought to find the joint coupling that resulted in all finger links making simultaneous contact with the target object. The results were not only specific to the size and inertia properties of their grasper, but were only appropriate for a single target object at a specific location. Studies related to the Laval hands, alternatively, provide a more generally applicable framework for hand design [28]. These studies, however, do not consider the hand with respect to the grasped object, instead focusing on generating positive forces throughout their configuration space without consideration of the effects of those forces.

Alternatively, we consider object size and location in order to find the best design to maximize the likelihood of a successful grasp. We showed that a single actuator for both gripper fingers performs just as well as one actuator per finger, in terms of

successful grasp range and unbalanced contact forces. For a single actuator, distal:proximal joint torque ratios of around 1:1 produced the best results both for cases in which sensory information available for the task was poor and for cases in which sensory information available for the task was good.

Another interesting observation from this investigation is that, for the scenarios considered, it is better to grasp the object some distance away from the centerline, i.e. approach the object off-center from the middle of the grasper. Contacting the object towards the center of the grasper results in high forces due to small lever arm on the proximal joint, less allowable travel forward after contact before the joint limits are reached, and a less stable enveloping grasp due to a smaller amount of object enclosure. However, in the presence of uncertainty in the object properties, approaching the object off-center runs the risk of the object being outside of the successful grasp range, particularly for large objects.

Chapter 4

Finger Design, Fabrication, and Evaluation

In this chapter, I begin to explore the benefits of using Shape Deposition Manufacturing (SDM) for constructing robotic hands for unstructured environments by focusing on the design of one of the most important components of a hand – the fingers. SDM uses polymeric materials to simultaneously create the rigid links and compliant joints of the fingers, with embedded sensing and actuation components [43,44]. In addition to simplifying the construction process, the result is an extremely robust part. Elastomeric polymers provide joint compliance, eliminating metal bearings, and tough rigid polymers fully encase the embedded components, eliminating the need for seams and fasteners that are often the source of mechanical failure. Our prototype is fully functional after impacts and other large loads due to unintended contact.

4.1 Shape Deposition Manufacturing (SDM)

To fabricate my experimental fingers, I used an emergent manufacturing technique called Shape Deposition Manufacturing (SDM) [43,44]. This rapid prototyping

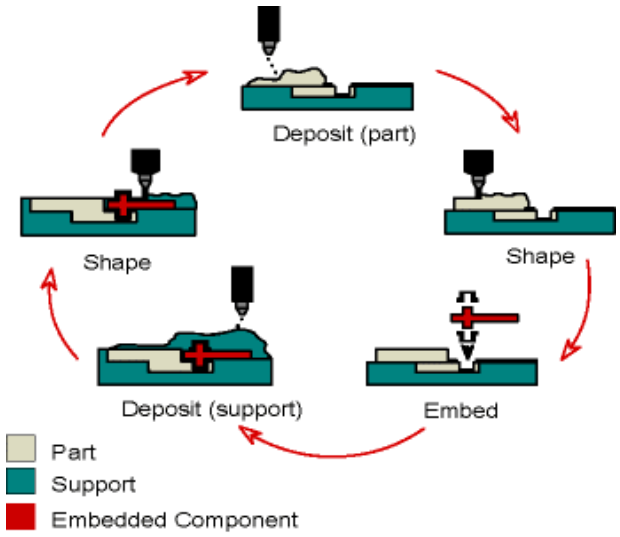

Figure 4.1. Diagram explaining the SDM process. Courtesy of Mark Cutkosky.

process involves a cycle of deposition of part material and shaping, building up the part in distinct layers, and resulting in the concurrent manufacture and assembly of the part. In this way, the part can be manufactured in multiple sections or layers, allowing manipulation of the internal parts of the final structure. A diagram detailing the process is shown in Figure 4.1 and an example use of the process with detailed steps is laid out in the next section.

SDM has a number of advantages over other prototyping techniques. The deposition of part material allows components to be embedded into the part during production, eliminating the need for fasteners, and reducing the likelihood of damage to the component by encasing it within the part structure. This is a particularly desirable property for the inclusion of fragile components such as sensors, greatly increasing the robustness of the part. Also, depositing the part in layers permits the use of dissimilar

materials, allowing for variation of mechanical properties within the same part. This property can be utilized to create complex mechanisms from a single part [14,53,54].

Due to its relative simplicity, custom tooling is not required to realize the SDM process. Complex part geometries can be attained using common computer numerical controlled (CNC) mill machines.

4.2 Finger Design and Fabrication

4.2.1 Fabrication Procedure

The diagram in Figure 4.2 shows the steps of the SDM process used to produce our compliant grasper fingers. Pockets corresponding to the shape of the stiff links of our fingers are machined into a high-grade machine wax (Freeman Manufacturing and Supply Co., Akron, Ohio, USA). The components in panel A are put into place in the pockets (panel B), and the polymer resin poured. Modeling clay is used to dam any areas to be blocked from the resin. After the layer cures, a second group of pockets is machined (both into the support wax and the stiff resin) and dammed (panel C). The polymer resins for the compliant finger joints (white) and soft fingerpads (clear) are then poured (panel D) and allowed to cure. The block is then faced off to level the surface and remove surface flaws (panel E), and the completed fingers removed from the wax support material. The entire process takes approximately 30 hours to complete, only 4 of which require human intervention.

The polymers used are two-part industrial polyurethanes. Different compositions are used for the soft fingerpads, compliant joints, and stiff links (IE35A, IE90A, and IE72DC, respectively, Innovative Polymers, St. Johns, Michigan, USA). Degassing at

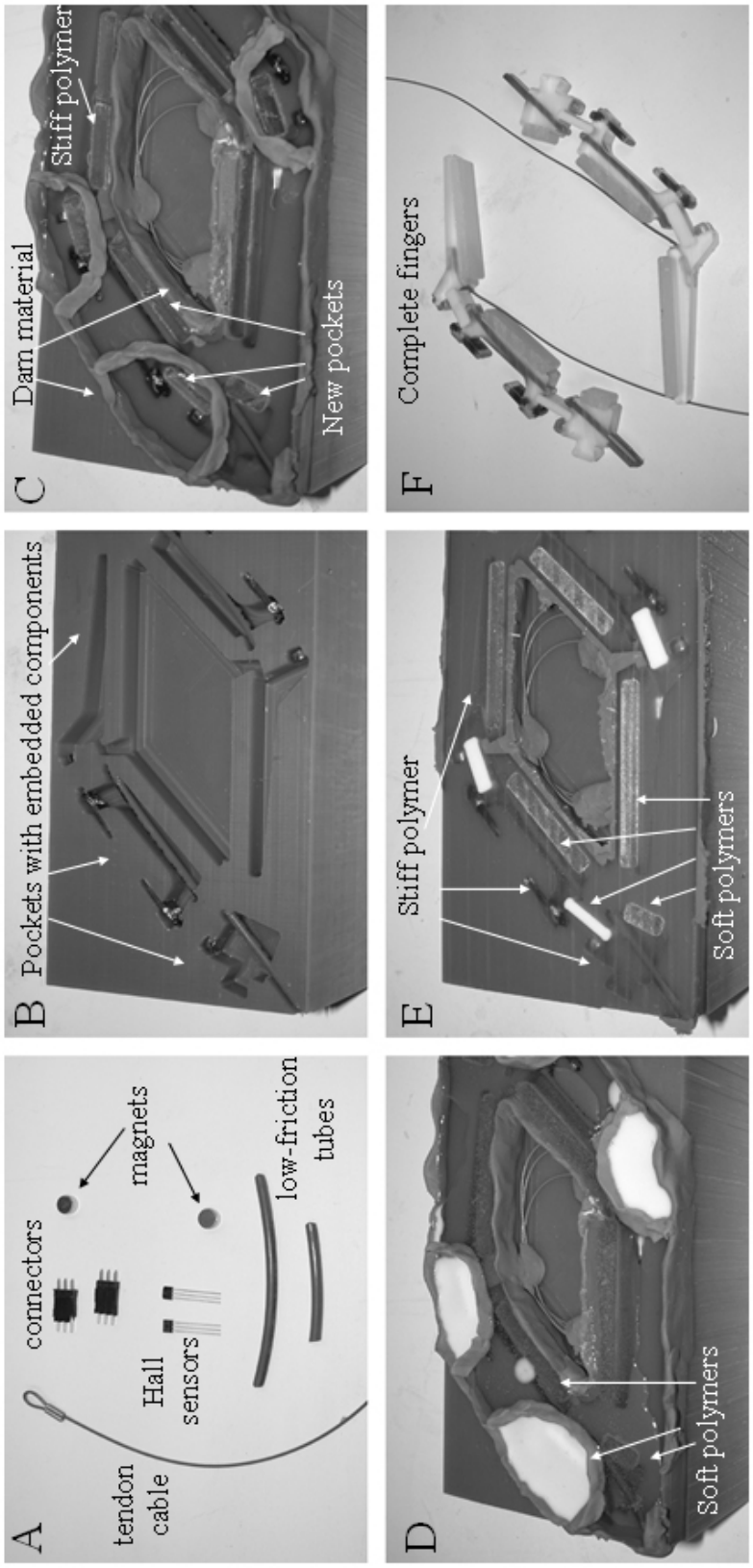

Figure 4.2. Steps of the Shape Deposition Manufacturing (SDM) process used to fabricate the grasper fingers.

TABLE 4.1
MATERIALS SPECIFICATIONS

	IE20AH	IE35A	IE90A	IE72DC
Hardness	15-25A	30-40A	85-95A	75-85D
Tensile Strength ASTM D-638 (ksi)	0.2	0.4	1.8	10
Elongation at Break	175%	470%	100%	2%
Tear Strength ASTM D-624 (pil)	25	50	250	N/A
Flex Modulus ASTM D-790 (ksi)	N/A	N/A	N/A	325
Ultimate Flex Strength D-790 (ksi)	N/A	N/A	N/A	13

-737mmHg (–29”Hg) was sometimes necessary to prevent voids in the cured resins. Table 4.1 shows material properties of these three polyurethanes as provided by the manufacturer.

4.2.2 Finger Design

Figure 4.3 diagrams the parts of the SDM finger. The concave side of each link contains a soft fingerpad to maximize friction and increase grasp stability [51,52]. The thin sections between links are the compliant joint flexures, designed to be compliant in the plane of finger motion and stiff out of plane. The joints are designed to have stiffnesses of 0.0421 Nm/rad and 0.224 Nm/rad for the proximal and distal joints, respectively, resulting in a proximal/distal stiffness ratio of 0.19.

Conveniently, the polymer used for the stiff links is transparent, allowing the embedded components to be clearly seen (also see Figure 4.2, panel A). Joint angle sensing is accomplished by embedding a low output impedance linear hall-effect sensor

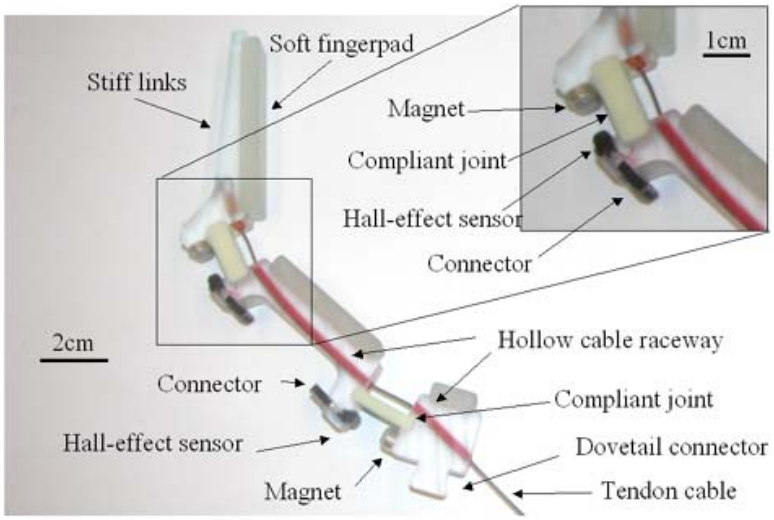

Figure 4.3. Details of finger parts and placement of components.

(A3517SUA, Allegro MicroSystems, Inc., Worcester, Massachusetts, USA) on one side of the joint, and a rare-earth magnet (6.35mm diam x 3.18mm, NdFeB, 10,800 Gauss strength, K&D Magnetics, Inc., Boca Raton, Florida, USA) on the other side. Joint motion changes the distance between the two, varying the sensor output (see Chapter 5 for more detail on this sensor). The sensors are wired to exposed connectors (2.5mm PC board header) for connection to external cables. A dovetail protrusion on the base link allows the finger to be securely connected to the grasper base.

For actuation, each finger has a pre-stretched, nylon-coated stainless steel cable (7x7 strand core, 0.94mm diam, 540N breaking strength) anchored into the distal link. This cable runs through the bodies of the proximal and base links through low-friction nylon 11 tubing (3.2mm OD, 2mm ID). Due to the joint compliance the finger can be underactuated, allowing for one tendon cable to drive both joints. The grasper is intended to be unactuated until contact is made with the target object and a successful grasp is

predicted based on the available sensory information. Before actuation, the tendon cable, which is in parallel with the compliant joints, remains slack and the finger is in its most compliant state. This method permits the use of actuators that are not backdrivable and prevents the inertial load of the actuator from increasing the passive stiffness. After actuation, the stiff tendon takes much of the compliance out of the fingers, resulting in a grasp with greater stability.

The link lengths, measured from the centers of the joint flexures, were chosen to be equal to enable the tip to reach the origin. The joint rest angles of the fingers (25 deg and 45 deg, for the proximal and distal joints, respectively) were carefully chosen based on the results of previous optimization studies (Chapter 2). The ratio of joint stiffnesses (0.19 proximal/distal) was chosen based on the optimization studies and additional material and geometric considerations to create a functional grasper. These angles and stiffnesses were shown to enable grasping of the widest range of object sizes with the greatest amount of uncertainty in object position.

The design is almost completely 2.5 dimensional (i.e. extruded 2 dimensional shapes) and symmetric about the center plane, allowing for the same finger to be used on the right or left side of the grasper.

For comparison to the single-part SDM finger, refer to a similar grasper made from aluminum that was shown in Chapter 2 (Figure 2.4). Each finger on this grasper contains over 60 distinct parts, 40 of which are fasteners! There is also a significant weight reduction in the SDM fingers (39g each) versus the aluminum fingers of similar size (~200g each).

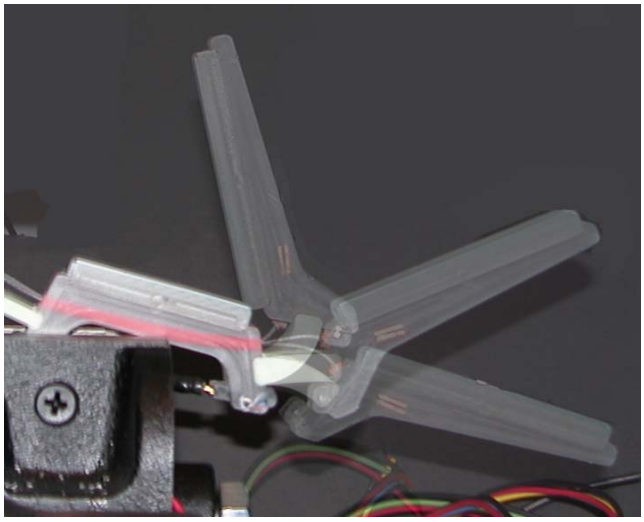

Figure 4.4. Superimposed photograph of joint deflection and link motion for three positions across the travel range of the distal joint of the fingers. The center image is the rest position.

4.3 Mechanism Behavior

Figure 4.4 shows the behavior of the finger joints through their range of motion. Note that the center of rotation varies slightly with joint angle. In order to characterize the behavior of the SDM grasper, a number of tests were performed. The polyurethane used for these joints (IE90A) demonstrates significant viscoelastic behavior, as shown in Figure 4.5. The sample tested corresponds to the dimensions of the distal joint flexure. A step angular displacement of 0.54 radians was applied, and the joint torsional stiffness was measured over a 30-minute interval.

The results show behavior consistent with a second-order Kelvin model [55], as shown in the figure. Note the non-zero origin of the vertical axis, highlighting the second-order fit

$$k_\theta = 0.176 + 0.0303e^{-0.0156t} + 0.0437e^{-0.00125t}, \qquad (4.1)$$

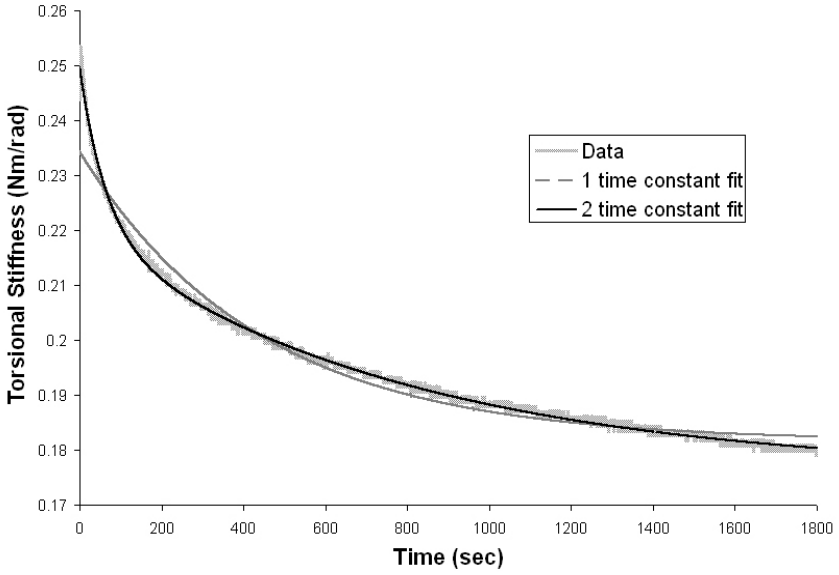

Figure 4.5. Force relaxation of the distal joint of the SDM finger, for an angular step displacement of 0.54 radians.

where k_θ and t have units of (Nm/rad, seconds), respectively. This fit was found using least-squares. Over the 30-minute time interval tested, the joint stiffness drops 29%. The time constants are much larger than typical grasp time, so the damping in the material has little effect on control of the grasper.

The viscoelastic properties of the joint material have the beneficial effect of damping out joint oscillations caused by grasper accelerations. In an undamped compliant grasper, these oscillations can be large due to the significant moment of inertia about the joints caused by long finger links. This effect was observed in our previous prototype that used music wire torsional springs in the joints (Chapter 2, Figure 2.4). In this conventionally-assembled grasper, oscillations due to large step displacements persisted for tens of seconds after release.

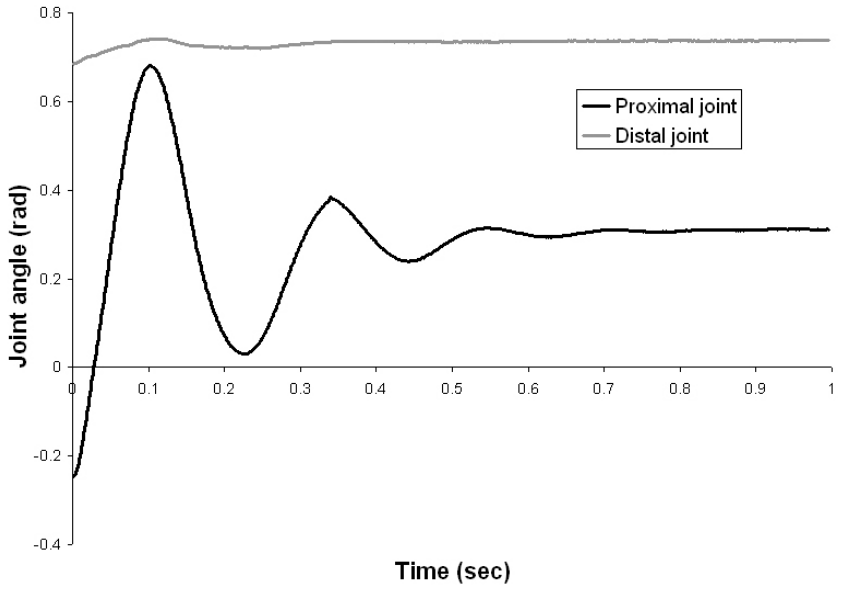

Figure 4.6. Joint response of the SDM finger to a tip step displacement released at time=0.

Low joint stiffness, although minimizing unwanted contact forces, increases the magnitude of resonant oscillations. Damping in the joints reduces the severity of these oscillations and therefore permits use of low joint stiffness. Figure 4.6 shows the joint response of the SDM finger to a large step displacement of the fingertip, released at time t=0. Note that the oscillations are negligible after less than 1 second.

Figure 4.7 shows the torque vs. angular deflection behavior of the joints of the grasper for different joint flexure sizes. Loads were applied and removed quickly in order to minimize the effects of the material viscosity. Note that the joint angular deflections are nearly linearly proportional to load torque even across large deflections, allowing for the assumption of simple cantilevered-beam bending behavior.

Figure 4.8 shows the joint deflection behavior as the finger is actuated without object contact. Note that the distal joint moves very little until the proximal joint completes its full range of motion, due to differences in joint stiffness and cable lever arm. This behavior is similar to that of the two distal joints of the human finger (PIP and DIP joints), and increases the chances that both links of the finger are in contact with the object, increasing contact area and friction. The "dip" in the theta1 curve is caused by out-of-plane motion that occurs when a joint has reached its travel limit. The hall-effect joint angle sensors are only calibrated for motion in the plane.

Figure 4.9 shows the force generated at the tip of the fingers due to displacement in the out-of-plane direction. The tip was displaced at a rate of approximately 1 cm/sec while mounted on an actuated linear slide mechanism (R2D series rodless actuator,

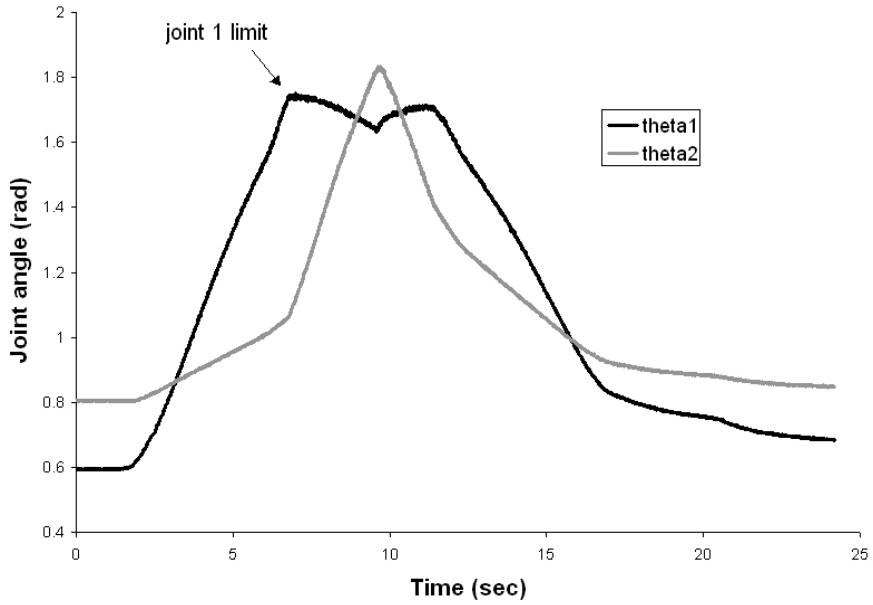

Figure 4.8. Joint behavior as the finger is actuated without object contact.

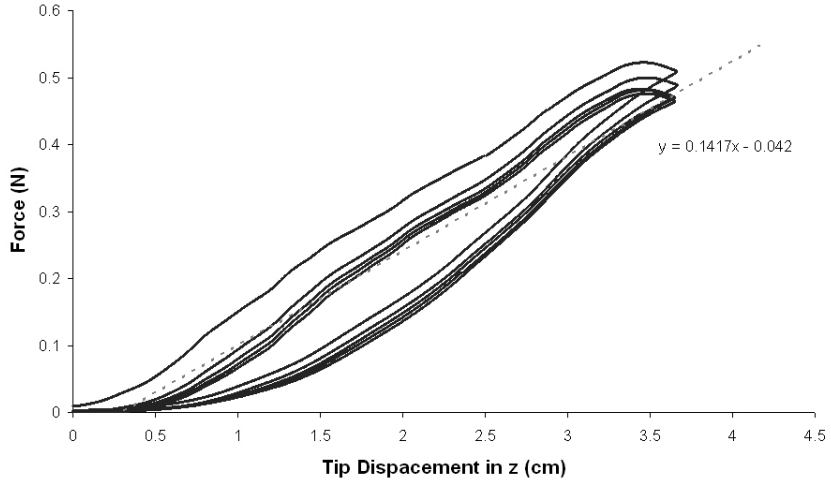

Figure 4.9. Out-of-plane force-deflection curve of the tip of the SDM finger with linear trendline. The data represents five cycles of tip motion.

Industrial Devices Corporation, Petaluma, CA). Force was measured with a multi-axis force/torque sensor (Gamma model, ATI Industrial Automation, Apex, NC). This data represents force generated due to motion of the tip across the tested range and back for a total of five cycles, low-pass filtered with a cut-off frequency of 1 Hz, to remove sensor noise. Note the hysteresis in the curves and the force relaxation due to viscoelasticity. The data is fitted with a trend line, to give an indication of the tip stiffness. The same tests were performed in the plane of actuation and show similar behavior. The approximate tip stiffness in the x, y, and z directions are 5.85, 7.72, and 14.2 N/m, respectively, according to the convention put forth in Chapter 3.

The SDM fingers, while exhibiting very low tip stiffness, can also undergo large deflections while remaining completely functional. In the test shown in Figure 4.9, the tip was displaced more than 3 cm in the out-of-plane direction without any degradation of mechanical properties. The advantages of this property are clear when considering the usual result of unplanned contact during use of traditional research robotic hands.

The grasper does not exhibit this amount of compliance during all phases of the grasping task, however. Although not quantitatively evaluated, the grasper becomes much stiffer after it is actuated by cable, a desirable characteristic allowing for more accurate manipulation of the grasped object.

To give a sense of the robustness of the mechanism to impact loads, a more informal test was performed. An SDM finger was repeatedly dropped from a height of over 15m (50') onto a stone floor. After two attempts, no noticeable damage had occurred. After three, a small piece broke off of the dovetail connector. After six

attempts, the outer link developed a large crack and one of the magnets broke off – but the sensors and joints remained intact and functional.

.

Chapter 5

Sensor Design and Evaluation

While they have demonstrated good performance and shown great promise for future work, the robot mechanisms that have been built using the Shape Deposition Manufacturing (SDM) process have been purely passive or open-loop mechanisms, devoid of sensing and control [53,56]. In order to expand the usefulness of SDM, sensors must be developed that both integrate with and exploit the unique characteristics of the process.

In this chapter, I describe the development of four types of sensors that take advantage of the special properties of the SDM process: an angular sensor for flexural joints, a force sensor with embedded strain gages, a compliant tactile sensor, and a low-threshold contact sensor. While they are broadly useful in many robotic applications, I evaluate these sensors in robotic graspers. Results show that SDM can bring the benefits of robustness and simplified construction to a wide variety of robotic sensing applications. For reference, a diagram of the SDM fingers described in Chapter 4 is shown in Figure 5.1.

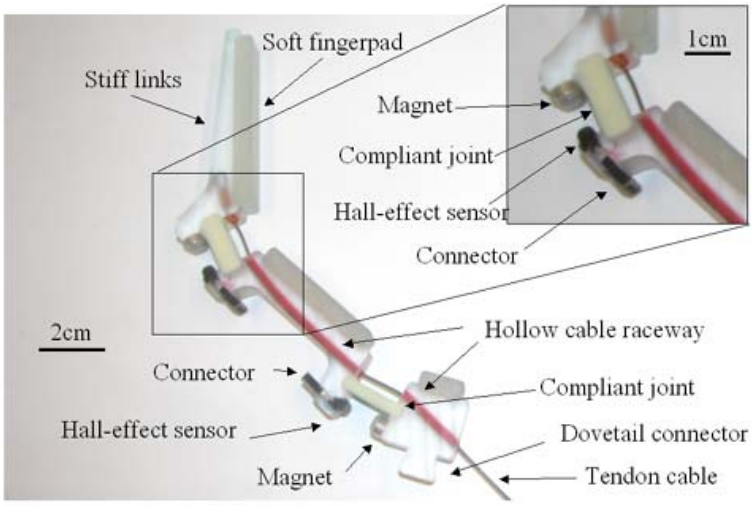

Figure 5.1. Details of finger parts and placement of components.

5.1 Joint Angle Sensor

Joint angle sensing in the robot fingers described above is accomplished by embedding a low output impedance linear hall-effect sensor (A3517SUA, Allegro MicroSystems, Inc., Worcester, Massachusetts, USA) on one side of the joint, and a rare-earth magnet (6.35mm diam x 3.18mm, NdFeB, 10,800 Gauss strength, K&D Magnetics, Inc., Boca Raton, Florida, USA) on the other side (Figure 5.1 inset). Joint motion changes the distance between the two, varying the sensor output. The sensors are wired to exposed connectors (2.5mm PC board header) for connection to external cables.

Figure 5.2 shows the output of the joint angle sensors (after amplification) and their fits versus joint deflection, θ, for the two fingers used in this study. The fit curves are of the form

$$\theta = (c_4 V^4 + c_3 V^3 + c_2 V^2 + c_1 V + c_0)^{-1} - 1, \qquad (5.1)$$

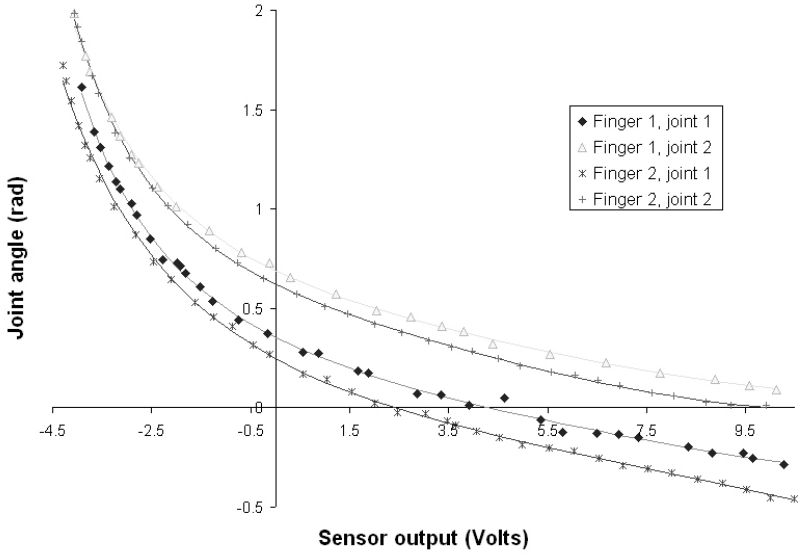

Figure 5.2. Joint angle sensor calibration data and fits

where c_i are the fit coefficients and θ and V have units of (radians, volts), respectively. These sensors give sufficient sensitivity across the entire range of motion of the joints to allow for use in the control of the grasper. The RMS sensor noise was found to be approximately 40 mV.

Note that the sensor gives better resolution as the finger opens (θ decreases) in order to optimize sensitivity during passive contact under. This enhances performance of the grasper when used as a "feeler". More about the usage and performance of the grasper can be found in Chapters 4, 6, and 7.

5.2 Strain Gage Force Sensor

Strain gages are often used as the basis of high quality force transducers due to their high sensitivity. The drawback of strain gages is that the bonding procedure is complicated and time consuming. Integrating SDM with strain gages allows devices to

be created with the high durability and ease of construction of SDM combined with the sensitivity of strain gages.

To determine the strain measuring capabilities of a strain gage embedded in a pourable plastic (IE72DC, Innovative Polymers, St. Johns, Michigan, USA), I embedded a full-bridge metal film strain gage (N2A-13-S056R-350, Vishay Micro-Measurements, Wendell, North Carolina, USA) in a beam (8.5 cm length, 1.27 cm x 0.64 cm cross-section). The beam was then loaded in tension (Series 900 Universal Test Machine, Applied Test Systems, Butler, PA, USA) and its strain at different loads was measured using a calibrated extensometer (model 2630-005, Applied Test Systems). Two types of beams were tested to examine the effects of wire placement; one with the strain gage wire leads exiting from the side of the beam, the other with wires running the axis of beam (Figure 5.3).

The stress strain curve of the beam with side-exit wires is shown in Figure 5.4. The measured strain from the gage matches the actual strain to less than 1 percent over the entire load. No significant difference was found between the side-exit or axial-exit beam in terms of strain measuring capability. A final observation is that the output of the strain gage matched the measured strain all the way to the ultimate failure of the specimens at 2% strain, showing the gage is well integrated into the material.

Based on the success of this proof of concept, and the relative ease of embedding strain gages versus bonding, SDM shows promise as a means of creating robust, high quality force sensors. These sensors can be built for relatively little cost due to the removal of the time consuming bonding procedure from the process of fabricating a transducer. Details and experimental results can be found in [66].

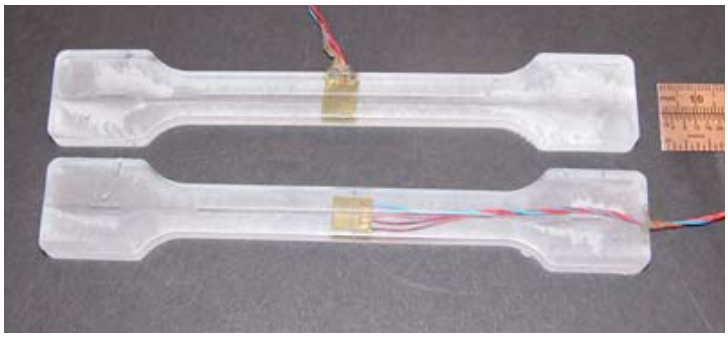

Figure 5.3. Metal film strain gages embedded in beam with side-exit wires (top) and axial-exit wires.

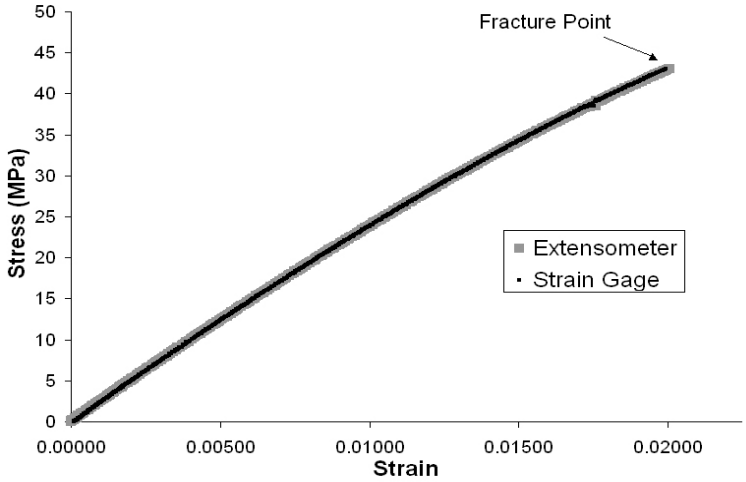

Figure 5.4. Measured and actual strain in side-exit beam.

5.3 Tactile Sensor

A tactile sensor has been developed for integration with the soft fingerpads (Figure 5.5). An array of these sensors can be used to sense a two-dimensional pressure distribution across the fingerpad. The sensor uses a reflective object sensor (OPB608R, 660 nm emitter wavelength, Optek Technology, Carrolton, TX, USA) that consists of an LED and photodetector. As the finger applies force to an object, the pad deforms

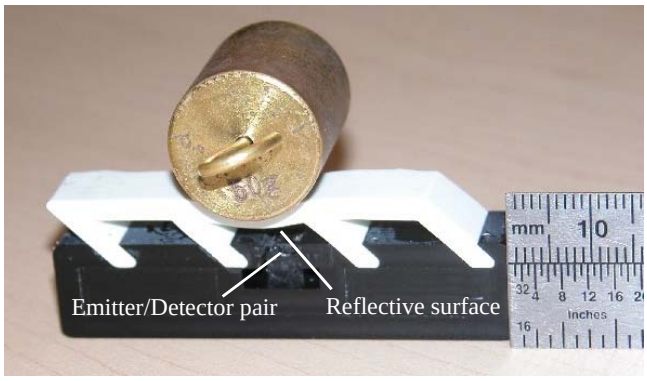

Figure 5.5. Tactile sensor prototype with 50g weight placed over the sensor. The angled strut flexures separate the reflective surface from the sensor face. Note the curvature of the reflective surface due to the applied load.

inwards, bringing the reflective inner surface of the fingerpad closer to the embedded sensor and causing a change in detector current. The slanted struts reduce stiffness in the normal contact direction. As shown in Figure 5.5, black and white dyes were used in the support and pad materials (IE72DC and IE20AH, Innovative Polymers, St. Johns, Michigan, USA) to shield the sensor from ambient visible light and increase reflectance. The sides of the sensor can also be easily enclosed.

The stiffness of the pad is very low - on the order of 1 kN/m, depending on contact location and geometry. Figure 5.6 shows the sensor output as a function of applied force for the various indenter diameters. It is clear from the figure that contact geometry plays a role in sensor output. This effect is due to both the difference in effective stiffness and the curvature of the reflective surface, which can deform with small objects to deflect light away from the detector. Note the higher sensitivity to smaller loads, a property useful in contact detection.

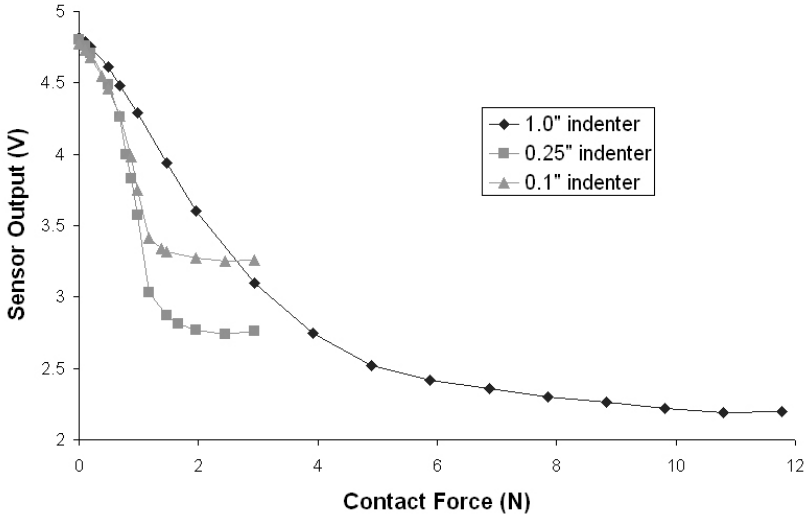

Figure 5.6. Optical sensor output vs. contact force for various spherical indenter geometries

Although this prototype contains only one optical sensor, multiple sensors can be embedded in the pad at about one every fifteen millimeters under the current design. Combining an array of the tactile sensors into a fingerpad will yield an inexpensive, compliant, distributed pressure sensor that can sense contact location on the fingerpad, as well as determine object geometry based on contact location. The array density, or contact position resolution, is limited only by the size of the emitter/detector package.

5.4 Piezofilm Contact Sensor

I have integrated a piezoelectric polymer film element (model LDTO-028K, MSI sensors, Hampton, VA, USA) into a compliant pad to make a robust, low-threshold contact sensor (Figure 5.7). These sensors generate an electrical charge in proportion to the applied strain, have excellent frequency sensitivity, but no static response. By

Figure 5.7. Piezofilm contact sensor.

embedding the flexible sensor just under the contact surface, I sense the transient when the fingerpad is deformed on initial contact.

To test the resolution of the sensor to a short contact, a load of 0.03 N was quickly removed from the sensor in less than 10 ms. This stimulus produced a 200 mV peak response, approximately 5 times the RMS sensor noise (40 mV). The sensor can therefore quickly respond to low force contact transients. This allows a manipulator to react quickly to minimize contact forces with the environment, yet still operate at a reasonable speed.

Similar sensors have been developed for contact and transient detection, as well as perception of small shapes and incipient slips [57]. The sensor was fabricated as a separate device and then assembled with the robot finger. While this provided good sensitivity, the need for assembly increased the complexity of the fabrication process and reduced the durability of the resulting gripper in comparison to the present SDM approach.

5.5 Future Work

Shape Deposition Manufacturing (SDM) has shown great promise in enabling biomimetic construction of robust robots that part from traditional design methods. The

capability to create spatially-varying materials for complex flexures and the added durability from embedded components will surely prove appealing to researchers frustrated with the fragility and complexity of robots built with traditional manufacturing methods. To further the usefulness of SDM, I have developed sensors for use with the process that cover four of the most utilized sensor types in robotics – joint angle, force, taction, and contact.

To continue the development and evaluation of these sensors, our next step is to create a more sensorized robotic hand by implementing combinations of sensors in an SDM grasper. The performance of these hands will be evaluated across a large range of grasping tasks, with particular attention to the information that can be gleaned from the different sensor suites. This analysis should speak not only to the sensors' effectiveness, but also to the nature of the information needed to complete the various grasping tasks.

Chapter 6

Hand Implementations

This chapter describes the design of two robot hands built using Shape Deposition Manufacturing (SDM). Both of these hands use the SDM finger design described in Chapter 4.

6.1 Two-fingered Hand

In this section, I describe the design and experimental evaluation of a prototype two-fingered gripper, including a quantitative study of its performance in grasping, in comparison to both simulation results and the metal prototype's performance. This gripper was developed as a proof-of-concept model for the ideas put forward in Chapter 2, as well as to guide the development of future generations of SDM hands.

Figure 6.1 shows the fully assembled grasper (two fingers, two motors, and base). The base was also produced using SDM, but is purely structural. The link lengths, measured from the centers of the joint flexures, were chosen to be equal to enable the tip to reach the origin. The joint rest angles of the fingers (25 deg and 45 deg, for the

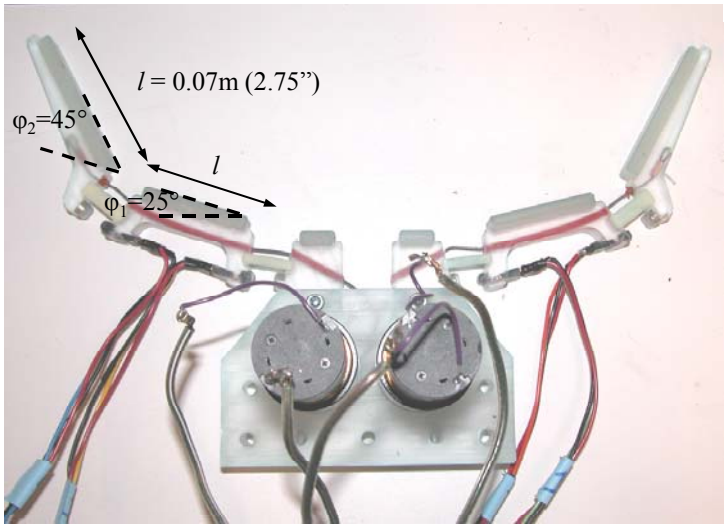

Figure 6.1. Overhead view of the 2-fingered SDM grasper.

proximal and distal joints, respectively) were chosen based on the results of the optimization study presented in Chapter 2. The ratio of joint stiffnesses (0.19 proximal/distal) was also chosen based on this study as well as additional material and geometric considerations to create a functional grasper. These angles and stiffnesses were shown to enable grasping of the widest range of object sizes with the greatest amount of uncertainty in object position.

6.1.1 Experimental Evaluation

6.1.1.1 Apparatus and Procedure

In an environment where sensing uncertainties are large, mechanical compliance can allow a robotic gripper to passively conform to the shape of the target object while minimizing contact forces. To maximize the effectiveness of the gripper, it should be designed to accommodate the largest range of target object size and location uncertainty. I evaluated the effectiveness of my compliant gripper by measuring the positions for

which a successful grasp could be obtained for various object sizes. To accomplish this, the grasper was mounted on a precision screw-driven linear positioner, which brought the grasper into contact with the target object. The objects were positioned at increasing distances x_c from the center of the grasper in the lateral x direction, and securely mounted to prevent motion due to gripper-object contact forces. A diagram of the experimental apparatus is shown in Figure 6.2. The objects were metal cylinders chosen to reflect the sizes used in Chapter 2, and were mounted on a multi-axis force/torque sensor (Gamma model, ATI Industrial Automation, Apex, NC) to record the contact forces in the plane. Force was recorded at a resolution of 0.016N.

Joint angles and contact forces were recorded as the grasper moved forward along the linear actuator at a rate of 2 cm/sec. Based on the joint angle information and knowledge of the object size and distance from the line of travel, the amount of object enclosure was calculated using the kinematics of the grasper and geometry of the object. If the grasper finger contacts can enclose greater than 180 degrees of the object surface, an enveloping grasp will be attained, and the grasp is deemed successful. For this evaluation of grasp range, the grasper is not actuated, but is allowed to passively conform to the shape of the target object. The kinematics of the grasper and object pair determines grasp success. See Chapter 2 for further discussion of this grasping scenario and success metric.

The performance of the grasper mechanism was evaluated for normalized object radius r/l=0.5 and 0.9, and object location, x_c/l, incremented by 0.023 from the center toward the outside of the grasping range, where l represents the grasper link length. The maximum normalized distance of the object from the centerline for which a successful

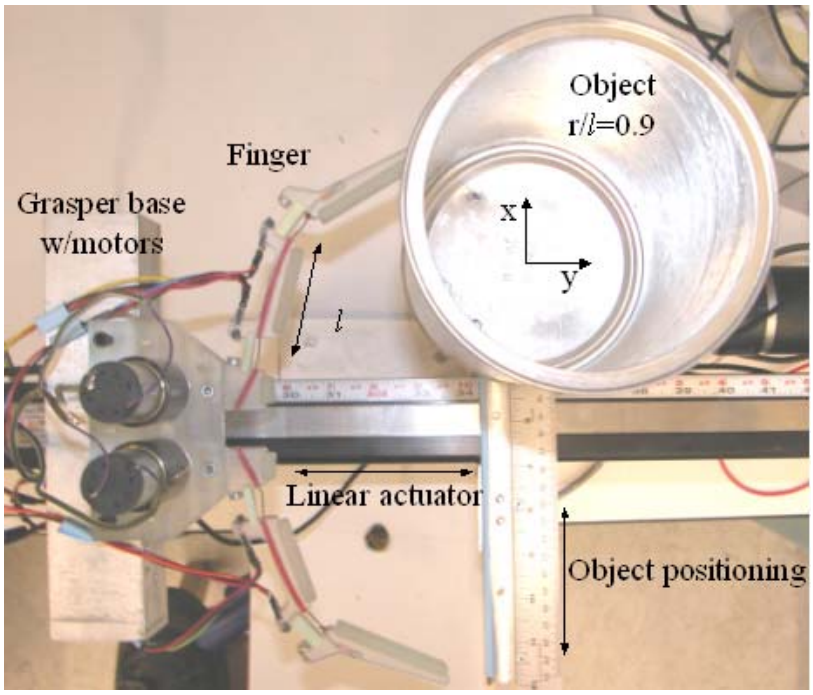

Figure 6.2. Experimental setup. The grasper is mounted on an actuated linear slider and the object, affixed to a six-axis force/torque sensor, can be positioned at distances normal to the actuation direction.

grasp was attained was recorded for each configuration. This value represents the successful grasp range and indicates the grasper's robustness to uncertainty in object location. The contact forces applied to the object during the grasping process were also recorded for each tested value of object location, x_c/l.

6.1.1.2 Results

Figure 6.3 shows an example plot (r/l=0.9 and x_c/l=0.45) of contact forces as the grasper moves forward against the object until a successful grasp configuration is obtained. As contact is made, the force causes deflection of the grasper, occurring primarily at the proximal joint, which is more compliant and is affected by a larger lever

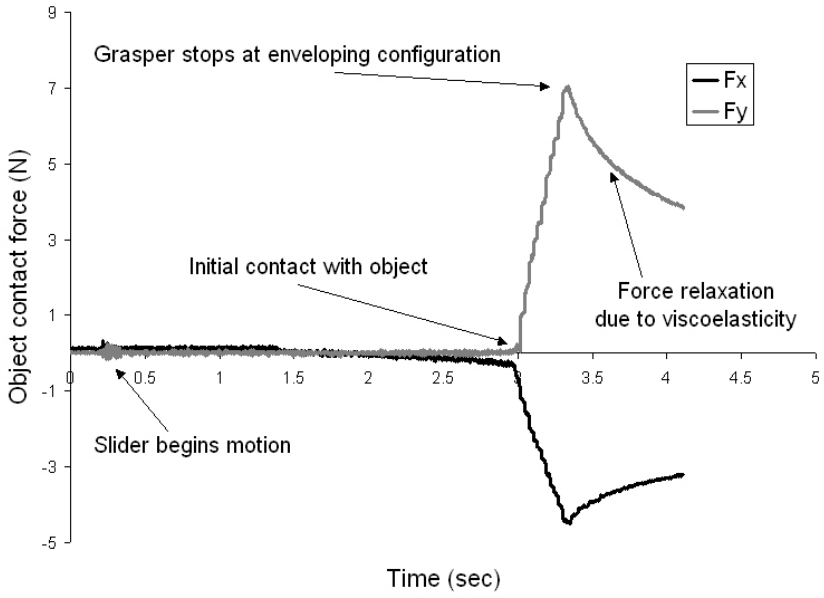

Figure 6.3. Object forces due to grasper contact. The grasper moves forward at a constant velocity of 2 cm/sec until a successful grasp configuration is reached.

arm than the distal joint. This deflection continues as the grasper moves forward, with object force increasing nearly linearly, until an enveloping configuration has been reached. Force on the object due to the passive contact then decreases due to the viscoelasticity in the joint flexures and fingerpads.

Figure 6.4 shows the successful grasp range of the SDM grasper and the analogous results from the aluminum grasper and simulation (both described in Chapter 2) for objects of radius r/*l*=0.5 and 0.9. The object can be successfully grasped anywhere within this range, indicating the allowable uncertainty in object position for a successful

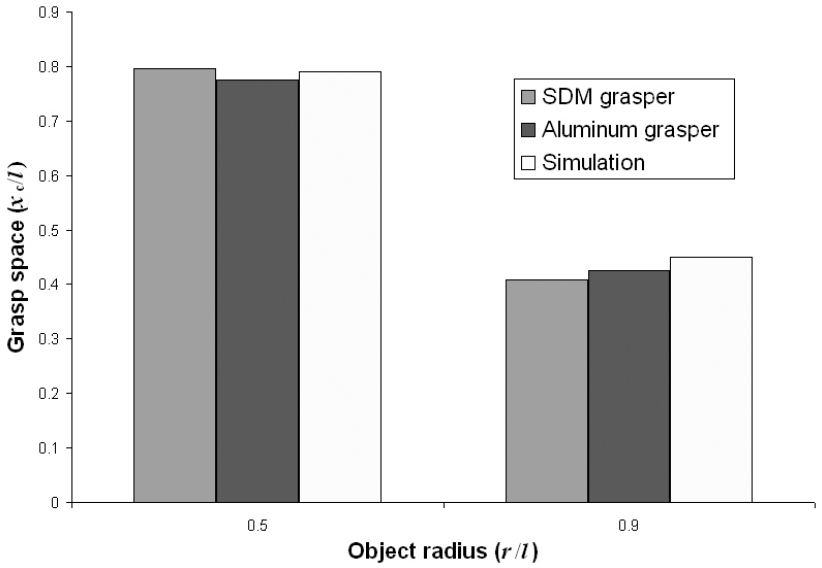

Figure 6.4. Successful grasp range of the SDM grasper compared to the aluminum grasper and simulation.

grasp. The results show that the center of an object of radius r/l=0.5 can be located anywhere within the range x_c/l=±0.80 from the centerline of the grasper. Similarly, a large object (r/l=0.9) can be located anywhere within the range x_c/l=±0.41. The values of the SDM grasp range show good agreement with the aluminum and simulated graspers.

6.2 Four-fingered Hand

Traditional approaches to grasping in unstructured environments involve hands that are complex, fragile, require elaborate sensor suites, and are difficult to control. In this section, I demonstrate a novel hand that is simple, adaptive, and robust (Figure 6.5).

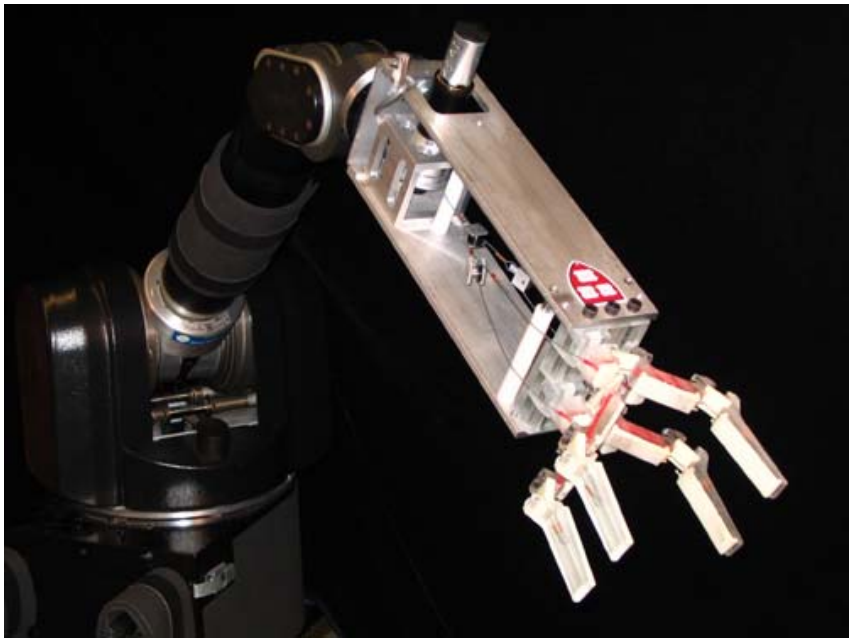

Figure 6.5. Four-fingered, underactuacted SDM hand mounted on a Whole-Arm Manipulator (Barrett Technology Inc., Cambridge, MA, USA). A single motor drives all eight joints of the hand.

The four-fingered hand is driven by a single actuator, yet can grasp objects spanning a wide range of size, shape, and mass.

6.2.1 Hand Design

Based on the results of the study presented in Chapter 2, a preshape configuration of φ_1=25º (angle with the horizontal in Figure 6.6) and φ_2=45º (angle with the proximal link) was chosen for my final hand design. In addition, the results showed that the proximal joint should be much stiffer than the distal joint, keeping the grasping surface concave and contact forces low.

6.2.1.1 Actuation

For actuation, each finger has a pre-stretched, nylon-coated stainless steel cable anchored into the distal link, and running through low-friction tubing to the base. The

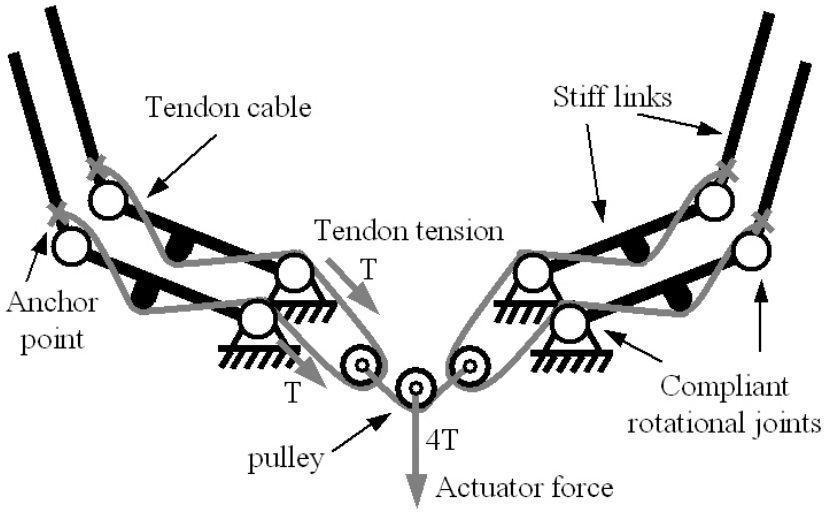

Figure 6.6. Actuation schematic of the hand

hand is unactuated until contact is made with the target object and a successful grasp is predicted based on the available sensory information. Before actuation, the tendon cable, which is in parallel with the compliant joints, remains slack and the finger is in its most compliant state. This method permits the use of actuators that are not backdrivable and prevents the inertial load of the actuator from increasing the passive stiffness. After actuation, the stiff tendon takes much of the compliance out of the fingers, resulting in a stiffer grasp with greater stability.

A single actuator drives the four fingers (eight joints) of the hand. This property not only makes the gripper simpler and lighter, but it also allows the gripper to be self-adapting to the target object (see Chapter 1 section 2 for an in-depth description of underactuation and adaptability). Figure 6.6 details the actuation scheme, by which motion of the distal links can continue after contact on the coupled proximal links occurs,

allowing the finger to passively adapt to the object shape. Additionally, the pulley design in this scheme allows the remaining fingers to continue to enclose the object after the other fingers have been immobilized by contact, ensuring that an equal amount of tension is exerted on each tendon cable, regardless of finger position or contact state.

The four fingers are staggered on the palm to allow them to completely close without interfering with one another.

The joint coupling scheme employed on each finger was determined based on the results of the optimization study presented in Chapter 3. The results of this study suggested that, for grasping in environments with large expected positioning errors, choosing a lower torque ratio $((\tau_2/\tau_1)/(k_2/k_1)=1.0)$ maximizes the likelihood of successfully grasping the target object while keeping unbalanced contact forces low.

6.2.2 Hand Performance

The series of images in Figure 6.7 show the hand grasping a number of different objects of varying size, shape, and mass. The performance of the hand is remarkable considering only one actuator drives all eight of the joints and the adaptability inherent with the underactuation scheme allows the hand to passively adapt to the target object without any sensory feedback.

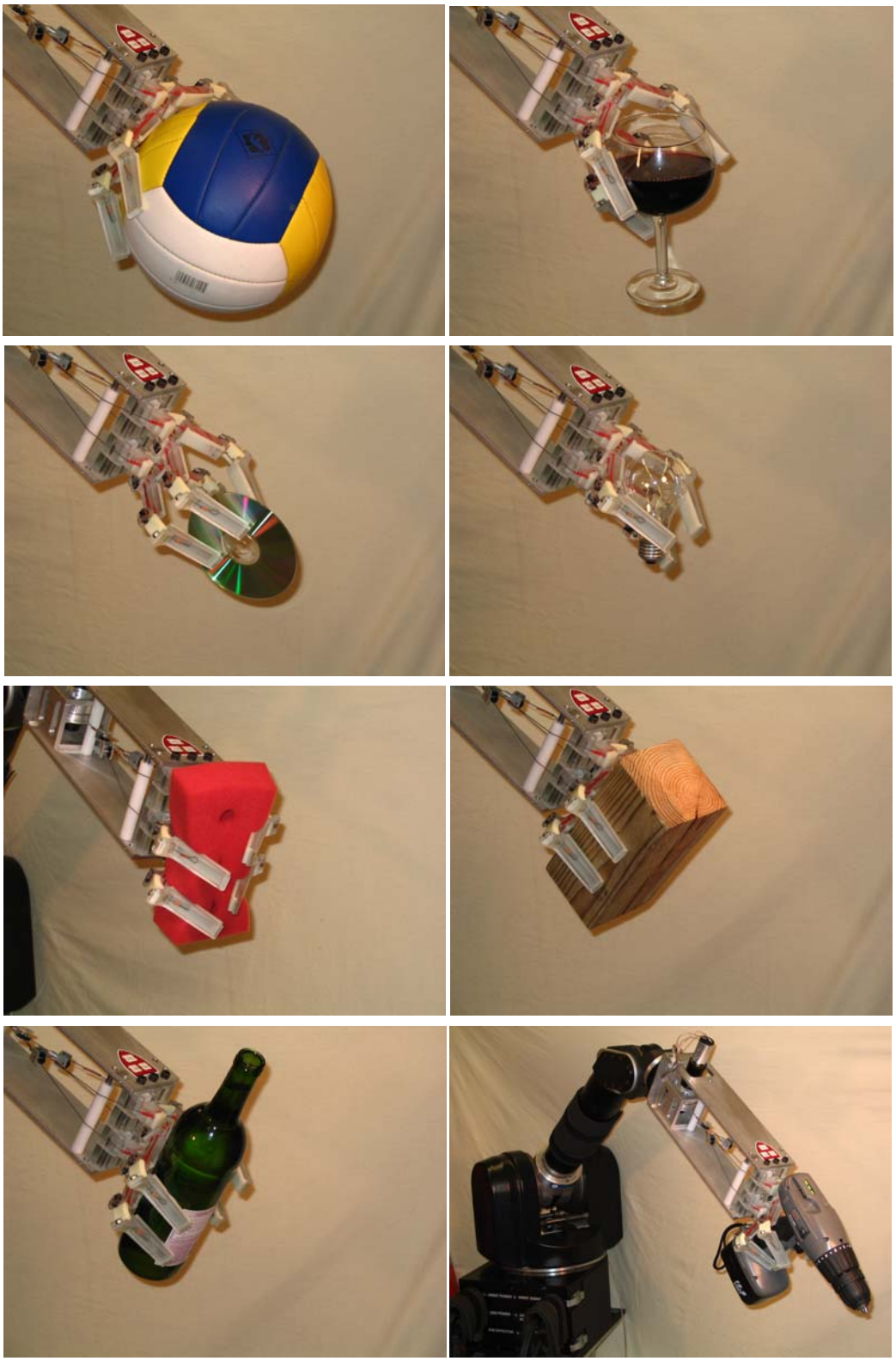

Figure 6.7. Holding a volleyball, glass of wine, compact disc, light bulb, foam block, wood block, full bottle of wine, and cordless drill.

Chapter 7

Autonomous Grasping Experiments

In order to determine the effectiveness of our hand at grasping objects in unstructured conditions, we experimentally evaluated the ability of the hand to grasp three-dimensional objects in a three-dimensional environment with large errors in the sensed target object location and a very simple control scheme.

7.1. Grasp Range and Contact Force Experiment

In this experiment, we examine the amount of positioning error allowable in order to obtain a stable grasp on the object, and record the forces on the object during the grasping task.

7.1.1. Experimental Setup

7.1.1.1. Robot Manipulator

The SDM Hand was mounted on a low-impedance robotic arm (Whole-Arm Manipulator (WAM), Barrett Technology, Cambridge, MA, USA) for positioning (Figure 7.1). Only three of the four joints of the WAM were utilized for a total of three

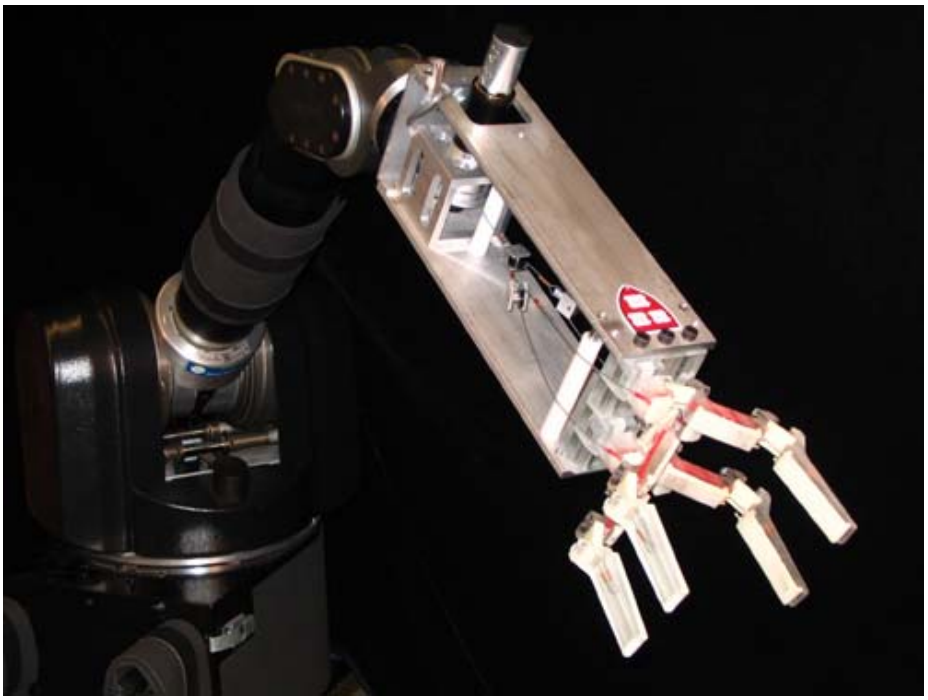

Figure 7.1. Four-fingered, underactuacted SDM hand mounted on a Whole-Arm Manipulator (Barrett Technology Inc., Cambridge, MA, USA). A single motor drives all eight joints of the hand.

positioning degrees of freedom: the base roll, shoulder pitch, and elbow pitch. Since there is no wrist, orientation of the hand was not controlled and was determined based on the kinematics of the manipulator at the target position.

The WAM was controlled using a 1000 Hz servo loop running on a DSP co-processor board (DS1103 PPC, dSPACE Inc., Novi, MI). The desired position was achieved using a PID controller with gains chosen so that the overall stiffness was dominated by the remote environment stiffness. To increase performance and allow for the use of lower gains, the robot controller uses a feedforward model of the forces on the arm (before contact with the object), including compensation for torque ripple, gravity, and friction.

7.1.1.2. Workspace

Target objects were mounted on a 6-axis force/torque sensor with a resolution of 0.1 N (Gamma model, ATI Industrial Automation, Inc, Apex, NC, USA). Objects were mounted to the force sensor via a square peg, such that position and orientation in the plane were fixed, yet the object could be lifted up out of the mount after grasping. Only contact forces in the plane of the workspace table were recorded, and torques were ignored. Robot inertial effects were minimized by using low accelerations during motion, reducing the task to nearly quasi-static conditions.

Two objects were tested at three positions, for a total of six conditions (Figure 7.2). The objects were a cylindrical PVC tube with a radius of 24mm (0.3 times the grasper link length l), and a wooden block with a 84 mm x 84 mm cross section (equivalent to 0.75 times the grasper link length l). This block was oriented such that a flat side was approximately normal to the approach direction. As shown in Figure 7.2, the difference in object position served to change the approach angle of the grasper with respect to the long axis of the objects, ranging from 25.6º to 42.8º.

7.1.2. Experimental Procedure

The experiment begins by manually finding the 'zero position' for the particular object and location. This position was taken as the point at which the hand contacts the object without any deflection, centered on the object; this represents the positioning of the hand under perfect visual sensing (hand is centered on the object) and perfect contact sensing (stopping the manipulator at the instant of initial contact). The y direction was taken along the line lying between the robot origin and the center of the object, normal to

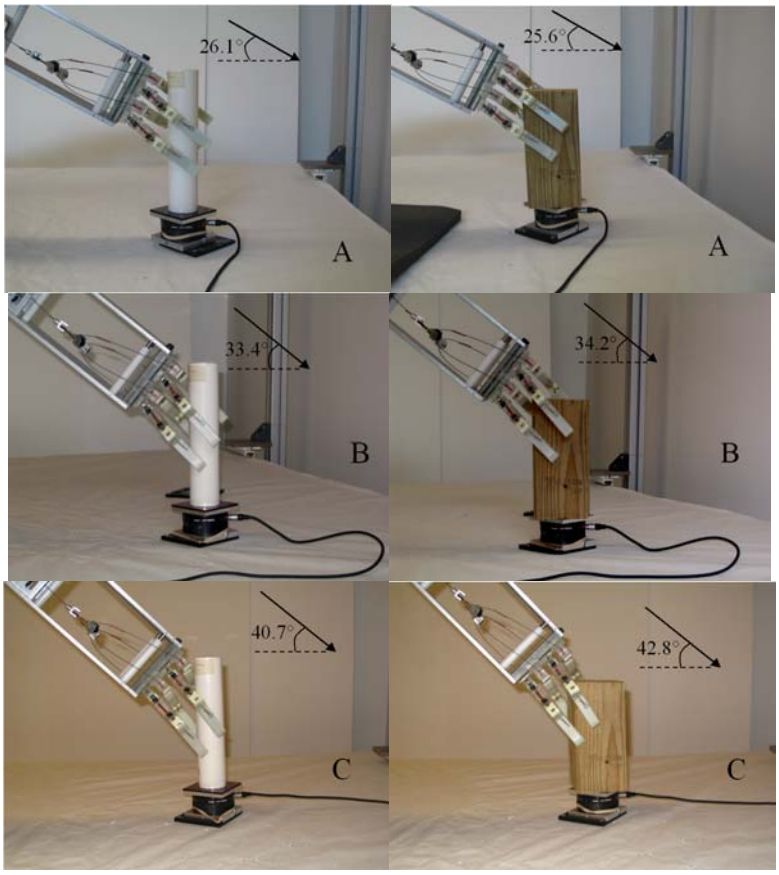

Figure 7.2. Two target objects (PVC cylinder of radius 24mm and wood block with square cross-section 90mm side length) at three locations (A, B, and C). Note the differences in approach angle for the locations, the main factor affecting the force and grasp space results.

the direction of gravity. The *x* direction is normal to the *y* direction, also normal to the direction of gravity (the *z* direction).

In order to examine the behavior of the grasping system for a range of "error" in positioning, a grid of positions from the zero position was calculated. The performance of the hand was tested at 10mm increments from the zero position in the positive *x* (symmetry in the positive and negative *x* direction was assumed) and positive and negative *y* directions (grasping behavior is not symmetric in *y*).

The manipulator joint angles were calculated using the inverse kinematics of the robot and rounded to the nearest tenth of a degree. For each position on the grid, the robot moves to within a tenth of a degree of the target joint configuration at each joint. The robot then initiates the grasp by driving the grasping motor to a preset torque (stall) and thus closing all fingers. When an encoder indicates motor stall, the motor current is reduced to a small amount required to prevent backdriving of the motor due to the tendon force. The arm then attempts to lift the object vertically out of the force sensor mount. Forces on the object and whether the grasp was successful were recorded for each position. The vertical position of the hand was kept constant across object position at approximately 19 cm above the table (Figure 7.2). The sensors on the hand are not used in this study. This simple, strictly feedforward hand control mode is used to evaluate the benefits of the optimized passive compliance and adaptive coupling approach to hand design.

Each location on the (x,y) grid of positions was tested three times, and the force results averaged. Force was recorded at 1000 Hz during the experiment. Data from the force sensor was filtered by taking the median of the previous 20 force samples (0.02 s).

A grasp was deemed successful if the object was lifted vertically out of the force sensor mount a distance of 150mm, and the grasp appeared to be stable (i.e. no slippage of the object was visually observed). Grasps could fail at a given position for a number of reasons: passive contact force pushes the object out of the sensor mount or pushes the sensor out of the table mount, too few fingers make contact with the object, or an imbalance of forces on the object due to undesirable positioning leads to it being ejected

from the grasp. Note that these failure modes may be avoided with appropriate sensory feedback in the grasping task.

7.1.3. Results

Figures 7.3 and 7.4 show the results of the force and successful grasp space study for the two objects at three configurations each. The left column ($F_{approach}$) indicates the magnitude of the maximum force applied to the object during the approach phase of the grasp (hand has not yet been actuated). The right column (F_{grasp}) indicates the magnitude of the maximum force applied to the object during the grasp phase (fingers are closing in on the object, before motion of the arm to lift the object out of the sensor mount).

The various points on the plots that are labeled correspond to interesting or demonstrative configurations. A description of the grasping behavior at these points is given in Tables 7.1 and 7.2.

The boundary of these plots is a rough approximation of the successful grasp range (the amount of allowable positioning error resulting in a successful grasp) for the particular object and position. Note that the successful grasp range is significantly affected by the approach angle of the hand. The steeper the approach angle, the less likely enough fingers will be in contact with the object to create a stable grasp (Figure 7.2).

The results show that the PVC cylinder (48mm diameter) could be successfully grasped at positions up to 50mm from the center in *x*, and +20mm,-30mm in *y*, for a total allowable positioning error of over 100% of the object size in each direction. Not surprisingly, shallow (more horizontal) hand orientations lead to larger successful grasp ranges. For the wooden block (84mm x 84mm cross section), positioning errors of up to

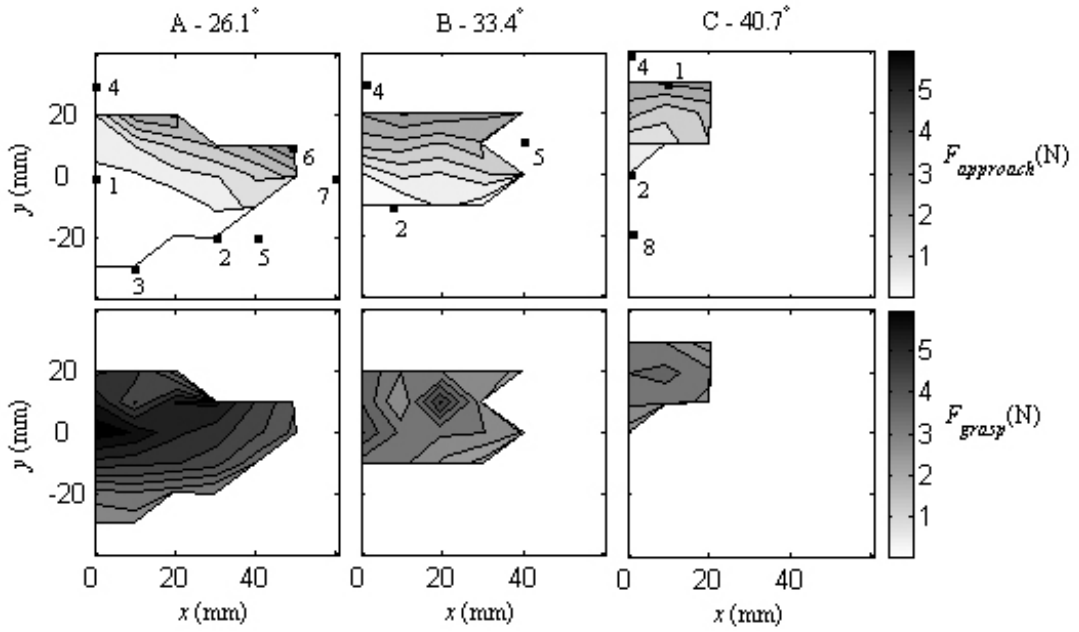

Figure 7.3. Forces on the PVC cylinder object during the approach (top row) and grasp (bottom row) phases for the three object locations (columns). Labeled configurations correspond to the behavior indicated in Table 7.1.

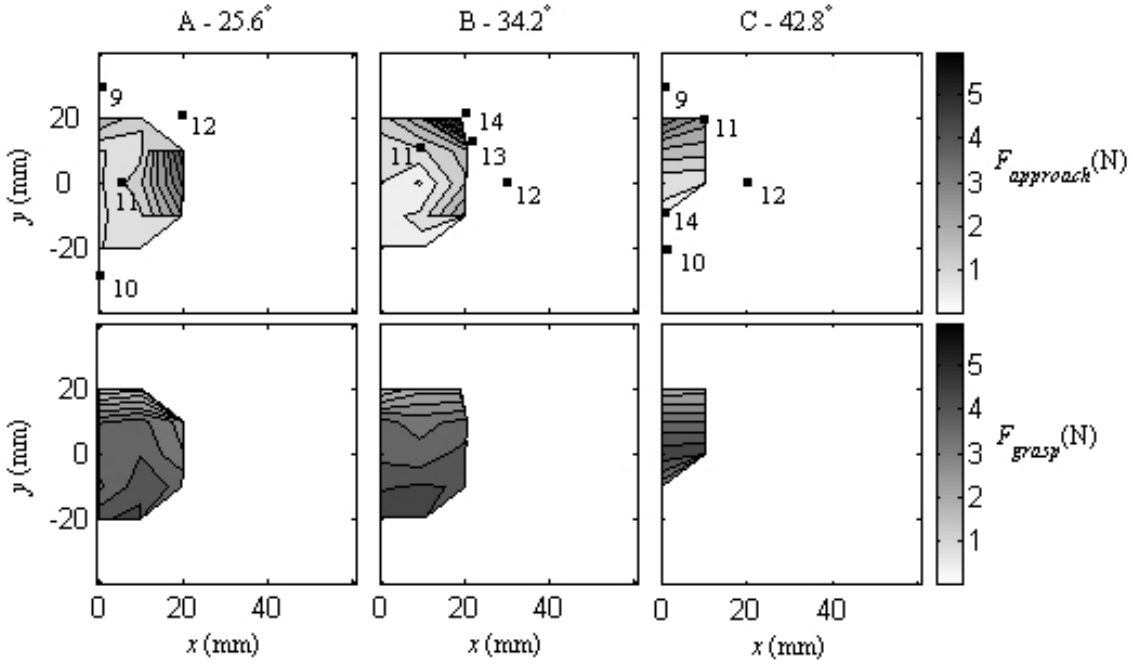

Figure 7.4. Forces on the wooden block during the approach (top row) and grasp (bottom row) phases for the three object locations (columns). Labeled configurations correspond to the behavior indicated in Table 7.2.

TABLE 7.1
CYLINDRICAL OBJECT

#	*Grasp behavior*
1	Four-fingered grasp
2	Three-fingered grasp
3	Two-fingered grasp
4	Object knocked from mount due to palm hitting object
5	Objects twists out of grasp
6	Left fingertip sticks, then slides into place
7	Miss object completely
8	Two fingers make contact - no grasp

TABLE 7.2
RECTANGULAR BLOCK

#	*Grasp behavior*
9	Object knocked from mount due to palm hitting object
10	Two fingers make contact - no grasp
11	Four-fingered grasp
12	Object knocked from mount due to finger jamming against object
13	Left fingertip sticks, then slides into place
14	Three-fingered grasp

20mm from the center in x, and +20mm,-20mm in y resulted in a successful grasp, for a total allowable positioning error of over 45% of the object size.

In general, the shape and orientation of these objects lend themselves better to a shallow or horizontal hand orientation, aligning the axis of the power grasp configuration with the major axis of the object. For this reason, additional manipulator or wrist degrees of freedom can greatly expand the amount of allowable positioning uncertainty across the manipulator workspace, particularly if the orientation of the major axis of the object can be estimated.

It can be seen from the contours that, in general, F_{approach} increases with increasing y. This is expected since motion forward increases the passive deflection of the joints due to contact, increasing the force. With decreasing y, the force goes to zero, as passive contact with the object is lost. The apparent discrepancy with this trend seen in Figure 7.4A is simply an artifact of the sampling and contour generation.

As x increases, $F_{approach}$ increases as well. This is particularly significant in the wooden block cases, where the forward-most finger first "jams" against the face of the block, eventually slipping to the side, enabling a successful grasp. As x increases, the amount of "slip" of this finger necessary for a successful grasp increases, thereby increasing the passive force. Note that, as in this example, the maximum passive force often occurs before the hand has reached the target position.

The trends in the F_{grasp} plots can be largely explained in terms of the object size relative to the fingers. For each object there is some "grasp equilibrium" position, located approximately with the object centered in the closed hand in the y direction, where the forces on the object would balance even without friction. Since the zero position for each object was based on the location of the front of the object and not the center, the size of the object affects the grasp equilibrium position. This position is in negative y for smaller objects (i.e. the object is "too close" to the base of the hand at the zero position) and positive y for larger objects (i.e. object is "too far" from the base at the zero position). In general, positions far away from the equilibrium position will result in high forces.

Figure 7.5 shows histograms of the standard deviation of the force measurements (three samples at each configuration) for the two objects. Note that the total number of samples are different for the two objects: 38 for the wooden block and 54 for the PVC cylinder. While the values of standard deviation are typically less than the sensor resolution (0.1N), there are a number of instances of large variation in the force measurements between trials, particularly during the approach phase for the wooden block. These instances occur at positions close to transition points between general grasp behaviors. For instance, when grasping the wooden block, if the tip of a finger is very

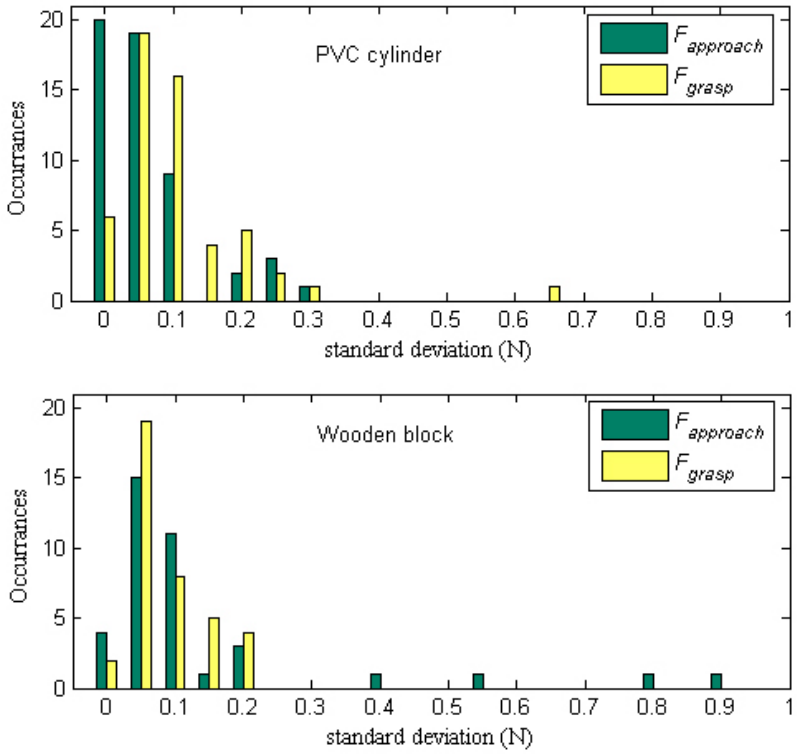

Figure 7.5. Histograms of the standard deviation of the force measurements for the PVC cylinder (top) and wooden block (bottom).

close to one of the edges, slight changes in hand or robot configuration can lead to drastically different behaviors (jamming against the object face vs. gently slipping to the side).

7.2. Visual-Guided Grasping Experiment

In order to demonstrate a further level of autonomy, we conducted a grasping experiment in which the location and size of a spherical target object were extracted from

a single image from an overhead camera and used to determine the target grasping position.

7.2.1. Experimental Setup

7.2.1.1. Robot Manipulator

The details of the manipulator and hand are the same as used in the previous experiment (section 7.1.1.1). Again, the hand was used without a wrist, for a total of three positioning degrees of freedom, and no control of orientation.

7.2.1.2. Workspace

To simplify the positioning of the robot, spherical target objects were chosen, spanning a wide range in size: a tennis ball (r=32mm), softball (r=44mm), small soccer ball (r=74mm), and volleyball (r=105mm). The tennis ball and volleyball are approximately the minimum and maximum size sphere that our hand can reliably grasp. Figure 7.6 shows the four objects as seen from an overhead camera. The spheres were set on a small stand to prevent them from rolling away during the grasping procedure, but were not fixed to the table.

A total of twelve trials for each of the four objects were conducted. The objects were pseudo-randomly placed on the workspace table in a manner such that all regions of the workspace were covered over the twelve trials. Only one object was placed on the table per trial. The workspace table is positioned approximately 22cm below the origin of the robot. As in the experiment presented in section 7.1, variations in target object position result in different approach angles of the robot hand due to the absence of a wrist and only three positioning degrees of freedom. Objects closer to the base are approached from above, while objects far from the base are approached from the front.

Figure 7.6. Overhead image of the workspace showing the four target objects and the robot arm. Images of the workspace taken from this camera were used to find the target object location and size.

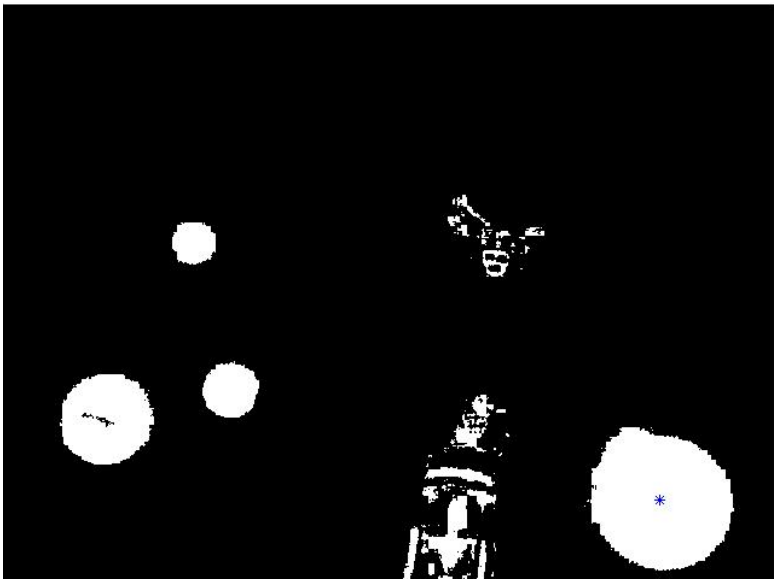

Figure 7.7. Image from Figure 7.6 after processing to find the 'color' pixels.

7.2.2. Experimental Procedure

The target configuration of the robot manipulator was determined based on a single overhead image of the workspace taken from a low-resolution USB camera (640x480 pixels, QuickCam Pro 3000, Logitech Inc., Fremont, CA USA). The camera was positioned at a height of 1.63m above the workspace, viewing a 1.26m x 0.94m portion of the workspace table. The lens distortion of the camera was accounted for by calibrating using a Matlab-based camera calibration toolbox [58]. The calibration was achieved to a mean pixel error of 0.40, corresponding to 0.79mm.

To register the camera to the robot workspace, a small black sphere was mounted to the end of the manipulator. The sphere was positioned within 3cm (+- 2cm) of the workspace table with a total of 32 images were taken spanning the robot workspace. The two spaces were registered using a linear least-squares fit, with an RMS error of 1.98mm. The mapping was found with a combination of the forward kinematics of the manipulator and the centroid of the sphere in the camera image. The resulting resolution of the camera is 1.97mm/pixel of the workspace table.

During experimental trials, the target object was located in the RGB image by detecting "colored" pixels. Pixels with a ratio of the red/green and red/blue channels between 0.9 and 1.1 were interpreted as 'gray', and part of either the table or robot. An example result of this method, performed on the image of Figure 7.6, is shown in Figure 7.7.

A bounding box was fit to the "color" blobs, and the largest taken as the target object. The largest leg of the target object box was taken as the object diameter (since the target objects are spherical). This value, in conjunction with knowledge of the height of

the workspace table, was used to locate the center of the object normal to the table. The centroid of the object pixels was taken as the object location in the plane of the workspace table.

The commanded target grasping position was the point on the surface of the sphere at which the hand is centered on the object, with the center of the hand was just touching the object. Once the target position is determined based on the camera image, the robot first moves to a position 15cm away from the target, normal to the sphere. This "approach" point ensures a consistent "approach" phase on the object regardless of initial manipulator configuration, and that the hand makes contact with the target in a way that maximizes the likelihood of a successful grasp. After reaching the approach point, the robot then moves in to the object, initiating the grasp once the target position has been reached (within approximately one tenth of a degree in all joints). The arm then lifts the object upwards 15cm, with the grasp deemed successful if the object appeared to be stable (i.e. no slippage of the object was visually observed). See Chapter 6 section 6.2.1.1 for further details on the actuation method of the hand. Figure 7.8 shows the hand in the rest configuration and grasping the smallest and largest objects.

7.2.3. Results

The results show that the objects can be grasped every time over the entire workspace. Figure 7.9 shows the placement of the target objects in the workspace. The axes correspond to the Cartesian robot space. The arc on the outer edge is the approximate limit of the robot workspace (i.e. arm fully extended) for the largest object (volleyball – r=105mm). The data points are the center of the target object as extracted from the camera image. Larger objects therefore can be grasped further from the base

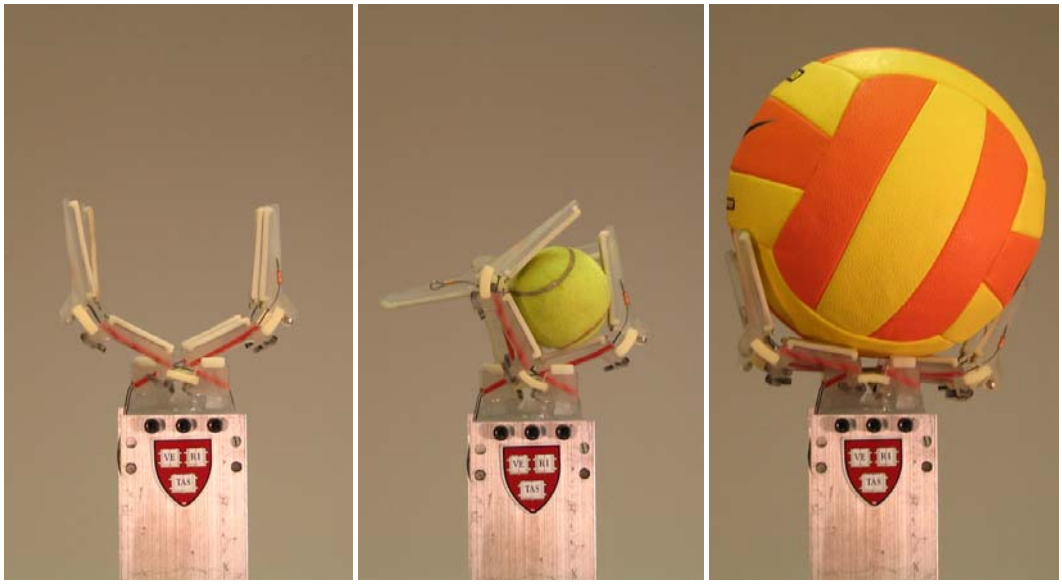

Figure 7.8. Images of the SDM hand (left to right) in the approximate "rest" configuration during this task, grasping the tennis ball (only three fingers make contact due to its small size), and grasping the volleyball (fingers must be pressed open by contact forces on the object). Note that due to the hand compliance, gravity tends to slightly open or close the hand from its normal "rest" configuration, depending on manipulator orientation.

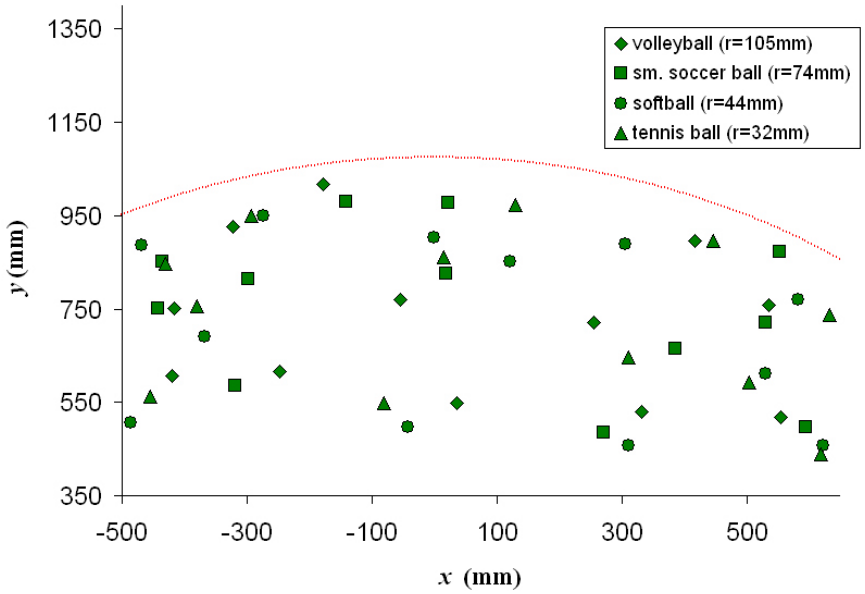

Figure 7.9. Placement of the four objects on the workspace table. The arc is the approximate robot workspace limit for the volleyball (r=105mm).

TABLE 7.3
OBJECT RADIUS MEASUREMENTS

object	*true r (mm)*	*est. r (mm)*	*error*	*std. dev*
Volleyball	105	116.3	11.3	2.1
Sm. Soccer ball	74	74.3	0.3	2.2
Softball	44	46.1	2.1	1.6
Tennis ball	32	34	2	1.3

than smaller objects by this classification, since the actual grasp target position is closer than the object center. Similarly, smaller objects can be grasped closer to the base and further to the sides since the entire object is more likely to be in the image space of the camera.

As expected due to symmetry in the object, the rotation of the robot base joint does not affect the performance of the task. Radial position from the base also does not affect the ability to establish a successful grasp.

Since we do not know the "true" object position, it is difficult to estimate the amount of positioning error inherent for each trial. However, from visual inspection, positioning of the hand was off-center from the object by as much as 8cm in the plane of the workspace, and 4cm in the normal direction.

Errors in each trial could have come from a number of sources. The calculation of the radius of the object (which was used in determining the target position of the hand) was subject to large errors (Table 7.3). Other factors that likely contributed to errors were camera resolution (1.97mm/pixel) and calibration error, shadows, errors in identifying "object" pixels in the workspace image, small robot positioning errors, and hysteresis in the viscoelastic joints of the hand.

7.3. Discussion

The intention in this study is not to suggest the details of a procedure to grasp objects in an unstructured environment, or to advance a specific grasper configuration. Rather, we empirically demonstrate that optimized passively compliant joints and adaptive coupling can allow the grasping system to adapt to the large positioning errors that can occur in these types of tasks. Even with simplified positioning and control (three degree of freedom arm with no wrist, a single actuator for the eight joints of the hand, and feedforward hand control), we are able to grasp 5 cm-scale objects in the presence of positioning error of up to 100% of the object size and 10 cm-scale objects in the presence of positioning error of up to 33% of the object size. We are also able to reliably grasp a wide range of spherical objects positioned arbitrarily across the robot workspace using only simple processing of a single image to guide the task.

Note that the use of the camera in the second experiment was intentionally simple. We are not interested in trying to extract the most information from the camera image, nor are we suggesting the best way to analyze the physical properties of the target object. Our aim is to test hardware system performance, even under large uncertainties due to poor sensing.

One of the main goals of this project is to simplify the amount of processing and control necessary to perform robust grasping. The use of the hand in these experiments is purely feedforward - once the target and size position is estimated based on a single workspace image, no further information about the object is used to execute the task. Additionally, such simple processing of the visual information and control of the hand

allows for easy implementation on microcontroller-based and other simplified robot platforms [e.g. 59].

There are a number of logical extensions to this work. The degree of autonomy demonstrated here can easily be expanded upon by utilizing the sensory information available from the joint angle and contact sensors already included in the hardware of the hand. This information, used in conjunction with an approximate model of object size and location from basic visual sensing, will make the grasping task even more robust to variations in object shape and position. Additional orientation degrees of freedom will also improve the performance by better relating hand and object geometry.

There are a number of directions for future work concerning the design of the hand. For instance, the compliance in the out-of-plane direction of finger motion, which seems to be important to both the adaptability and durability of the hand, has not yet been studied. Additionally, the arrangement of the fingers can be done in a number of alternate configurations. While an equal number of fingers on both sides of the hand creates more equivalent forces on the object, there is an additional moment applied to the object due to this arrangement that might be avoided with an alternate arrangement. The amount of space between the fingers and the affect on performance is another area to be considered.

The ability of the hand to perform complicated grasping tasks can be further evaluated by operating the manipulator in teleoperation mode, allowing for more precise and dexterous positioning in order to perform more sensitive tasks. Preliminary study of use of this mode indicates that a broad range of difficult tasks can be performed even with simple kinematics and hand control.

Chapter 8

Conclusions and Future Directions

This project set out to explore the design space of mechanically compliant and adaptive robot hands, determining how variations in joint stiffness, grasper preshape, and actuation scheme affect the ability to grasp objects in the presence of large sensing uncertainties. The first step along this path was a simulation of the grasping process to evaluate the effect of variations in joint stiffness and grasper preshape on grasping performance (Chapter 2). An optimum grasper preshape and joint stiffness ratio was determined based on both the maximum range of object size and location that could be successfully grasped and the magnitude of contact forces.

The second step was the determination of the role of actuation in the design of the graspers (Chapter 3). This work shows that much of the functionality of a hand can be retained while reducing the number of actuators by careful selection of joint coupling schemes. The result is a grasper that is much lighter, easier to control, and less expensive than a comparable fully-actuated hand. Finally, a prototype of a robust, adaptive hand was designed and fabricated using Shape Deposition Manufacturing (SDM) (Chapters 4-

6). Experimental results with this hand showed superior robustness to positioning errors, durability under misuse, adaptability to a wide range of target objects, and extremely simple means of control (Chapter 7).

8.1. Implications

8.1.1. New Approach

Perhaps the biggest surprise of this research was not that it works, but how *well* it works. With such simple control and positioning, the grasping system presented in Chapters 6 and 7 is able to robustly grasp objects spanning a surprisingly large range of size, shape, and mass, even under large errors in sensing and positioning. The combination of compliant flexural joints and highly coupled actuation scheme provides my hand with adaptability previously unseen and simplicity desirable in a number of arenas. The small number of required sensors and actuators also enables it to be produced very inexpensively.

One of the key concepts to the success of my approach is the increase in stiffness when the hand is actuated, due to the arrangement of the tendons in parallel with the flexural joints. While very low joint stiffness is desirable during the approach phases, the hand must become rigid after actuation in order to achieve a stable grasp. This property is particularly important for heavier objects.

Another aspect of my approach that has lent to its success is the focus on constructing durable hardware. While this is an area that has been largely overlooked in

the research community, it will be proven exceedingly important as robotics progresses in areas requiring physical interaction with the environment.

8.1.2. New Frameworks

This research established new frameworks for a number of issues surrounding grasping in the presence of uncertainty. I identified what are likely two of the most important quality metrics when evaluating the performance of the design of a hand in an unstructured task: successful grasp range and unbalanced contact force (Chapters 2 and 3). The first of these speaks to the amount of error or uncertainty allowable in the task while resulting in a successful grasp. For cases in which sensing is very noisy, the successful grasp range should be large to maximize the likelihood of a successful grasp. The second of these, unbalanced contact force, relates to the likelihood that the grasper will displace the object during acquisition, also relating to the likelihood of establishing a successful grasp.

I also established a method for modeling sensing uncertainty in a grasping task as a way to address tradeoffs in choices of certain design parameters. By assuming some normal distribution of the object from the expected or sensed position, a strategy for positioning the hand with respect to the object can also be adopted in order to minimize the unbalanced forces on the object and increase the likelihood of achieving a successful grasp.

In addition, I provided one of the first quantitative analysis of tradeoffs in the design of multi-purpose robot hands. To this point, the vast majority of robot hands have been designed on purely anthropomorphic principles or intuitive configurations. Instead of focusing on the mechanical design of these devices, researchers took the approach that

the getting these hands to function effectively was a problem solved by layering extensive sensing and control on top of complicated hardware.

8.2. Applications

8.2.1. Within Robotics

The premise of reliable grasping without complicated sensing and control lends itself to application in a number of different areas of robotics that require work in human environments. However, the problem of developing machines that interact with our surroundings is immense. A seemingly simple task such as walking on moderately uneven surfaces has proved to be difficult to accomplish. Grasping and manipulation in unstructured environments is a sort of "holy grail" for the field [60].

Highly functional graspers with minimum mechanical and sensing complexity are likely to be successful in built-for-human environments. These grasping tasks have often been attempted using complex anthropomorphic robot hands. However, after years of relatively unsuccessful work, researchers have largely abandoned these complicated, fragile devices. Alternatively, my approach reduces the need for the construction of a precise model of the task environment and is simple to operate - greatly increasing the reliability and speed of grasping tasks.

Other potential applications within robotics include military and police robots for the handling of hazardous materials and space robotics both for planetary rovers and on-board manipulators. These areas all involve grasping in unstructured environments and are enjoying an increase in funding and commercialization.

8.2.2. Outside of Robotics

8.2.2.1. Prosthetics

Over 10,000 major amputations of the upper extremities occur every year in America. And while technology has improved drastically, very few advances in prosthetic technology have been adopted by the amputee community in the last century. Most patients choose hooks or other simple mechanisms as terminal devices, rather than realistic looking prostheses that have little function and are mostly chosen for cosmetic purposes [61]. My approach lends itself well towards the development of a hand prosthesis that is both multi-functional and realistic.

Size and weight constraints as well as limitations inherent with both myoelectric and body-powered methods of actuation limit the number of actuators that can reasonably be incorporated into a prosthesis. Indeed, current state-of-the-art commercial products are limited to 1 or 2 degrees of freedom. For these reasons, there will always be a desire to minimize degrees of actuation while maximizing functional use and durability. The strategy I have taken with my grasper design fits well with this problem – careful choice of compliance, smart design of coupling, and an emphasis on durability.

8.2.2.2. MEMS

Motion is most often achieved in MEMS devices by means of flexures, and my approach to compliant grasping lends itself well to developing dexterous microgrippers. The creation of effective MEMS devices requires a systems-level design approach, and my work in smart joint coupling to reduce degrees of actuation lends itself well to this area.

8.2.2.3. Medical devices

A number of direct applications of this research to the medical industry include end-effectors for catheters, dexterous laparoscopic instruments, and surgical robotic instruments. Additionally, Shape Deposition Manufacturing shows potential for use in devices compatible with ultrasound and MRI procedures due to its nonmetallic materials, embedded components, and lack of fasteners.

8.2.2.4. Biomechanics

One interesting indirect application of this work is the possibility of studying biological hands/graspers using the approach presented in this dissertation. What is the exact role of compliance in biological hands? How does it reduce the need for sensing, actuation, and control? What is the role of the joint coupling between the DIP and PIP joints of human fingers, and how does it affect manipulation?

8.3. Limitations

8.3.1. Current Hardware Implementation

There are a few limitations to the current implementation of the four-fingered SDM hand. Perhaps the biggest limitation is that the number of tasks that can be performed is limited due to the small number of degrees of freedom of the manipulator arm. Having no orientation control (i.e. only three degrees of freedom) means that the hand cannot be aligned to best fit the shape and orientation of the target object, often greatly decreasing the quality of the grasp. One or two more degrees of freedom from a

wrist or more elaborate manipulator arm are necessary for a more generally useful grasping system.

Another potential limitation to the current version of the hand is the residual compliance in the hand after a grasp has been attained. While there are many applications in which some amount of passive compliance around the grasped object is useful ([8]-[13]), there are also applications in which a greater degree of positional accuracy is desired. The compliance in the grasp is even more significant when an object is grasped further from the palm, due to the increased lever arm.

8.3.2. Overall Approach

There are also a number of limitations to the overall approach that I have taken to address these issues. As mentioned above, compliance in the structure of the hand leads to lower grasp stiffness and makes for poor precision in positioning. Depending on the application, this may make the use of passive compliance in the structure of the hand undesirable.

While the use of SDM has a great number of desirable properties, there are also fallbacks. Due to the strength of the polymers, a hand fabricated with SDM may not be able to be as powerful as a similar-sized metal hand, and therefore may be inappropriate for certain high-force applications. However, the simplification of the design of the fingers may somewhat counteract that fact, since what may be one single rigid part in the SDM hand would likely be replaced by many much smaller (and perhaps weaker) parts in a metal prototype.

The viscosity in the polyurethane joints, while passively damping out oscillatory behavior, also leads to undesirable creep and force-relaxation. While these may be

outside of the time-scale for most grasping tasks, they will adversely affect performance in certain applications.

8.4. Future Work

8.4.1. Extension to Manipulation

Robotic hands that have been built for the purpose of performing dexterous tasks have typically employed little if any adaptability (Chapter 1 section 1.3). This fact likely comes from the belief that performing dexterous tasks requires fixed control of each of the joints involved. However, it is not clear that such restrictive control is necessary or even desirable to perform dexterous tasks. For example, an adaptive mechanism with passive stiffness can help ensure contact while an object is actively perturbed by another finger, simplifying the control required to execute the task.

Along these lines, the scope of this research can be expanded by addressing design methodologies for adaptive hands with a focus on manipulation capabilities as well as grasping. As in the work presented here, approaching the problem with an aim to simplify the design and control of the manipulators while retaining the majority of the function will surely make an impact on the field of study.

8.4.2. Quality Measures for Grasping in Unstructured Environments

While there has been extensive research in the areas of grasp planning, the vast majority of grasp quality measures are based on precise knowledge of the target object (e.g. [62]-[65]), which is an unrealistic expectation for tasks in unstructured environments. And while I have begun to address these issues in the process of

conducting the design optimization studies presented in Chapters 2 and 3, there is a need to further develop performance metrics and subsequent planning for grasping objects whose geometry and mechanical properties are unknown. These measures might be based on proprioceptive information such as force and grasper configuration, imaging information from a camera or 3-D range scanner, or a combination of these.

8.4.3. Sensing for Unstructured Grasping Tasks

One of the largest remaining holes in this research is investigating of the role of sensing in unstructured grasping tasks. While it will always be necessary to have some sort of imaging modality such as vision to identify target objects and their approximate location, how rich does this information need to be? Is there a significant advantage to being able to complete the task using lower-fidelity sensing, in simplified processing or savings in hardware expense? Can grasping be reliably done in complex environments without using imaging information in the feedback control of the manipulator and hand?

In keeping with my mantra of simplicity, what is the most basic sensor suite, both in imaging and in sensors on-board the hand that can allow for reliable grasping? What design features can be implemented to reduce the need for expensive and fragile tactile sensors? Certainly, all of these questions and more have multiple layers of complexity and provide a rich offering of future research directions.

Bibliography

[1] E. Schlicht, P. Schrater, "Effects of Visual Uncertainty on Grasping Movements," submitted to Experimental Brain Research, Springer, 2006.

[2] K. J. Salisbury, "Active stiffness control of a manipulator in Cartesian coordinates," *19th IEEE Conf. Decision and Control*, pp..95-100, 1980.

[3] J. Loncaric, "Geometrical analysis of compliant mechanisms in robotics," Ph.D. thesis, Harvard University, 1985.

[4] M. R. Cutkosky, I. Kao, "Computing and controlling the compliance of a robotic hand," *IEEE Transactions on Robotics and Automation*, vol. 5 (2), pp. 151-165, 1989.

[5] Q. Lin, J. Burdick, E. Rimon, "Computation and analysis of compliance in grasping and fixturing," *Proceedings of the 1997 IEEE International Conference on Robotics and Automation*, pp. 93-99, 1997.

[6] H. Bruyninckx, S. Demey, V. Kumar, "Generalized stability of compliant grasps," *Proceedings of the 1998 International Conference on Robotics and Automation*, pp. 2396-2402, 1998.

[7] J. P. Desai and R. D. Howe, "Towards the development of a humanoid arm by minimizing interaction forces through minimum impedance control," *Proceedings of the 2001 IEEE Int. Conf. on Robotics and Automation*, pp. 4214-4219, 2001.

[8] J. Nevins, D. Whitney, "Computer controlled assembly," *Scientific American*, vol. 238(2), pp. 62—74, 1978.

[9] S.H. Drake, "Using Compliance in Lieu of Sensory Feedback for Automatic Assembly," Ph.D. dissertation, MIT, 1977.

[10] N. Ciblak, H. Lipkin, "New Properties of the Remote Center of Compliance," *Proceedings of the 1997 IEEE International Conference on Robotics and Automation,* pp. 921-926, 1997.

[11] S. Joo, N. Yoshihara, F. Miyazaki, "Development of Variable RCC Using Elastomer Shear Pads," JSME *International Journal, Series C,* vol. 44 (4), pp. 867-876, 1998.

[12] C. Francois, K. Ikeuchi, M. Hebert, "A Three-Finger Gripper for Manipulation in Unstructured Environments," *Proceedings of the 1991 IEEE International Conference on Robotics and Automation,* pp. 2261-2266, 1991.

[13] J. M. Schimmels, S. Huang, "A Passive Mechanism that Improves Robotic Positioning through Compliance and Constraint," *Robotics and Computer-Integrated Manufacturing,* vol. 12 (1), pp. 65-71, 1996.

[14] J. E. Clark, J. G. Cham, S. A. Bailey, E. M. Froehlich, P. K. Nahata, R. J. Full, M. R. Cutkosky, "Biomimetic design and fabrication of a hexapedal running robot," *Proceedings of the 2001 International Conference on Robotics and Automation,* Seoul, Korea, 2001.

[15] U. Saranli, M. Buehler, and D. E. Koditschek, RHex: "A simple and highly mobile hexapod robot," *International Journal of Robotics Research,* vol. 20(7), pp. 616-631, July 2001.

[16] Q. Lin, J. Burdick, E. Rimon, "A Stiffness-Based Quality Measure for Compliant Grasps and Fixtures," *IEEE Transactions on Robotics and Automation,* vol. 16 (6), pp. 675-688, 2000.

[17] S. Govindarajan, G.S. Rajulu, "Presence of Resilin in a Scorpion Palamnaeu swammerdami and its Role in the Food-Capturing and Sound-Producing Mechanisms," *Experientia,* volume 30, pp. 908,909, 1974.

[18] S. A. Andersen, T. Weis-Fogh, "Resilin: A Rubberlike Protein in Arthropod Cuticle," *Advances in Insect Physiology*, volume 2, pp. 1-65, 1965.

[19] M. Higashimori, M. Kaneko, A. Namiki, M. Ishikawa, "Design of the 100G Capturing Robot Based on Dynamic Preshaping," *The International Journal of Robotics Research*, vol. 24 (9), pp. 743-753, 2005.

[20] W. T. Townsend, "The BarrettHand Grasper - Programmably Flexible Part Handling and Assembly," *Industrial Robot – An International Journal*, vol 10 (3), pp. 181-188, 2000.

[21] M. Rakic, "Multifingered Robot Hand with Self-Adaptability," *Robotics and Computer Integrated Manufacturing*, vol. 5(2/3), pp. 269-276, 1989.

[22] G. A. Bekey, R. Tomovic, I. Zeljkovic, "Control Architecture for the Belgrade/USC Hand" in *Dextrous Robot Hands*, Springer-Verlag, New York, 1990.

[23] J. Butterfass, G. Hirzinger, S. Knoch, H. Liu, "DLR's Multisensory Articulated Hand Part I: Hard- and Software Architecture," *Proceedings of the 1998 IEEE International Conference on Robotics and Automation*, pp. 2081-2086, 1998.

[24] J. Butterfass, M. Grebenstein, H. Liu, G. Hirzinger, "DLR-Hand II: Next Generation of a Dextrous Robot Hand," *Proceedings of the 2001 IEEE International Conference on Robotics and Automation*, pp. 109-114, 2001.

[25] A. Edsinger-Gonzales, "Design of a Compliant and Force Sensing Hand for a Humanoid Robot," *Proceedings of the 2004 International Conference on Humanoid Manipulation and Grasping (IMG04)*, 2004.

[26] J. Crisman, C. Kanojia, I. Zeid, "Graspar: A Flexible, Easily Controllable Robotic Hand," *IEEE Robotics and Automation Magazine*, pp. 32-38, June 1996.

[27] S. Hirose and Y. Umetani, "The Development of Soft Gripper for the Versatile Robot Hand," *Mechanism and Machine Theory*, vol. 13, pp. 351-359, 1978.

[28] T. Laliberte, L. Birglen, C. Gosselin, "Underactuation in Robotic Grasping Hands," *Machine Intelligence & Robotic Control*, vol. 4 (3) pp. 1-11, 2002.

[29] J. Ueda, Y. Ishida, M. Kondo, T. Ogasawara, "Development of the NAIST-Hand with Vision-based Tactile Fingertip Sensor," *Proceedings of the 2005 IEEE International Conference on Robotics and Automation*, pp. 2343-2348, 2005.

[30] E. Torres-Jara, "Obrero: A platform for sensitive manipulation," *Proceedings of the 2005 IEEE-RAS International Conference on Humanoid Robots*, pp. 327-332, 2005.

[31] C. S. Lovchik, M. A. Diftler, "The Robonaut Hand: A Dexterous Robot Hand for Space," *Proceedings of the 1999 IEEE International Conference on Robotics and Automation*, pp. 907-912, 1999.

[32] K. DeLaurentis, C. Mavroidis, "Mechanical design of a shape memory allow actuated prosthetic hand," *Technology and Health Care*, vol. 10, pp. 91-106, 2002.

[33] D. Caldwell, N. Tsagarakis, ""Soft" grasping using a dextrous hand," *Industrial Robot: An International Journal* vol. 27 (3), pp. 194-199, 2000.

[34] A. M. Dollar and R. D. Howe, "Designing Robust Robotic Graspers for Unstructured Environments," *proceedings of the Workshop on Manipulation for Human Environments, 2006 Robotics: Science and Systems Conference,* 2006.

[35] The Shadow Dextrous Hand, http://www.shadowrobot.com

[36] R. Crowder, V. Dubey, P. Chappell, D. Whatley, "A Multi-Fingered End Effector for Unstructured Environments," *Proceedings of the 1999 IEEE International Conference on Robotics and Automation,* pp. 3038-3043, 1999.

[37] M. C. Carrozza, C. Suppo, F. Sebastiani, B. Massa, F. Vecchi, R. Lazzarini, M. R. Cutkosky, P. Dario, "The SPRING Hand: Development of a self-Adaptive Prosthesis for Restoring Natural Grasping," *Autonomous Robots* 16, pp. 125-141, 2004.

[38] N. Dechev, W. Cleghorn, S. Naumann, "Multiple finger, passive adaptive grasp prosthetic hand," *Mechanism and Machine Theory* 36, pp. 1157-1173, 2001.

[39] F. Lotti, P. Tiezzi, G. Vassura, L. Biagiotti, G. Palli, C. Melchiorri, "Development of UB Hand 3: Early Results," *Proceedings of the 2005 IEEE International Conference on Robotics and Automation,* pp. 4499 –4504, 2005.

[40] iRobot Corporation, Government and Industrial Robotics Division, Burlington, MA, USA, (www.irobot.com/governmentindustrial).

[41] D. F. Hougen et al., "A Miniature Robotic System for Reconnaissance and Surveillance," *Proceedings of the 2000 IEEE International Conference on Robotics and Automation,* pp. 501-507, San Francisco, CA, April 2000.

[42] D. A. Theobald et al., "Autonomous Rock Acquisition," *Proceedings of the AIAA Forum on Advanced Developments in Space Robotics,* Madision, Wisconsin, August, 1-2, 1996.

[43] R. Merz, F. B. Prinz, K. Ramaswami, M. Terk, L. Weiss, "Shape Deposition Manufacturing," *Proceedings of the Solid Freeform Fabrication Symposium,* University of Texas at Austin, August 8-10, 1994.

[44] M. Binnard and M. R. Cutkosky, "A Design by Composition Approach for Layered Manufacturing," *ASME Transactions, J. Mech. Design,* vol. 122, no. 1, pp 91-101, 2000.

[45] S. C. Jacobsen, E. K. Iversen, D. F. Knutti, R. T. Johnson, K. B. Biggers, "Design of the Utah/MIT dextrous hand," *Proceedings of the 1986 IEEE Int. Conf. on Robotics and Automation,* pp. 1520-1532, 1986.

[46] L. Biagiotti, F. Lotti, C. Melchiorri, G. Vassura, "Mechatronic design of innovative fingers for anthropomorphic robot hands," *Proceedings of the 2003 IEEE International Conference on Robotics and Automation*, pp. 3187 –3192, 2003.

[47] J. C. Trinkle, R. C. Ram, A. O. Farahat, P. F. Stiller, "Dexterous manipulation planning and execution of an enveloped slippery workpiece," *Proceedings of the 1993 IEEE International Conference on Robotics and Automation,* vol. 2, pp 442-448, May 1993.

[48] W. S. Howard, V. Kumar, "Modeling and Analysis of the Compliance and Stability of Enveloping Grasps," *Proceedings of the 1995 IEEE Intl. Conference on Robotics and Automation,* pp. 1367-1372, 1995.

[49] M. T. Mason, J. K. Salisbury, "Robot Hands and the Mechanics of Manipulation," MIT Press, Cambridge, USA, 1985.

[50] M. Kaneko, K. Harada, T. Tsuji, "Dynamic friction closure," *Proceedings of the 2002 IEEE International Conference on Robotics and Automation,* pp.1584-1589, 2002.

[51] K. B. Shimoga, A. A. Goldenberg, "Soft materials for robotic fingers," *Proceedings of the 1992 IEEE International Conference on Robotics and Automation,* pp. 1300-1305, 1992.

[52] M. R. Cutkosky, J. M. Jourdain, P. K. Wright, "Skin materials for robotic fingers," *Proceedings of the 1987 IEEE International Conference on Robotics and Automation*, pp. 1649-1654, 1987.

[53] C. Stefanini, M. R. Cutkosky, P. Dario, "A high force miniature gripper fabricated via shape deposition manufacturing," *Proceedings of the 2003 International Conference on Robotics and Automation,* Taipei, Taiwan, 2003.

[54] B. H. Park, M. Shantz, F. B. Prinz, "Scalable rotary actuators with embedded shape memory alloys," *Proceedings of SPIE, The International Society for Optical Engineering,* vol. 4327, pp. 79-87, 2001.

[55] Y. C. Fung, "Biomechanics: Mechanical properties of living tissues," Springer-Verlag, 2nd edition, 1993.

[56] A. T. Asbeck et al., "Scaling Hard Vertical Surfaces with Compliant Microspine Arrays," *Proceedings of Robotics: Science and Systems*, Cambridge, MA, 2005.

[57] R. D. Howe and M. R. Cutkosky, "Dynamic tactile sensing: Perception of fine surface features with stress rate sensing," IEEE *Trans. on Robotics and Automation* 9(2):140-151, April 1993.

[58] J-Y Bouguet, http://www.vision.caltech.edu/bouguetj/calib_doc/

[59] Pioneer 3-DX8 mobile robot platform, MobileRobots Inc., Amherst, NH, USA.

[60] R. Brooks et al., "Sensing and Manipulating Built-for-Human Environments", International Journal of Humanoid Robotics, vol. 1(1), 2004.

[61] D.G. Shurr and T.M. Cook, eds., "Prosthetics and Orthotics," Appleton and Lange, Norwalk, CT, 1990.

[62] D. Montana, "The Kinematics of Contact and Grasp," The International Journal of Robotics Research, vol. 7(3), pp. 17-32, June 1988.

[63] D. Montana, "Contact Stability for Two-Fingered Grasps," IEEE Transactions on Robotics and Automation, vol. 8(4), pp. 421-430, August 1992.

[64] V. Nguyen, "Constructing Force-Closure Grasps," The International Journal of Robotics Research, vol. 7(3), pp. 3-16, June 1988.

[65] V. Nguyen, "Constructing Stable Grasps," The International Journal of Robotics Research, vol. 8(1), pp. 26-37, February 1989.

[66] A. M. Dollar, C. R. Wagner, and R. D. Howe, "Embedded Sensors for Biomimetic Robotics via Shape Deposition Manufacturing," proceedings of the first IEEE/RAS-EMBS International Conference on Biomedical Robotics and Biomechatronics (BioRob), Pisa, Italy, Feb. 20-22, 2006.